2012

Hollow hydroxyapatite microspheres as devices for controlled delivery of proteins and as scaffolds for tissue engineering

Hailuo Fu

Department: Materials Science and Engineering

HOLLOW HYDROXYAPATITE MICROSPHERES AS DEVICES FOR CONTROLLED DELIVERY OF PROTEINS AND AS SCAFFOLDS FOR TISSUE ENGINEERING

by

HAILUO FU

A DISSERTATION

Presented to the Faculty of the Graduate School of the

MISSOURI UNIVERSITY OF SCIENCE AND TECHNOLOGY

In Partial Fulfillment of the Requirements for the Degree

DOCTOR OF PHILOSOPHY

in

MATERIALS SCIENCE AND ENGINEERING

2012

Approved by

Mohamed N. Rahaman, Advisor

Delbert E. Day

Richard K. Brow

Roger F. Brown

Lynda F. Bonewald

PUBLICATION DISSERTATION OPTION

The body of this dissertation has been compiled in the format for publication in peer-reviewed journals. Five papers have been included in the following order. The first paper, “Effect of Process Variables on the Microstructure of Hollow Hydroxyapatite Microspheres Prepared by A Glass Conversion Method,” was published in Journal of the American Ceramic Society in 2010, Volume 93, Issue 10, pages 3116−3123. The second paper, “Effect of Pyrophosphate Ions on the Conversion of Calcium-Lithium-Borate Glass to Hydroxyapatite in Aqueous Phosphate Solution,” was published in Journal of Materials Science: Materials in Medicine in 2010, Volume 21, pages 2733−2741. Paper number three titled “Hollow Hydroxyapatite Microspheres as a Device for Local Delivery of Proteins,” was published in Journal of Materials Science: Materials in Medicine in 2011, Volume 22, pages 579−591. The fourth paper, “Evaluation of Protein Release Behavior from Hollow Hydroxyapatite Microspheres into PEG Hydrogel,” was submitted to Materials Science and Engineering C. The fifth paper, “Evaluation of Bone Regeneration in Implants Composed of Hollow HA Microspheres Loaded with TGF–β1 in a Rat Calvarial Defect Model” was prepared for submission to Acta Biomaterialia.

One paper not included in the main body of the dissertation is given in the appendix. Titled “Long-term Conversion of 45S5 Bioactive Glass–Ceramic Microspheres in Aqueous Phosphate Solution,” the paper was accepted for publication in Journal of Materials Science: Materials in Medicine, 2012.

ABSTRACT

Hollow HA microspheres were prepared by converting $Li_2O–CaO–B_2O_3$ glass microspheres in a K_2HPO_4 solution. Process parameters, such as reaction temperature (25°C–60°C) and concentration of the phosphate solution (0.02–0.25 M) significantly influenced the microstructure of the hollow HA microspheres. Microspheres with the largest hollow core size were obtained at lower temperature or with low K_2HPO_4 concentration. In comparison, microspheres with high surface area (~140 m^2/g) were obtained at higher K_2HPO_4 concentration (0.25 M). Upon heat treatment (up to 900°C), the surface area of the hollow HA microspheres decreased (from ~100 m^2/g to ~2 m^2/g), and the rupture strength increased (from ~11 MPa to ~30 MPa). The release kinetics of a model protein, bovine serum albumin (BSA) from the hollow HA microspheres were evaluated in two different media, phosphate-buffered saline (PBS) and poly(ethylene glycol) (PEG) hydrogel, used to mimic different environments in vivo. Implants composed of individual hollow HA microspheres or three-dimensional (3D) scaffolds composed of hollow HA microspheres were evaluated for their ability to regenerate bone in non-healing rat calvarial defects. The individual microspheres showed better ability to regenerate bone than the 3D scaffolds. Larger microspheres (150–250 μm in diameter) showed better ability to regenerate bone than smaller microspheres (106–150 μm). Loading the hollow HA microspheres with transforming growth factor-β1 (TGF-β1) (5 μg/defect) enhanced bone regeneration in the implants after 6 weeks. The results indicate that implants composed of hollow HA microspheres could potentially be used as an osteoconductive matrix for local growth factor delivery in bone regeneration.

ACKNOWLEDGMENTS

I am grateful to my advisor, Dr. Mohamed N. Rahaman, who has supported me in many ways during the past four years. He has provided numerous valuable suggestions and discussions to make this dissertation possible. His great enthusiasm and meticulous attitude towards research have inspired me to work for excellence.

I sincerely appreciate the assistance of Dr. Roger F. Brown, Department of Biological Sciences, for his assistance with the *in vitro* and *in vivo* experiments in my research. I am also grateful to Dr. Delbert E. Day, Dr. Richard K. Brow and Dr. Lynda F. Bonewald, who provided valuable comments and constructive suggestions throughout my PhD education. I would like to thank Dr. Wenhai Huang, Tongji University, China, for introducing me to the idea of studying in the USA.

Several persons provided assistance to enable me to complete my research or provided guidance with the direction of my research, and I would like to express my thanks to them: Dr. Ted Day (Mo-Sci Corp.), Ms. Yiyong He (Mo-Sci Corp.), Clarissa Wisner (Missouri S&T), Dr. Eric Bohannan (Missouri S&T), Xiaoming Cheng (Missouri S&T), Yinan Lin (Missouri S&T), Dr. Qiang Fu (Corning Incorporated), and Dr. Steven Jung (Mo-Sci Corp.).

All of my friends and colleagues deserve many thanks as well. Dr. Shichang Zhang, Dr. Tieshu Huang, Dr. Liying Zhang, Xin Liu, Lina Ma, Yifei Gu, and Jiye Wang. I greatly appreciated working and learning with you.

Last but not least, I would like to thank those who made this possible: my parents, Zhencai Fu and Xiuzhi Bao, and my husband, Jun Tao. Their love, belief, and encouragement kept me moving forward with my research.

TABLE OF CONTENTS

Page

Page

Page

Page

Page

APPENDIX

LIST OF ILLUSTRATIONS

PAPER 1 Page

Page

Page

PAPER 3

Page

Page

PAPER 5

Page

ADDITIONAL WORK AND SUGGESTIONS FOR FUTRUE WORK

LIST OF TABLES

PAPER 1 Page

PAPER 2

PAPER 3

PAPER 4

PAPER 5

1. PURPOSE OF THIS DISSERTATION

The purpose of this Ph.D. research was to prepare and evaluate hollow hydroxyapatite (HA) microspheres as an inorganic system for local growth factor delivery in the regeneration of hard tissues. HA is the main inorganic constituent of human bone. Synthetic HA has several attractive properties as a scaffold material for bone regeneration. It is biocompatible, bioactive, and osteoconductive, with a proven ability to support bone regeneration and to bond to surrounding tissue. Composed of the same ions as the mineral constituent of bone, HA produces no systemic toxicity or adverse immunological reaction. In the present work, hollow HA microspheres were produced by a glass conversion process developed elsewhere. The HA microspheres had a hollow core and a mesoporous porous shell wall. In addition to their biocompatibility and osteoconductivity, these hollow HA microspheres can potentially provide a device for local growth factor delivery in the regeneration of bone.

The first phase of this study determined the process variables that controlled the microstructure of the hollow HA microspheres formed by the glass conversion process. Once hollow HA microspheres could be prepared reliably and reproducibly, the next phase of the study was to evaluate their biocompatibility, their ability to serve as a device for protein delivery in vitro, and their ability to regenerate bone in a standard bone defect model (non-healing rat calvarial defect model).

PAPER

1. EFFECT OF PROCESS VARIABLES ON THE MICROSTRUCTURE OF HOLLOW HYDROXYAPATITE MICROSPHERES PREPARED BY A GLASS CONVERSION METHOD

Hailuo Fu, Mohamed N. Rahaman, Delbert E. Day

Department of Materials Science and Engineering, Center for Bone and Tissue Repair and Regeneration, Missouri University of Science and Technology, Rolla, Missouri 65409, USA

1.1 ABSTRACT

Solid microspheres (diameter = 106–150 μm) of a Li_2O–CaO–B_2O_3 glass were reacted in a K_2HPO_4 solution to form hollow hydroxyapatite (HA) microspheres. The effect of the temperature (25–60°C), K_2HPO_4 concentration (0.01–0.25M), and pH (9–12) of the solution on the diameter (*d*) of the hollow core normalized to the diameter (*D*) of the HA microspheres, the surface area, and the pore size of the microsphere wall was studied. The statistically significant process variables that influenced these microstructural characteristics were evaluated using a factorial design approach. While the pH had little effect, the concentration of the solution had a marked effect on *d*/*D*, surface area, and pore size, whereas temperature markedly influenced *d*/*D* and pore size, but not the surface area. The largest hollow core size (*d*/*D* value ≈ 0.6) was obtained at the lowest temperature (25°C) or the lowest K_2HPO_4 concentration (0.02M), while microspheres with the highest surface area (140 m^2/g), with pores of size 10–12 nm were obtained at the highest concentration (0.25M). The consequences of these results for

potential application of these hollow HA microspheres as devices for local delivery of proteins, such as drugs or growth factors, are discussed.

1.2 INTRODUCTION

Over the past few decades, there has been considerable interest in the development of controlled delivery devices for local delivery of proteins such as drugs or growth factors [1]. A controlled-release system consists of a biologically-active agent (e.g., protein) in a carrier material (commonly a polymer or ceramic). The objective of the controlled-delivery device is to provide a means for local delivery of the protein to the target site at concentrations within the therapeutic limits and for the required duration. Because the delivery device is implanted, injected, or inserted into the body, the biocompatibility and toxicity of the carrier material are of critical importance.

Natural and synthetic biodegradable polymers have found wide application as carrier materials for protein delivery [2]. The delivery systems include microspheres, hydrogels, and three-dimensional porous scaffolds [3, 4]. These polymers degrade *in vivo*, either enzymatically or nonenzymatically, to produce biocompatible or nontoxic by-products along with progressive release of the dispersed or dissolved protein. Natural polymers and their derivatives in the form of gels or sponges have been used extensively as delivery vehicles. In particular, collagen is a readily available extracellular matrix component that allows cell infiltration and remodeling, making it an attractive delivery system for protein growth factors [5, 6]. Biodegradable synthetic polymers, such as poly(lactic acid), and poly(glycolic acid), as well as their copolymers, poly(lactic coglycolic acid), are the most widely used delivery systems. In addition to being widely

available, they can be prepared with well-controlled, reproducible chemical and physical properties [2–4, 7]. They are also among the few synthetic biodegradable polymers approved by the Food and Drug Administration for *in vivo* use.

Inorganic (bioceramic) materials which have been utilized as carriers for protein delivery consist primarily of β-tricalcium phosphate or hydroxyapatite (HA).[1] These materials, composed of the same elements as bone, are biocompatible and produce no systemic toxicity or immunological reactions. The delivery systems typically consist of porous particles, granules, or substrates in which the protein is adsorbed or attached to the surfaces of the porous material, or encapsulated within the pores. [8–11] Hollow HA microspheres (diameter = 1500–2000 μm), consisting of a hollow core and a mesoporous shell, have been prepared by coating chitin microspheres with a composite layer of chitin and HA, followed by thermal decomposition of the chitin and sintering of the porous HA shell. [12]

Day and Conzone [13] invented a process for the preparation of porous phosphate materials with high surface area by converting borate glasses with special compositions in an aqueous phosphate solution near room temperature. [14, 15] This process is shown schematically in Fig. 1, using as an example the conversion of a $Li_2O–CaO–B_2O_3$ glass in the shape of a sphere to form HA. In the conversion process, Ca^{2+} and other ions are released as the glass dissolves, while $(PO_4)^{3-}$ and OH^- from the solution react with Ca^{2+} ions to form an amorphous calcium phosphate (ACP) layer on the glass surface. The glass core continues to dissolve as the ACP converts to HA, until finally a fully reacted shape, hollow or porous, composed of mesoporous HA, is formed. A characteristic

feature of the process is that it is pseudomorphic, so the HA product retains the same external shape and dimensions of the starting glass object.

Wang *et al*. [16] reacted solid glass microspheres (106–125 μm) with the composition (wt%) 4.7Li_2O, 13.2CaO, 82.1B_2O_3 in 0.25 M K_2HPO_4 solution for 5 days at 37°C and pH = 10.0–12.0. They found that the product consisted of hollow microspheres of a calcium phosphate material, which, on heating for 4 h at 600°C, converted to HA. Huang *et al*. [17] prepared hollow HA microspheres by reacting glass microspheres with the composition 10Li_2O, 10CaO, 80B_2O_3 (wt%) for 5 days (microsphere diameter = 106–125 μm) or 14 days (microsphere diameter = 500–800 μm) under similar conditions used by Wang *et al*. [16] They measured the surface area of the smaller HA microspheres (135 m^2/g) and the rupture strength of the larger HA microspheres (1.6 MPa), and studied the effect of heat treatment on the surface area and rupture strength. Heating the as-prepared HA microspheres for 8 h at 600°C and at 800°C resulted in a marked decrease in surface area and a sharp increase in strength.

The objective of this work was to comprehensively evaluate how the process parameters influence the microstructure of hollow HA microspheres prepared by reacting Li_2O–CaO–B_2O_3 glass microspheres in an aqueous phosphate solution. In contrast to previous studies that used only a single set of reaction conditions, [16, 17] we used a factorial design approach to evaluate the statistically significant process variables, which influenced the microstructure of the HA microspheres. The effect of the K_2HPO_4 concentration (0.02–0.25 M), temperature (25–60°C), and pH (9–12) of the solution on the diameter of the hollow core and surface area of the HA microspheres, as well as the average pore size of the microsphere wall was studied. Knowledge of the relationships

between the process parameters and the resulting microstructure is vital for the preparation of hollow HA microspheres with characteristics optimized for potential application as carriers for controlled protein delivery.

1.3 EXPERIMENTAL PROCEDURE

1.3.1 Preparation of Hollow HA Microspheres.

Borate glass, with the composition (wt%): 15CaO, 10.63Li_2O, 74.37 B_2O_3, designated CaLB3-15, was prepared by melting reagent grade $CaCO_3$, Li_2CO_3 and H_3BO_3 (Alfa Aesar, Haverhill, MA) in a Pt crucible at 1200ºC for 45 min, and quenching between cold stainless steel plates. This glass composition was used because it had been shown in previous work to produce hollow HA microspheres by the glass conversion process. [14] Particles of size 106–150 μm were obtained by grinding the glass in a hardened steel mortar and pestle, and sieving through 100 and 140 mesh sieves. Solid glass microspheres were obtained by dropping the crushed particles down a vertical tube furnace at 1000°C, as described in detail elsewhere. [14]

Hollow HA microspheres were prepared by reacting the glass microspheres with K_2HPO_4 solution for 2–7 days. In all the experiments, 1 g of glass microspheres was placed in 200 ml solution, and the system was gently stirred continuously. A range of temperature (25, 37, and 60°C), K_2HPO_4 concentration (0.02, 0.10, and 0.25 M), and pH (9 and 12) of the solution was used to study the effect of these process variables on the microstructure of the synthesized HA microspheres. Upon completion of the conversion process, the HA microspheres were washed three times with distilled water, soaked in

anhydrous ethanol to displace residual water, dried for at least 12 h at room temperature, then for at least 12 h at 90^{o}C, and stored in a desiccator before being characterized.

1.3.2 Factorial Design of Experiments.

An approach based on factorial design of experiments was used to evaluate the statistically significant process variables that influenced the microstructure of the hollow HA microspheres. The three process variables investigated were the temperature of the conversion reaction, the K_2HPO_4 concentration of the phosphate solution, and the pH value of the solution. Each of these variables was set at two levels, as shown in Table I. The factorial design required eight sets of experimental conditions, which were carried out in a random order given in Table II. The microstructural properties evaluated in the experiments were specific surface area (SSA), pore size, and the ratio of the hollow core diameter (*d*) to the external diameter (*D*) of the hollow HA microspheres. Analysis of the data to determine the statistically significant process variables that influenced these microstructural characteristics was performed using the software package Minitab 15.1 (Minitab Inc., State College, PA).

1.3.3 Characterization of Hollow HA Microspheres.

The phase composition of the as-prepared HA microspheres was checked using X-ray diffraction, XRD (D/mas 2550 v; Rigaku; The Woodlands, TX) and Fourier transform infrared (FTIR) spectroscopy (Model 1760-X; Perkin Elmer, Norwalk, CT). XRD was performed using Cu K_α radiation (λ = 0.15406 nm) at a scan rate of 1.8° /min in the 2θ range 20–70°. The HA microspheres were ground to a powder for the XRD and FTIR analyses. FTIR was performed in the wavenumber range of 400–4000 cm^{-1}

(resolution = 8 cm^{-1}). A mass of 2 mg of the powder was mixed with 198 mg KBr, and pressed to form pellets for the FTIR analysis.

The microstructure of the external surface and the cross section of the HA microspheres was observed using scanning electron microscopy (SEM) (S-4700; Hitachi, Tokyo, Japan), at an accelerating voltage of 10 kV and working distance of 12 mm. The diameter of the hollow core and the external diameter of the microspheres were determined from at least five measurements for each group of microspheres. Local composition of the external surface and across the wall of the microspheres was determined using energy dispersive X-ray (EDS) analysis in the SEM, with an electron beam spot size of 1 μm. X-ray mapping in the SEM was used to analyze the elemental distribution across the cross section of the HA microspheres.

The SSA of the hollow HA microspheres and the pore size distribution of the microsphere wall were measured using nitrogen adsorption (Autosorb-1; Quantachrome, Boynton Beach, FL). Before the measurement, a known mass of HA microspheres (in the range 300–500 mg) was weighed, and evacuated for 15 h at 120°C to remove adsorbed moisture. The volume of nitrogen adsorbed and desorbed at different relative gas pressures was measured and used to construct adsorption–desorption isotherms. The first five points of the adsorption isotherm, which initially followed a linear trend implying monolayer formation of adsorbate, were fitted to the Brunauer–Emmett–Teller equation for the determination of the SSA. [18] The pore size distribution was calculated using the Barrett–Joiner–Halenda method applied to the desorption isotherms. [19] The surface area and average pore size were determined from two measurements for each group of microspheres.

1.4 RESULTS

1.4.1 Geometry and Composition of Converted Microspheres.

Figure 2 shows SEM images of CaLB3-15 glass microspheres (Fig. 2a), and the surface of a converted microsphere formed by reacting the glass microspheres for 2 days in 0.02 M K_2HPO_4 solution at 37°C and pH = 9.0 (Fig. 2(b) and (c)). The converted microspheres had a porous, nanostructured surface with a plate-like particle morphology (Fig. 2(c)). Measurement of the microsphere diameter from SEM images showed no significant difference between the average diameter of the starting glass microspheres and that of the converted microspheres, confirming that the conversion reaction was pseudomorphic. [14–16]

XRD patterns of the starting glass microspheres and the converted microspheres formed by reacting the glass microspheres for 2 days in 0.25M K_2HPO_4 solution at 37°C and 60°C and pH = 9 and 12 are shown in Fig. 3. The starting CaLB3-15 glass had a diffraction pattern with no measurable peaks, typical of an amorphous glass. On the other hand, the patterns of the converted microspheres contained peaks that corresponded to those of a reference HA (JCPDS 72-1243), confirming the formation of the HA phase. The fairly broad width of the peaks in the XRD patterns may indicate that phases were poorly crystallized, or consisted of nanometer-sized crystals, or a combination of both.

Figure 4 shows FTIR spectra of the starting glass microspheres and the converted microspheres prepared under the conditions described above for the XRD analysis. The spectrum of the as-prepared glass was similar to that of a binary $Li_2O–3B_2O_3$ glass, [20, 21] consisting of two broad resonances, at 600–750 and 1200–1600 cm^{-1}, which corresponded to vibrations of the trigonal BO_3 groups in the borate glass. The resonance

centered at ~975 cm^{-1} corresponded to the vibration of tetrahedral BO_4 groups. The most dominant resonances for the converted microspheres were the phosphate v3 resonance, centered at ~1040 cm^{-1}, and the phosphate v4 resonance, with peaks at ~605 cm^{-1} and 560 cm^{-1}, which are associated with crystalline HA. [22, 23] These FTIR spectra provided further evidence that the converted microspheres consisted of HA. Additional resonances in the spectra of the conversion products included a weak shoulder at ~962 cm^{-1} corresponding to the phosphate v1 band, [24] and a resonance at ~878 cm^{-1} corresponding to the vibrations of CO_3^{2-} ions substituting for PO_4^{3-} ions in the HA lattice. [24]

The XRD and FTIR patterns of the converted microspheres formed under the remaining conditions summarized in Table II were generally similar to those described above, and they are omitted for the sake of brevity. Together, the XRD and FTIR analyses showed that the converted microspheres had a phase composition corresponding to that of HA.

A back-scattered SEM image of the polished cross section of a microsphere formed at 37°C in 0.02 M K_2HPO_4 solution with a pH = 9.0 is shown in Fig. 5a. The cross section was prepared by vacuum impregnation of the as-prepared microspheres with epoxy resin, followed by grinding and polishing. This image (as well as other similar images not shown) confirmed that the HA microspheres were hollow. X-ray maps of Ca(K) and P(K) across the section (Fig. 5(b) and (c)), showed that the microsphere wall was composed of Ca and P, which is consistent with the formation of HA as determined by XRD, FTIR spectroscopy, and EDS analysis.

Examination of the cross section at higher magnification in the SEM showed that the HA microsphere wall was not homogeneous in structure. Instead, it consisted of at least two distinct layers. An SEM image (Fig. 6(a)) of the cross section of a hollow microsphere prepared by reacting glass microspheres for 48 h in 0.02M K_2HPO_4 solution at 37°C and pH = 9.0 showed that the microsphere wall consisted of two layers. The denser surface layer (Fig. 6(b)) was 3–5μm thick, whereas the remainder of the microsphere wall consisted of a more porous microstructure (Fig. 6(c)). The factors responsible for this layered structure of the microsphere wall are not clear. Experiments are currently underway to provide a clearer understanding of the formation of this layered structure, and the results will be reported in a subsequent publication.

1.4.2 Statistical Significance of Process Variables.

As described earlier, a factorial design approach was used to identify the process variables (temperature, concentration, and pH), which had a statistically significant effect on the microstructural properties (d/D, surface area, and average pore size) of the hollow HA microspheres. The results are shown in the form of Pareto charts (Fig. 7), which provide a useful graphical tool for illustrating the magnitude and significance of an effect. The chart displays, in decreasing order, the absolute value of the standardized effect of the variables (X-axis), together with a reference line giving the level of significance, taken as $p = 0.05$ in this work. An effect that extends past this reference line is statistically significant. In the present analysis, two-way interactions between the process variables, as well as three-way interactions among the variables were also considered.

The most dominant factor influencing the surface area of the hollow HA microspheres was the concentration of the K_2HPO_4 solution (Fig. 7(a)). An interaction

between the reaction temperature and the concentration had a significant effect on the surface area. Surprisingly, temperature by itself did not have a significant effect on the surface area. The interaction among temperature, K_2HPO_4 concentration, and pH was not found to have a significant effect. Temperature and concentration each had a significant effect on the ratio (d/D) of the hollow core diameter to the microsphere diameter (Fig. 7(b)) and on the average pore size (Fig. 7(c)).

1.4.3 Relationships Between Process Variables and Microstructural Characteristics.

Contour plots were selected to show the main effects of the individual process variables and combinations of these variables on the microstructural characteristics of the hollow HA microspheres. The plots in Fig. 8 show the variations in the SSA, average pore size, and the *d*/*D* ratio with changes in two process variables, while holding the third variable constant. The constant values of the third variable were temperature = 37°C, K_2HPO_4 concentration = 0.25 M, and pH = 9, respectively. The results in these plots could be used to identify optimized solution conditions for preparing hollow HA microspheres with a given set of microstructural characteristics.

Inspection of the plots in Fig. 8(a) shows that high surface area (> 130–140 m^2/g) can be achieved by using higher K_2HPO_4 concentration (0.25M) or using a combination of higher concentration (0.25M) and higher temperature (60ºC). Figure 8(b) shows that the diameter of the hollow core (or the *d*/*D* ratio) increased with decreasing temperature or with decreasing K_2HPO_4 concentration. Increasing temperature produced a reduction in the pore size, whereas increasing K_2HPO_4 concentration produced an increase in the pore size (Fig. 8c). Larger pore sizes (>18 nm) are obtained for a combination of lower

temperature (37°C) and higher concentration (0.25M). A change in pH of the solution, between 9.0 and 12.0 had little effect on the microstructural characteristics.

1.4.4 Diameter of Hollow Core.

The diameter (*d*) of the hollow core of the HA microspheres, (or the *d*/*D* ratio) is of particular interest because it determines the amount of a substance that could be encapsulated within the hollow core of the microsphere. Based on the factorial design approach, two additional sets of experimental conditions were used (designated as Runs 9 and 10 in Table II) to provide further information on the dependence of *d*/*D* on the key process variables of temperature and K_2HPO_4 concentration of the solution.

SEM images (Fig. 9) of cross sections of hollow HA microspheres prepared at different temperatures (pH = 9; K_2HPO_4 concentration = 0.25) and different K_2HPO_4 concentrations (pH = 9; temperature = 37°C) show a marked change in the diameter, *d*, of the hollow core (or the *d*/*D* ratio). The microspheres in Fig. 9 were broken deliberately to show the cross sections. Increasing the temperature from 25°C to 60°C almost resulted in the disappearance of the hollow core (Fig. 9(a)). The diameter of the hollow core also decreased markedly with an increase in the concentration of the K_2HPO_4 solution. Based on measurements from at least five spheres in each group, the results showed that *d*/*D* decreased from 0.62 ± 0.08 at 25°C to 0.19 ± 0.11 at 60°C (Fig. 10(a)), while it decreased from 0.61 ± 0.03 for a K_2HPO_4 concentration of 0.02M to 0.36 ± 0.02 for a concentration of 0.25M (Fig. 10(b)).

1.5. DISCUSSION

The present investigation showed that solid microspheres of a $Li_2O–CaO–B_2O_3$ glass, designated CaLB3-15, can be reproducibly converted to hollow HA microspheres when reacted in an aqueous phosphate solution. Furthermore, by varying the temperature, concentration, and pH of the K_2HPO_4 solution, hollow microspheres with controlled microstructural characteristics (diameter of hollow core, surface area, and pore size) can be prepared. The conversion reaction is pseudomorphic, so not only the microstructural characteristics but also the external diameter of the hollow HA microspheres can be controlled.

The ability to control the geometry and microstructure of these hollow HA microspheres is critical for evaluating the potential of the microspheres for their intended application as delivery devices for proteins, such as drugs or growth factors, in tissue repair and regeneration. Key microstructural characteristics for this application are the ratio of the diameter of the hollow core relative to the external diameter of the hollow HA microspheres, *d/D*, the SSA of the microspheres, and the average pore size of the microsphere wall. A larger *d/D* value means that a larger amount of protein can be encapsulated within the hollow core, whereas a larger surface area indicates better ability for a protein to be adsorbed to the surfaces of the microsphere wall. The average pore size controls the permeability of the HA microsphere wall, and therefore the ability of a protein to migrate through the microsphere wall, during incorporation of the protein into the hollow core, or release of the protein from the hollow core into a surrounding medium.

Previous investigations studied the ability to prepare hollow HA microspheres by the glass conversion method using a selected set of temperature, solution concentration, and pH conditions. [16, 17] In contrast, the factorial design approach used in this work allowed an investigation of the statistically significant process variables which influenced the microstructural characteristics of the hollow HA microspheres. By varying the temperature (25–60°C), K_2HPO_4 concentration (0.02–0.25M), and pH (9–12) of the solution over practically useful ranges, we were able to determine the key individual variables, as well as combinations of these individual variables, which had a significant influence on the microstructure.

The temperature and K_2HPO_4 concentration of the solution had the most dominant effect on the three microstructural properties (*d*/*D*, surface area, and pore size) of the HA microspheres investigated in this work (Figs. 7 and 8). The basic pH values (9 and 12) of the phosphate solution used in this work, while favorable for the formation of HA, [25] had little effect on the microstructure (Fig. 7 and 8).

The achievement of high surface area is promoted by higher K_2HPO_4 concentration of the solution. Interestingly, higher temperature leads to high surface area only when the solution concentration is high (Fig. 7(a)). The highest surface area (145 ± 5 m^2/g) was obtained for a temperature of 60°C and a concentration of 0.25M. Apparently, a high concentration of phosphate ions is required for the rapid formation of fine nuclei at the reaction interface, whereas a rapid reaction rate (higher temperature) is beneficial for the formation of fine HA particles (high SSA).

Lower temperature or lower K_2HPO_4 concentration is beneficial for the formation of hollow cores with larger *d*/*D* (equal to ~0.6) (Figs. 8 and 9). In the conversion reaction

(Fig. 1), if it is assumed that all the CaO in the glass reacts with the phosphate ions in the solution to form HA, then the amount of HA formed is ~27 wt% of the starting glass, regardless of the conditions used. The occurrence of the largest *d/D* at low concentration (0.02M) or low temperature (25°C) indicates that under these conditions, the fine HA particles in the microsphere wall are more efficiently packed. Presumably the low temperature or low solution concentration lead to slower growth of the HA nuclei, allowing the smaller HA crystals to achieve a more efficient packing in the microsphere wall. A large *d*/*D* value may result in high strength of the HA microspheres, which is an important property for the application of these microspheres. A detailed study of the rupture strength of the microspheres is currently underway.

The average pore size of the microsphere wall varied by a factor of ~2, from ~10 to ~20 nm, for the temperature, K_2HPO_4 concentration, and pH conditions used in this work, with the smallest pore size obtained for lower concentration (0.02M) and for higher temperature (60°C) (Table II). The pore size, as outlined earlier, controls the ability of a molecule to migrate through the microsphere wall. Based on hydrodynamic experiments, bovine serum albumin (BSA), one of the most widely studied proteins, is reported to take up the shape of an oblate ellipsoid with dimensions of 14 and 4 nm along the long and short-axis, respectively. [26] Some groups of HA microspheres prepared in this work, with the larger pore sizes (15–20 nm), could potentially serve as delivery devices for BSA, as well as other proteins with dimensions approximately equal to, or smaller than, the length of the BSA long-axis. Our current work shows that the pore size can be enlarged by a thermal treatment at temperatures up to ~600°C, which could serve as a

further method for controlling the pore size and, therefore, the release rate of a protein from the microspheres.

In these experiments, the reaction time was chosen to ensure complete conversion of the starting glass microspheres to HA. The reaction time was 2 days, except for experiments involving the lowest K_2HPO_4 concentration (0.02M) or the lowest temperature (25°C), when the reaction time was 7 days (Table II). For the same conditions (temperature, concentration, and pH), varying the reaction time could result in changes to the microstructure. However, a thermal treatment of the as-prepared HA microspheres, as outlined above, may provide a more efficient method for modifying the microstructure.

1.6 CONCLUSIONS

Solid microspheres (106–150 μm in diameter) of a Li_2O–CaO–B_2O_3 glass were completely converted within 2–7 days in an aqueous phosphate solution to hollow HA microspheres with a mesoporous wall. The conversion reaction was pseudomorphic, with the hollow HA microspheres retaining the external shape and diameter of the starting glass microspheres. A factorial design approach, used for designing the conversion experiments, allowed a determination of the statistically significant process variables, which influenced the microstructure of the HA microspheres. Although the pH had little effect, the K_2HPO_4 concentration of the solution had a marked effect on the diameter of the hollow core, surface area, and pore size, whereas temperature markedly influenced the hollow core diameter and pore size, but not the surface area. The surface area increased with the K_2HPO_4 concentration, reaching ~140 m^2/g at 0.25M. The hollow core

diameter increased with decreasing temperature or with decreasing K_2HPO_4 concentration, reaching a value of ~0.6 times the microsphere diameter at 25°C or 0.02M. The largest pore sizes (~20 nm) were obtained at higher concentration or lower temperature. These hollow HA microspheres could provide potential biocompatible inorganic systems for local delivery of proteins, such as drugs and growth factors in tissue repair and regeneration.

1.7 ACKNOWLEDGEMENT: The authors would like to thank Y. He, MO-SCI Corp., for assistance with surface area and pore size measurements.

1.8 REFERENCES

1. S. K. Mallapragada and B. Narasimhan, “Drug Delivery Systems”; pp. 425–37 in Handbook of Biomaterials Evaluation, 2nd edition, Edited by A. F. von Recum. Taylor & Francis, Philadelphia, PA, 1999.
2. V. R. Sinha and A. Trehan, “Biodegradable Microspheres for Protein Delivery,” J. Control Release, 90, 261–80 (2003).
3. Y. Tabata, “Tissue Regeneration Based on Growth Factor Release,” Tissue Eng., 9 [Suppl 1] S5–S15 (2003).
4. R. R. Chen and D. J. Mooney, “Polymeric Growth Factor Delivery Strategies for Tissue Engineering,” Pharm. Res., 20, 1103–12 (2003).
5. S. Ma, G. Chen, and A.H. Reddi, “Collaboration Between Collageneous Matrix and Osteogenin is Required for Bone Induction,” Ann. NY Acad. Sc.i, 580, 525–5 (1990).
6. J. M. McPherson, “The Utility of Collagen-based Vehicles in Delivery of Growth Factors for Hard and Soft Tissue Wound Repair,” Clin. Mater., 9, 225–34 (1992).
7. R. L. Cleek, K. C. Ting, S. G. Eskin, and A. G. Mikos, “Microparticles of Poly(DL-Lactic-Co-Glycolic Acid)/Poly(Ethylene Glycol) Blends for Controlled Drug Delivery,” J. Control Release, 48, 259–68 (1997).
8. I. Ono, T. Ohura, M. Murata, H. Yamaguchi, Y. Ohnuma, and Y. Kuboki, “A Study on Bone Induction in Hydroxyapatite Combined with Bone Morphogenetic Protein,” Plast. Reconstr. Surg., 90, 870–9 (1992).

9. U. Ripamonti, S. Ma, B. Van den Heever, and A. H. Reddi. “Osteogenin, a Bone Morphogenetic Protein, Adsorbed on Porous Hydroxyapatite Substrata, Induces Rapid Bones Differentiation in Calvarial Defects of Adult Primates,” Plast. Reconstr. Surg., 90, 382–93 (1992).
10. U. Ripamonti, “Osteoinduction in Porous Hydroxyapatite Implanted in Heterotopic Sites of Different Animal Models,” Biomaterials, 17, 31–5 (1996).
11. T. Matsumoto, M. Okazaki, M. Inoue, S. Yamaguchi, T. Kusunose, T. Toyonaga, Y. Hamada, and J. Takahashi, “Hydroxyapatite Particles as a Controlled Release Carrier of Protein,” Biomaterials, 25, 3807–12 (2004).
12. Q. Peng, L. Ming, C. X. Jiang, B. Feng, S. X. Qu, and J. Weng, “Preparation and Characterization of Hydroxyapatite Microspheres with Hollow Core and Mesoporous Shell,” Key Eng. Mater., 309–311, 65–8 (2006).
13. D. E. Day and S. A. Conzone, “Method for Preparing Porous Shells or Gels from Glass Particles,” US Patent No. 6,358,531, March 19, 2002.
14. D. E. Day, J. E. White, R. F. Bown, and K. D. McMenamin, “ Transformation of Borate Glasses into Biologically Useful Materials,” Glass Technol., 44, 75–8 (2003).
15. S. D. Conzone, and D. E. Day, “Preparation and Properties of Porous Microspheres Made from Borate Glass,” J. Biomed. Mater. Res. Part A, 88A, 531–542 (2009).
16. Q. Wang, W. Huang, D. Wang, B. W. Darvell, D. E. Day, and M. N. Rahaman, “Preparation of Hollow Hydroxyapatite Microspheres,” J. Mater. Sci.: Mater. Med., 17, 641–6 (2006).

17. W. Huang, M. N. Rahaman, D. E. Day, and B. A. Miller, “Strength of Hollow Microspheres Prepared by a Glass Conversion Process,” J. Mater. Sci.: Mater. Med., 20, 123–9 (2009).
18. N. J. Coleman and L. L. Hench, “A Gel-Derived Mesoporous Silica Reference Materials for Surface Analysis by Gas Sorption, Part1 – Textural Features,” Ceram. Int., 26, 171–8 (2000).
19. E. P. Barrett, L. G. Joyney, and P. P. Halenda, “The Determination of Pore Volume and Area Distributions in Porous Substances I: Computations from Nitrogen Isotherms,” J. Am. Chem. Soc., 73, 373–80 (1951).
20. A. H. Verhoef and H. W. DenHartog, “Infrared Spectroscopy of Network and Cation Dynamics in Binary and Mixed Alkali Borate Glasses,” J. Non-Crystalline Solids, 182, 221–34 (1995).
21. A. H. Verhoef and H. W. DenHartog, “Structure and Dynamics of Alkali Borate Glasses: A Molecular Dynamics Study,” J. Non-Cryst. Solids, 182, 235–47 (1995).
22. A. E. Clark and L. L. Hench, “Early Stages of Calcium-Phosphate Layer Formation in Bioglass,” J. Non-Cryst. Solids, 113, 195–202 (1989).
23. M. R. Filgueiras, G. LaTorre, and L. L. Hench, “Solution Effects on the Surface Reaction of a Bioactive Glass,” J. Biomed. Mater. Res., 27, 445–53 (1993).
24. I. Rehman, and W. Bonfield, “Characterization of Hydroxyapatite and Carbonated Apatite by Photo Acoustic FTIR Spectroscopy,” J. Mater. Sci.: Mater. Med., 8, 1–4 (1997).

25. G. H. Nancollas and J. Zhang, “Formation and Dissolution Mechanisms of Calcium Phosphates in Aqueous Systems”; PP. 473–81 in Hydroxyapatite and Related Materials, Edited by P. W. Brown and B. Constantz. CRC Press, Boca Raton, FL, 1994.

26. T. Peters, “Serum Albumin,” Adv. Protein Chem., 37, 161–245 (1985).

Table I. Control factors used in the statistical design of the experiments

Code	Control factor	Experimental level 1	Experimental level 2
T	Temperature	37^{o}C	60^{o}C
C	Concentration	0.02M	0.25M
P	pH value	9	12

Table II. Experimental design with three factors (temperature, K_2HPO_4 concentration, and pH of the Solution) varied at two levels

Run	Temperature (^oC)	Concentration (M)	pH value	Surface area (m^2/g)	Pore size (nm)	d/D	Reaction time (d)
1	60	0.25	9	145 ± 5	13 ± 2	0.19 ± 0.11	2
2	60	0.02	9	82 ± 5	10 ± 2	0.34 ± 0.03	7
3	37	0.02	12	89 ± 5	12 ± 2	0.55 ± 0.02	7
4	37	0.25	12	123 ± 5	17 ± 2	0.34 ± 0.03	2
5	37	0.02	9	101 ± 5	15 ± 2	0.61 ± 0.03	2
6	37	0.25	9	127 ± 5	19 ± 2	0.36 ± 0.02	2
7	60	0.25	12	140 ± 5	12 ± 2	0.14 ± 0.07	2
8	60	0.02	12	78 ± 5	8 ± 2	0.37 ± 0.09	7
9	37	0.10	9	108 ± 5	17 ± 2	0.54 ± 0.03	2
10	25	0.25	9	101 ± 5	20 ± 2	0.62 ± 0.08	7

The measured properties of the hollow hydroxyapatite microspheres (ratio of hollow core diameter to microsphere diameter [*d*/*D*] specific surface area, and average pore size) prepared under each condition for the reaction time used are also shown.

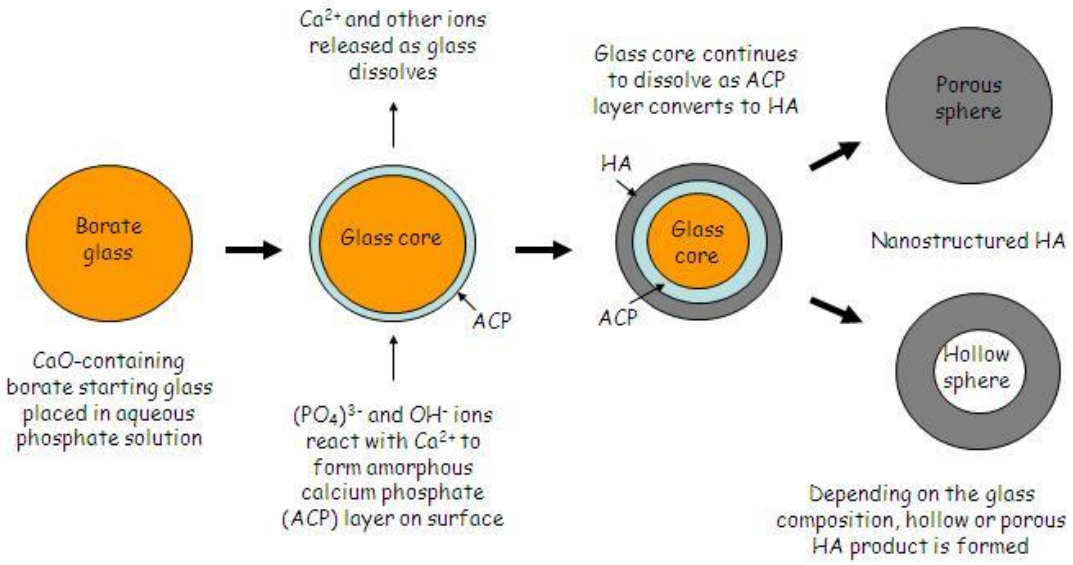

Figure 1. Schematic diagram illustrating steps in the reaction process for converting calcium-borate glass microsphere to hollow or porous hydroxyapatite (HA) microsphere in an aqueous phosphate solution.

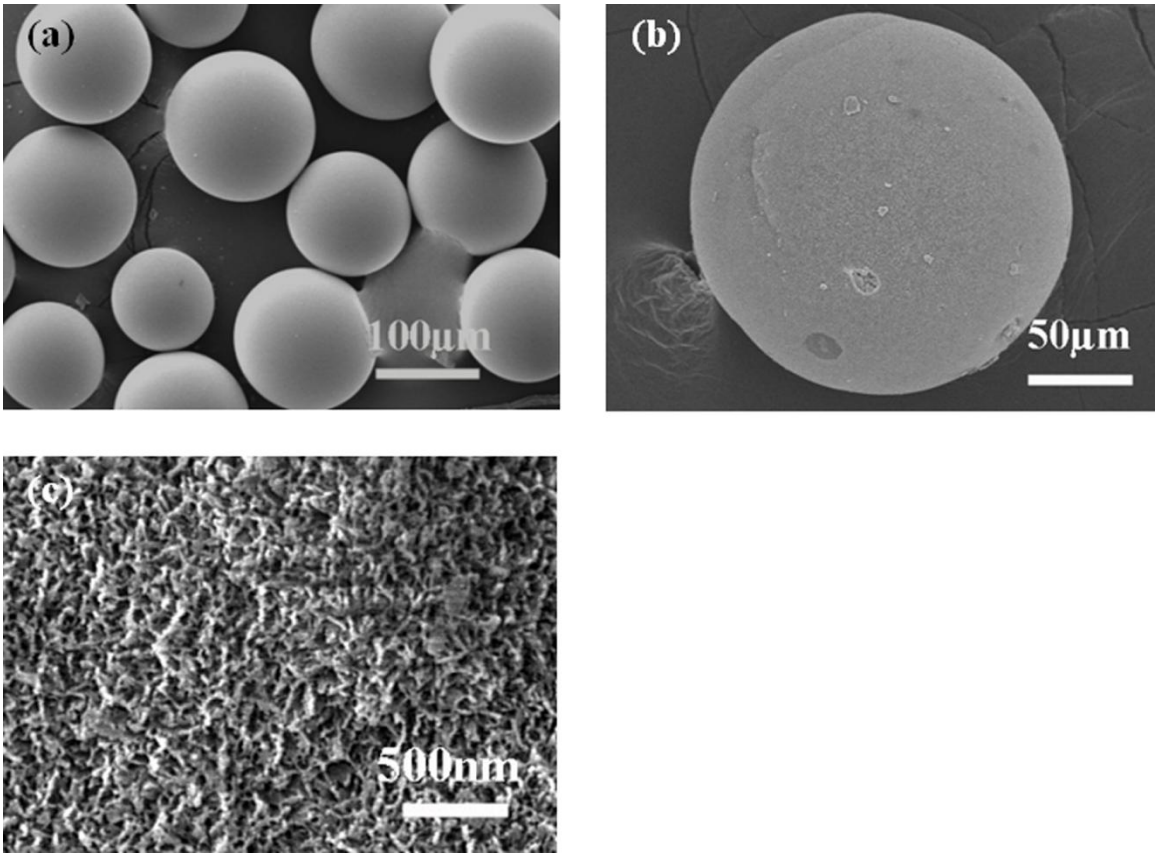

Figure 2. Scanning election microscopy images of (a) starting glass (CaLB3-15) microspheres, (b) external surface of hollow hydroxyapatite (HA) microsphere formed by conversion of glass microspheres in 0.02M K_2HPO_4 solution at 37°C and pH = 9 for 48 hours, and (c) external surface of hollow HA microsphere at high magnification.

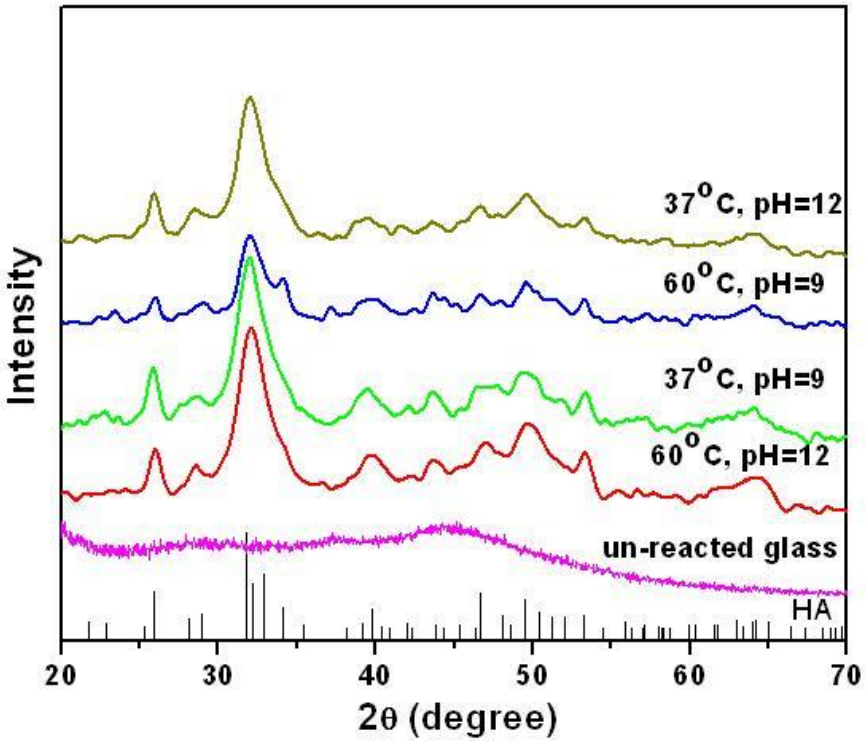

Figure 3. X-ray diffraction of the starting glass microspheres (unreacted glass) and the microspheres formed by reacting the glass microspheres in 0.25 M K_2HPO_4 solution under the conditions shown for 48 h. The pattern of a reference hydroxyapatite (HA) (JCPDS 72-1243) is also shown.

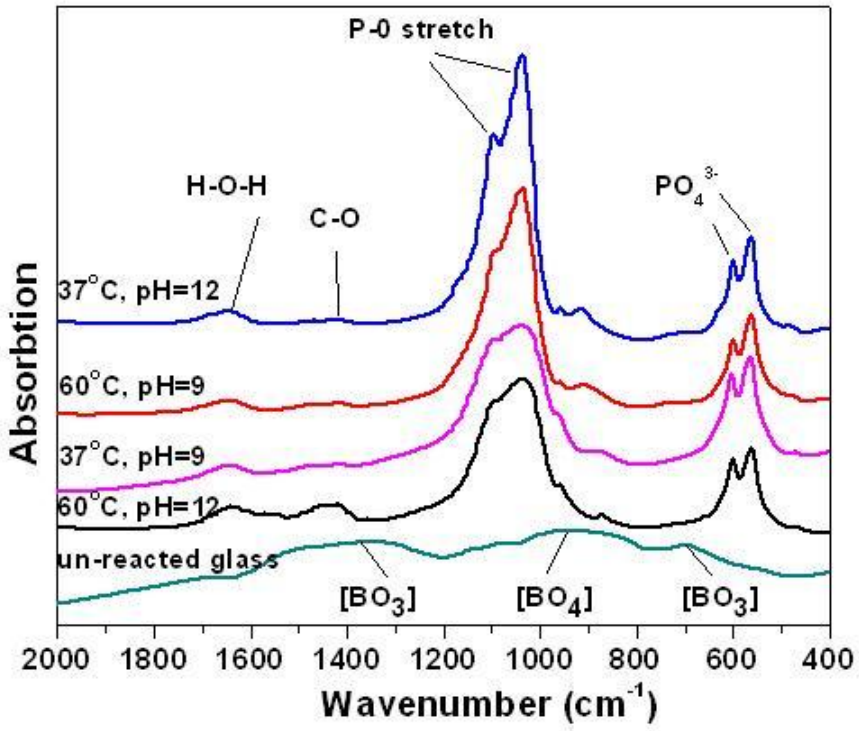

Figure 4. Fourier transform infrared of the starting glass microspheres (unreacted glass) and the hollow microspheres formed by reacting the glass microspheres in 0.25 M K_2HPO_4 solution under the conditions shown for 48 h.

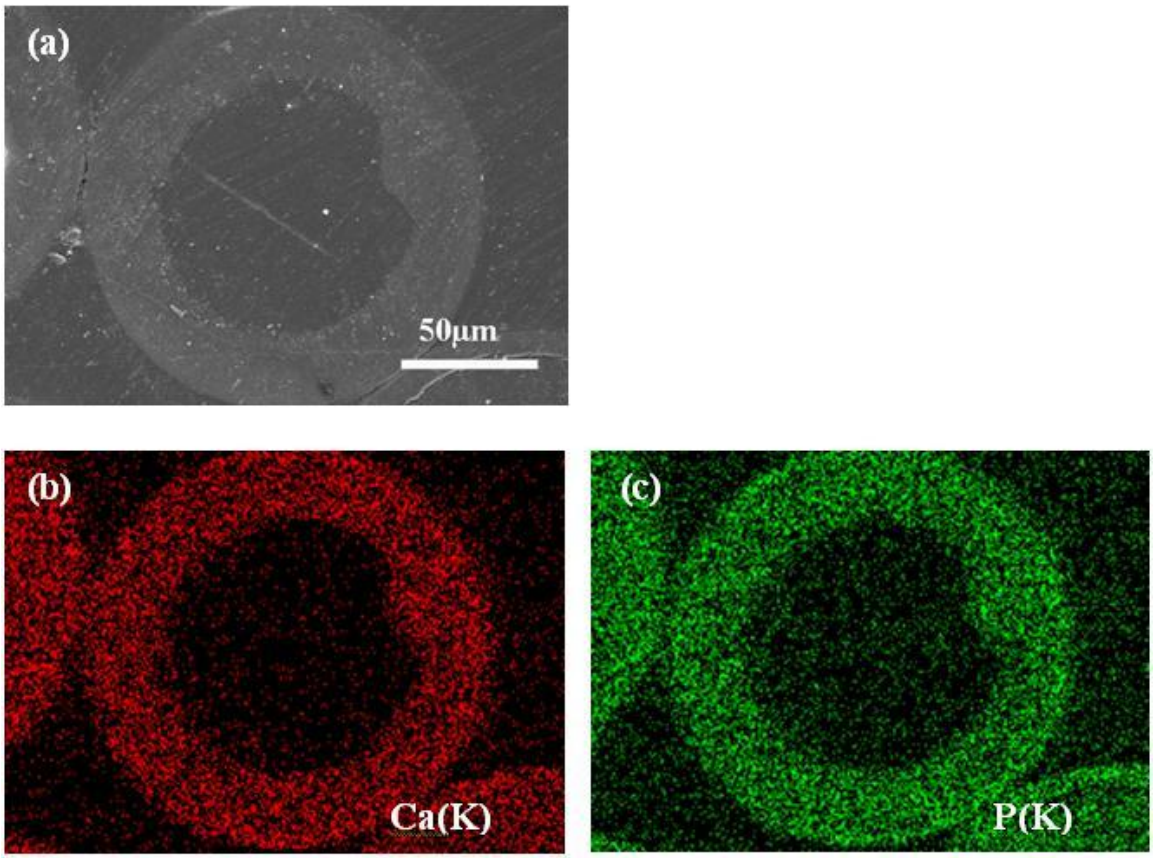

Figure 5. (a) Scanning electron microscopy image in back-scattered mode of a polished cross section of a hollow hydroxyapatite microsphere formed by reacting glass microspheres in 0.02M K_2HPO_4 solution at 37°C and pH = 9 for 48 h; (b) and (c) X-ray maps of Ca(K) and P(K) across the planar section shown in (a).

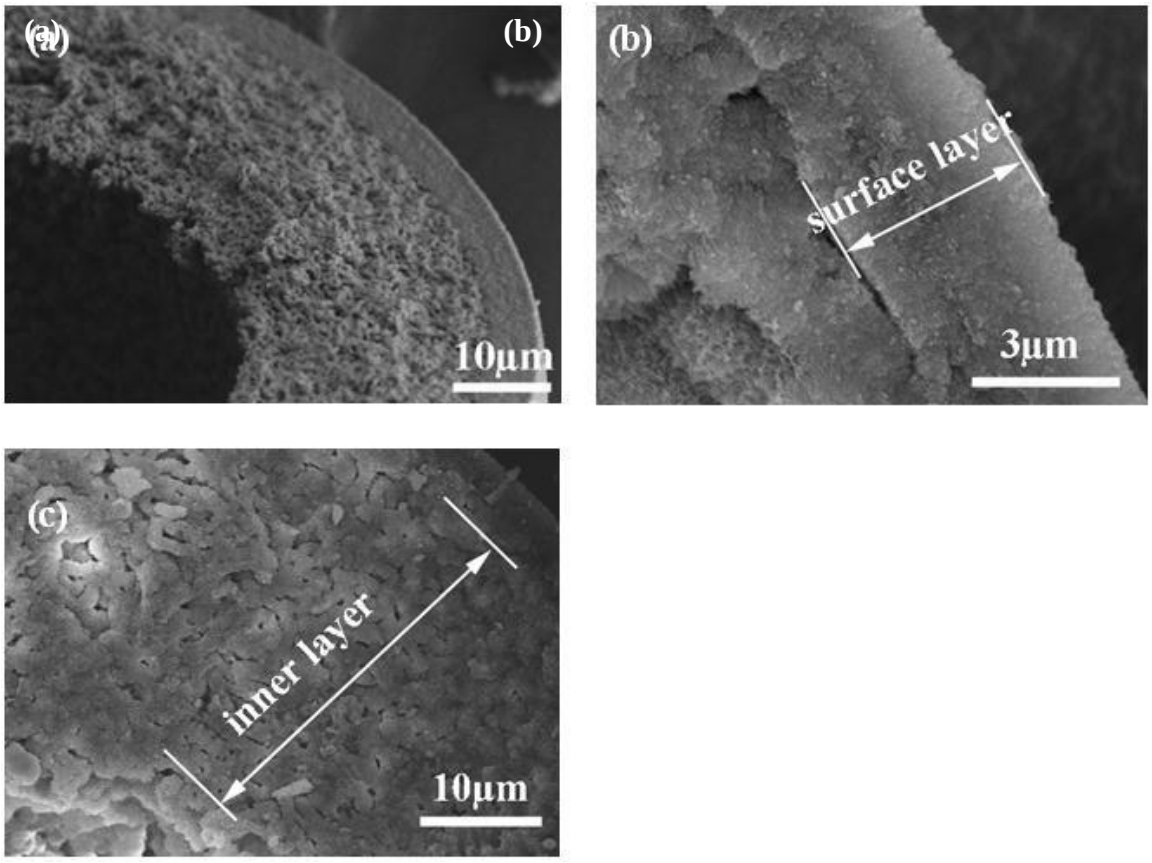

Figure 6. Sanning electron microscopy images of the fractured cross section of a hollow hydroxyapatite microsphere formed by reacting glass microspheres in 0.02M K_2HPO_4 solution at 37°C and pH = 9 for 48 h: (a) concentric bilayered structure, (b) denser surface layer, and (c) more porous inner layer.

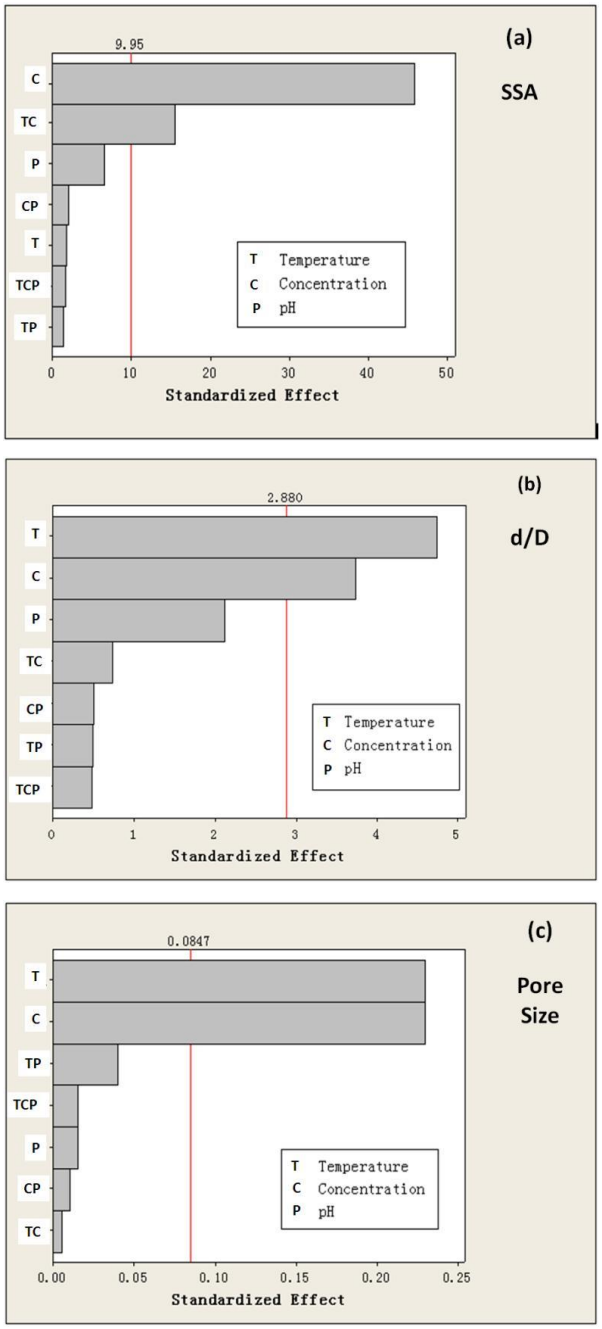

Figure 7. Pareto charts showing the standardized effect for the process variables and their significance on (a) the specific surface area (SSA), (b) ratio of hollow core diameter to the microsphere diameter (*d*/*D*), and (c) pore size of the microsphere wall.
T, temperature; C, concentration of K_2HPO_4; P, pH value.

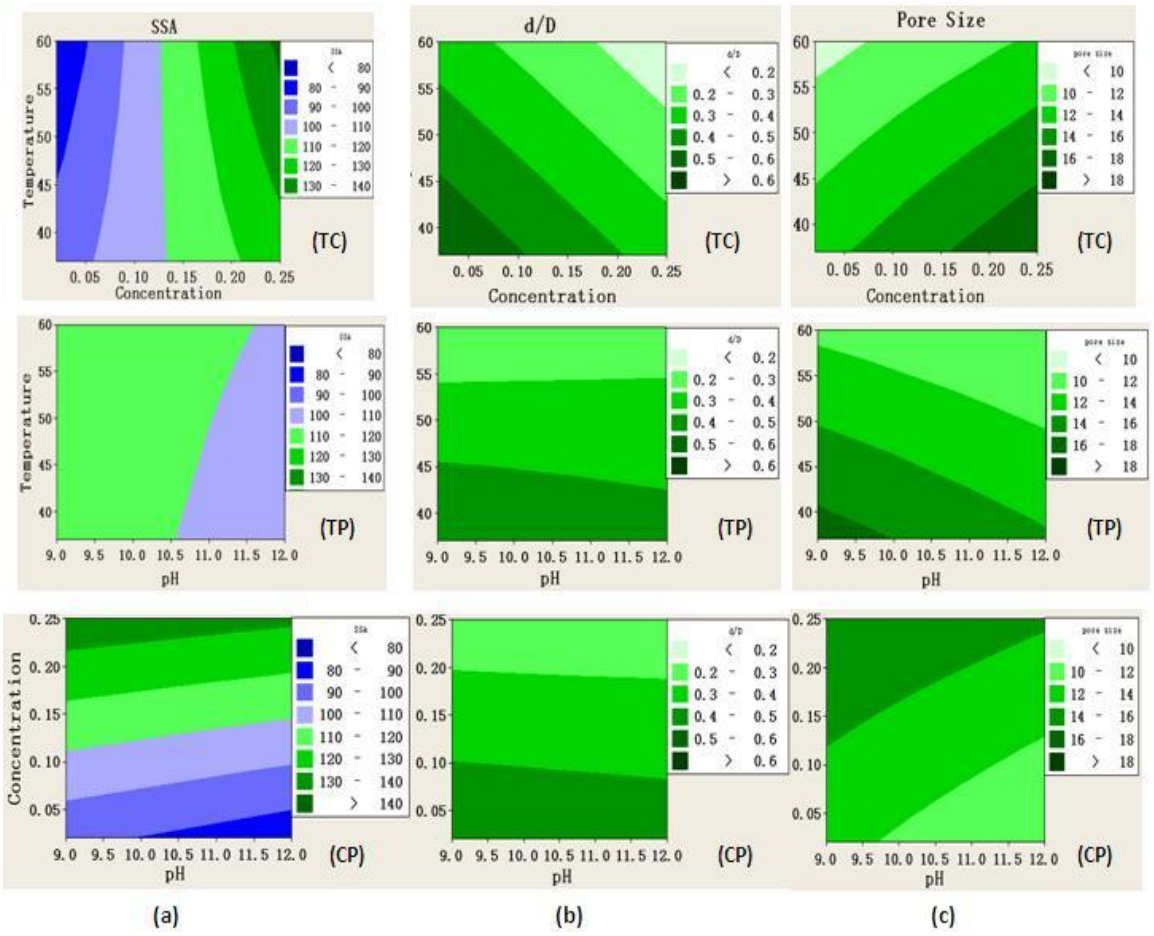

Figure 8. Contour plots showing the effect of the process variables on the microstructural characteristics: (a) specific surface area (SSA), (b) ratio of hollow core diameter to the microsphere diameter (*d*/*D*), and (c) pore size of the microsphere wall.
T, temperature (ºC); C, concentration of K_2HPO_4 (M), and P, pH value.

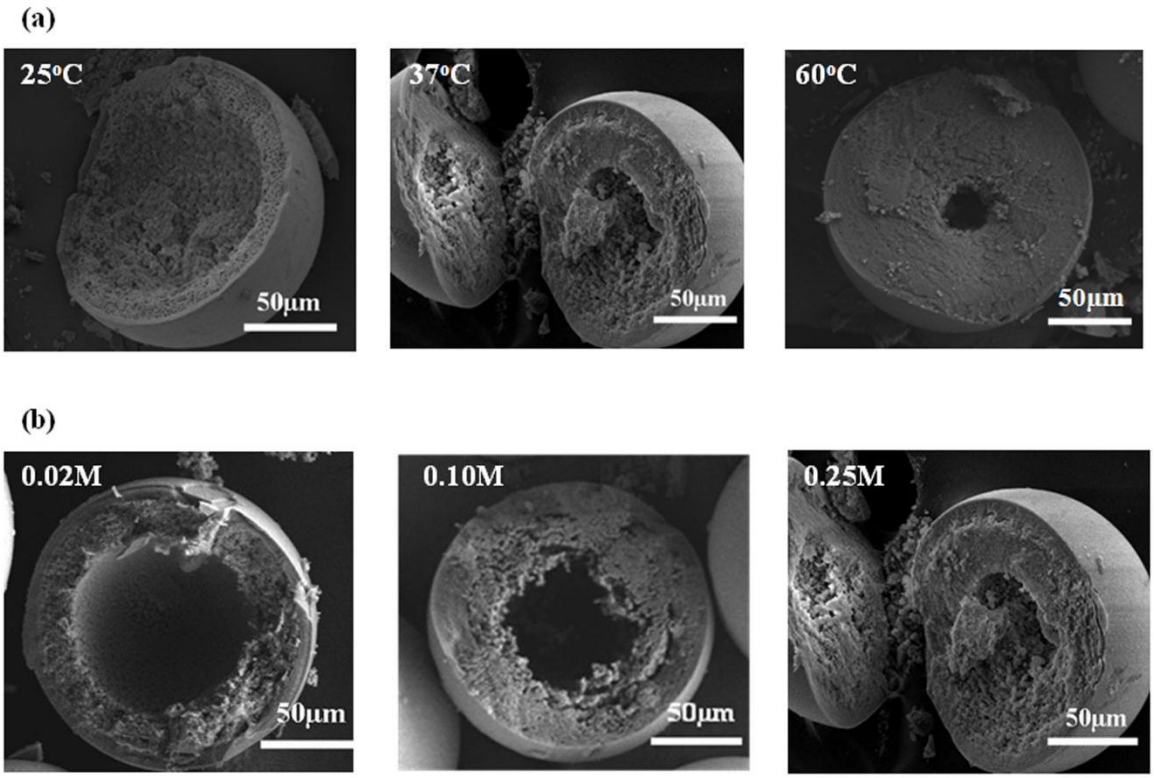

Figure 9. Scanning electron microscopy images of the fractured cross sections of hollow hydroxyapatite microspheres, showing (a) the effect of temperature on the hollow core size for microspheres prepared under constant conditions of pH (9.0) and K_2HPO_4 concentration (0.25 M), and (b) the effect of K_2HPO_4 concentration on the hollow core size for microspheres prepared at constant conditions of pH (9.0) and temperature (37°C).

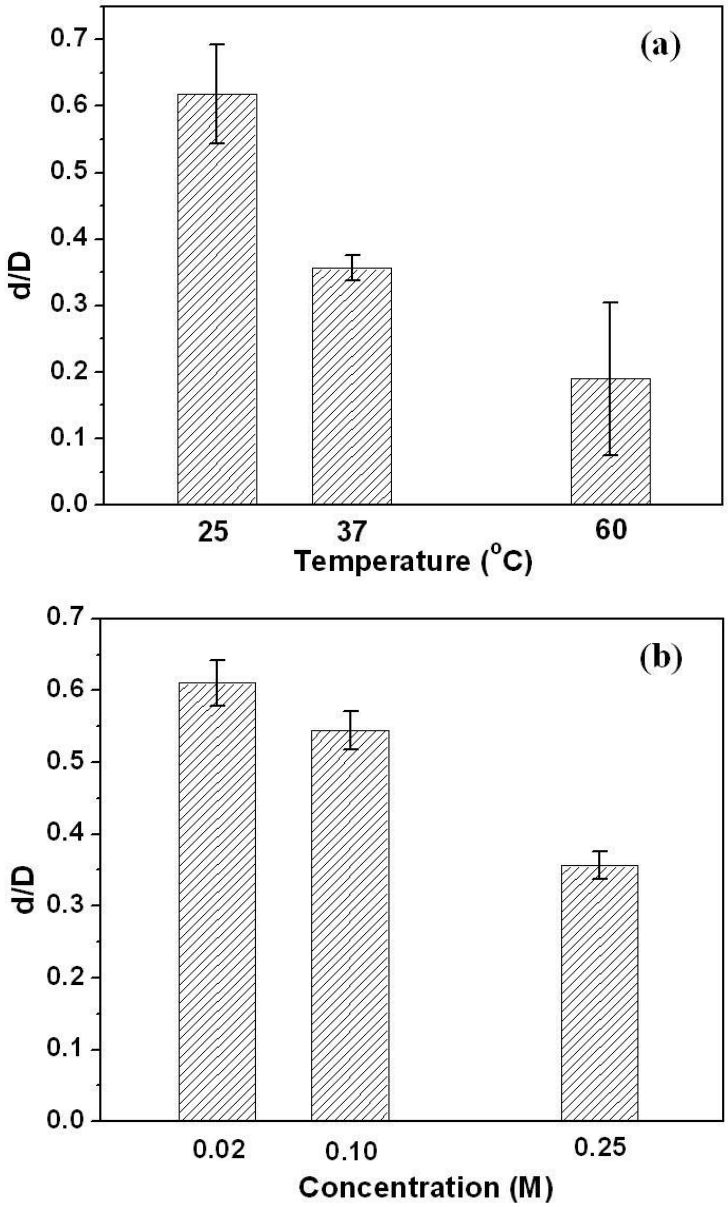

Figure 10. The relationship between the measured values of *d*/*D* and (a) temperature, and (b) K_2HPO_4 concentration of the solution, where *d*/*D* is the ratio of the hollow core diameter to the microsphere diameter.

2. EFFECT OF PYROPHOSPHATE IONS ON THE CONVERSION OF CALCIUM-LITHIUM-BORATE GLASS TO HYDROXYAPATITE IN AQUEOUS PHOSPHATE SOLUTION

Hailuo Fu[1], Mohamed N. Rahaman[1], Delbert E. Day[1], Wenhai Huang[2]

[1]Department of Materials Science and Engineering, and Center for Bone and Tissue Repair and Regeneration, Missouri University of Science and Technology, Rolla, MO 65409, USA

[2]Institute of Bioengineering and Information Technology Materials, Tongji University, Shanghai 200092, China

2.1 ABSTRACT

The conversion of glass to a hydroxyapatite (HA) material in an aqueous phosphate solution is used as an indication of the bioactive potential of the glass, as well as a low temperature route for preparing biologically useful materials. In this work, the effect of varying concentrations of pyrophosphate ions in the phosphate solution on the conversion of a calcium−lithium−borate glass to HA was investigated. Particles of the glass (150–355 μm) were immersed for up to 28 days in 0.25 M K_2HPO_4 solution containing 0–0.1 M $K_4P_2O_7$. The kinetics of degradation of glass particles and their conversion to HA were monitored by measuring the weight loss of the particles and the ionic concentration of the solution. The structure and composition of the conversion products were analyzed using X-ray diffraction, scanning electron microscopy, and Fourier transform infrared spectroscopy. For $K_4P_2O_7$ concentrations of up to 0.01 M, the glass particles converted to HA, but the time for complete conversion increased from 2 days (no $K_4P_2O_7$) to 10 days (0.01 M $K_4P_2O_7$). When the $K_4P_2O_7$ concentration was

increased to 0.1 M, the product consisted of an amorphous calcium phosphate material, which eventually crystallized to a pyrophosphate product (predominantly $K_2CaP_2O_7$ and $Ca_2P_2O_7$). The consequences of the results for the formation of HA materials and devices by the glass conversion route are discussed.

2.2 INTRODUCTION

Bioactive glasses have attractive properties for biomedical applications [1−3]. When placed in an aqueous phosphate solution, such as the body fluid, bioactive glasses undergo specific surface reactions, leading to the formation of a hydroxyapatite (HA)-type surface layer that is responsible for developing a firm bond with hard and soft tissues.[4−6] The conversion of a bioactive glass (or glass−ceramic) to HA *in vitro*, when immersed in an aqueous phosphate solution such as a simulated body fluid (SBF), provides a measure of its bioactive potential *in vivo* [7]. Therefore, it is important to understand the factors that influence the conversion of bioactive glass to HA *in vitro*.

The conversion of bioactive glass to HA in an aqueous phosphate solution is also of interest because the method can be used as a low temperature route for the formation of biologically useful materials, such as hollow or porous HA microspheres [8−11]. CaO-containing alkali-borate glass with special compositions in the system $Li_2O−CaO−B_2O_3$ or $Na_2O−CaO−B_2O_3$ have been observed to convert rapidly to HA when placed in an aqueous phosphate solution near room temperature, such as the body temperature, 37ºC [8, 12]. Porous or hollow HA microspheres prepared by this route have a mesoporous structure of nanosized particles and high surface area (100–200 m^2/g). As such, the glass conversion method provides a novel route for the production of biologically active HA

materials and devices for biomedical applications which cannot be obtained by other known methods.

The conversion of silicate and borate bioactive glass to HA in an aqueous phosphate solution has been the subject of several studies [1, 13–16]. It is well established that an initial step in the conversion of silicate bioactive glass (such as 45S5 and 13-93 glass) to HA is the formation of a SiO_2-rich gel layer on the glass surface by ion exchange reactions. Dissolution of Ca^{2+} ions from the glass, their diffusion through the SiO_2-rich layer, and reaction with $(PO_4)^{3-}$ ions from the solution, leads to the precipitation of an amorphous calcium phosphate (ACP) layer on the SiO_2-rich layer, which subsequently converts to HA. The reaction interface moves inward with time. Because of their lower chemical durability, some borate glasses convert faster and more completely to HA than silicate 45S5 or 13-93 glass. The mechanism of converting borate bioactive glass to HA is similar to that for silicate bioactive glass, but without the formation of a SiO_2-rich layer [14, 15].

In addition to factors such as glass composition, reaction temperature, and concentration of the aqueous phosphate solution, the conversion of silicate bioactive glass (13-93) to HA has also been shown to depend on the presence of polyanions in the aqueous phosphate solution [17]. In particular, the conversion rate of 13-93 glass in 0.25 M K_2HPO_4 solution was found to increase linearly with alginic acid concentration in the range 0−1 wt% alginic acid (based on the dry mass of the glass). At a given alginic acid concentration, the conversion rate increased almost 6 times when compared to that for the reaction without alginic acid. The acceleration of the conversion rate was explained in

terms of chelation of the electron donating moieties of alginic acid, such as carboxyls and hydroxyls, to the leached Ca^{2+} from the glass.

Inorganic phosphates such as dipotassium phosphate, K_2HPO_4, used for preparing the aqueous phosphate solution in the glass conversion process often contain varying concentrations of other phosphates resulting from incomplete purification. In particular, tetrapotassium pyrophosphate, $K_4P_2O_7$, is a common 'impurity' in commercial K_2HPO_4. Although the specific charge (charge per unit anion group) of the $(P_2O_7)^{4-}$ anion is the same as that for the $(HPO_4)^{2-}$ anion, the higher molecular weight could result in preferential adsorption at the reaction interface. This could result in a modification of the rate of formation of HA by the glass conversion method, or in the formation of new phases based on calcium pyrophosphate.

The objective of this work was to study the effect of varying concentrations of $K_4P_2O_7$ on the conversion of calcium−lithium−borate glass particles to HA in K_2HPO_4 solution (0.25 M). The kinetics of conversion were monitored by measuring the weight loss of the glass particles and the concentration of ions dissolved from the glass into the aqueous phosphate solution. The structure and composition of the solid conversion products were analyzed using X-ray diffraction (XRD), Fourier transform infrared spectroscopy (FTIR), and scanning electron microscopy (SEM).

2.3 EXPERIMENTAL PROCEDURE

2.3.1 Conversion of Calcium−Lithium−Borate Glass Particles in Aqueous Phosphate Solution.

Borate glass, with the composition (wt%): 15.00CaO, 10.63Li_2O, 74.37 B_2O_3, designated CaLB3-15, was prepared by melting reagent grade $CaCO_3$, Li_2CO_3 and

H_3BO_3 (Alfa Aesar, Haverhill, MA, USA) in a Pt crucible for 1 h at 1200ºC, and quenching the melt between cold stainless steel plates. This glass composition was used because previous work had shown that particles of the glass could be converted rapidly (within 2 days) to a HA-type material in an aqueous phosphate solution [11]. Particles of size 150–355 μm were obtained by grinding the glass in a hardened steel mortar and pestle, and sieving through 45 and 100 mesh sieves. The particles were washed three times with ethanol prior to being used in the conversion reaction.

Conversion of the borate glass particles to HA was studied in 0.25 M K_2HPO_4 solution containing 0-0.1 M $K_4P_2O_7$ (compositions and reaction times shown in Table I). The K_2HPO_4 solution was used as the parent solution for the conversion reaction because it had been used previously in several studies [14–16]. The solutions were prepared by dissolving 0.25 mol of $K_2HPO_4.3H_2O$ (99+%; Acros Organics, Morris Plains, NJ, USA) in 1 l distilled water, and then dissolving the required amount of $K_4P_2O_7$ (98%; Acros Organics). The pH of the as-prepared solutions was 9.0.

In the conversion reaction, 1 g glass particles was placed in a bag consisting of nylon sieve cloth (140 mesh; nominal opening = 106 μm), and immersed in the aqueous phosphate solution. Each bag of particles was placed in a sealed polyethylene bottle containing 100 mL solution and kept at 37°C for up to 28 days (Table I). After selected immersion times, the particles were removed from the solution, rinsed twice with distilled water, then twice with anhydrous ethanol, and dried at 90ºC. For each immersion time, the weight loss was determined from three samples.

2.3.2 Evaluation of Conversion Kinetics.

Measurement of the weight loss of the borate glass particles as a function of immersion time in the phosphate solution was used to monitor the conversion kinetics of the particles to HA, as described previously [14–16]. The weight loss is defined as $\Delta W/W_o = (W_o - W)/W_o$, where W_o is the initial mass of the particles (prior to immersion) and W is the mass after time t. Since the conversion of the calcium–lithium–borate glass to HA is also accompanied by dissolution of ions such as Li^+ and $(BO_3)^{3-}$, the concentration of Li and B in the phosphate solution as a function of immersion time was also used to evaluate the conversion process. The concentration of Ca, B, Li and P in the phosphate solution was measured using inductively-coupled plasma optical emission spectrometry (ICP-OES) at a commercial laboratory (Research Analytical Lab, University of Minnesota, St. Paul, MN, USA).

2.3.3 Characterization of Conversion Products.

The phase composition and microstructure of the solid products of the conversion reaction were analyzed using XRD and SEM. XRD was performed using Cu K_α radiation (λ = 0.15406 nm) at a scan rate of 1.8°/min in the 2θ range 5–70° (D/mas 2550 v; Rigaku; The Woodlands, TX, USA). The conversion product was ground to a powder for the XRD analysis. The microstructure of the external surface of the product was observed using SEM (S-4700; Hitachi, Tokyo, Japan), at an accelerating voltage of 10 kV and working distance of 12 mm. Composition analysis of the conversion product was performed using FTIR spectroscopy (NEXUS 670 FTIR; Thermo Nicolet; Madison, WI, USA) in the wavenumber range 400–4000 cm^{-1} (resolution = 8 cm^{-1}). A mass of 2 mg of

the product was ground into a powder, mixed with 198 mg KBr, and pressed to form pellets for the FTIR analysis.

2.4 RESULTS

2.4.1 Structure and Composition of Conversion Products.

XRD patterns of the starting glass (CaLB3-15) and the products formed by reacting the glass particles in 0.25 M K_2HPO_4 solution with varying concentration of $K_4P_2O_7$ at 37°C and pH = 9.0 are shown in Fig. 1. The starting glass had a diffraction pattern with no identifiable peaks, typical of an amorphous glass. (A small peak at ~13° 2θ is due to the instrument). For the conversion products formed by reacting the glass particles in the K_2HPO_4 solution (without $K_4P_2O_7$) and in the K_2HPO_4 solution containing 0.001 M and 0.01 M $K_4P_2O_7$, the XRD patterns showed diffraction peaks corresponding to those of a reference HA (JCPDS 72-1243). The peaks in the XRD patterns appeared to be broad, which might indicate that the conversion products were poorly crystallized, or consisted of nanometer-sized crystals, or a combination of both.

In comparison, the product formed when the glass particles were reacted in the K_2HPO_4 solution containing 0.1 M $K_4P_2O_7$ had a markedly different XRD pattern (Fig. 1). The major peaks corresponded to those of a dipotassium calcium pyrophosphate, $K_2CaP_2O_7.4H_2O$ and a calcium pyrophosphate, $Ca_2P_2O_7.nH_2O$. Only minor peaks corresponding to HA were identified in the XRD pattern, indicating little formation of HA. The XRD pattern showed the presence of additional phases that could not be clearly identified.

FTIR spectra of the conversion products formed when the glass particles were reacted in the K_2HPO_4 solution (without $K_4P_2O_7$) and in the K_2HPO_4 solution containing 0.001 M and 0.01 M $K_4P_2O_7$ are shown in Fig. 2. The most dominant resonances were the phosphate v3 resonance, centered at ~1040 cm^{-1}, and the phosphate v4 resonance, with peaks at ~605 and 560 cm^{-1}, which are associated with HA [18, 19]. These FTIR spectra provided further evidence that the products formed by reacting the glass particles in these three solutions consisted of HA. Additional resonances in the spectra of these conversion products included a weak shoulder at ~962 cm^{-1} corresponding to the phosphate v1 resonance [20], and a resonance at ~878 cm^{-1} corresponding to the vibrations of CO_3^{2-} ions substituting for PO_4^{3-} ions in the HA lattice [20].

In comparison, the FTIR spectrum of the product formed in the K_2HPO_4 solution containing 0.1 M $K_4P_2O_7$ was markedly different from those described above. The asymmetric and symmetric terminal stretching vibrations of PO_2 groups usually occur in the region 1250−980 cm^{-1} [21−23]. The intense band observed at 1175 cm^{-1} is attributed to the asymmetric P−O stretching, while the symmetric P−O stretching is located at 1109 and 1024 cm^{-1}. The P−OH vibrations are observed at 916 cm^{-1} and 487 cm^{-1}. The resonance observed at 723 cm^{-1} is attributed to symmetric P−O−P bridge vibration, while the resonance centered at ~580 cm^{-1} might be produced by the phosphate v4 and asymmetric δ PO_3 vibration. Taken together, the FTIR spectrum showed that the product formed in K_2HPO_4 solution with 0.1 M $K_4P_2O_7$ contained the function groups $P_2O_7^{4-}$, $HP_2O_7^{3-}$ and PO_4^{3-}, indicating the presence of a pyrophosphate, as well as a phosphate.

2.4.2 Reaction Kinetics.

Data for the weight loss, $\Delta W/W_o$, of the glass particles as a function of immersion time in the K_2HPO_4 solution with or without $K_4P_2O_7$ are shown in Fig. 3. The average weight loss and deviation for each immersion time were determined from three samples under the same conditions. In the K_2HPO_4 solution without $K_4P_2O_7$, the weight loss increased rapidly with immersion time, reaching a steady, limiting value of 63% after 48 h. The presence of 0.001 M $K_4P_2O_7$ in the K_2HPO_4 resulted in a small decrease in the $\Delta W/W_o$ value at a given immersion time, so the weight loss curve was shifted slightly to longer immersion times. For the glass particles reacted in the K_2HPO_4 solution containing 0.01 M $K_4P_2O_7$, the weight loss data showed a marked decrease at any immersion time, when compared to the data for particles reacted in K_2HPO_4 solution without $K_4P_2O_7$. The weight loss reached the same final limiting value (63%), but only after 200–250 h.

The weight loss curve for the particles immersed in K_2HPO_4 solution with 0.1 M $K_4P_2O_7$ showed a markedly different behavior (Figs. 3a, b). The weight loss first increased with immersion time, reaching a maximum value of 57% after an immersion time of 300–350 h, but then decreased at longer immersion times. After an immersion time of 672 h when the experiment was terminated, the final weight loss was 39%. According to XRD analysis, the product formed by reacting the particles for 336 h, corresponding to approximately the maximum on the weight loss curve, was amorphous (Fig. 4a). (A small peak at ~13° 2θ, as indicated earlier, is due to the instrument). The FTIR spectrum of the amorphous product also showed differences from that of the final product, particularly in the wavenumber range 1000-1200 cm^{-1} (Fig. 4b).

Table II shows data for the concentration of B, Ca, Li, and P in the K_2HPO_4 solution (with or without $K_4P_2O_7$) after different immersion times. For the K_2HPO_4 solution containing 0–0.01 M $K_4P_2O_7$, the concentration of B and Li showed trends similar to those described earlier for the weight loss data. With increasing $K_4P_2O_7$ concentration, the B and Li concentration decreased at a given immersion time, indicating a reduction in the degradation of the glass due to the presence of increasing $K_4P_2O_7$ concentration in this range. However, when the $K_4P_2O_7$ was increased to 0.1 M, this trend of decreasing B and Li concentrations at any given immersion time was not observed. Instead, the concentrations of B and Li at earlier emersion times (e.g., 1 day or earlier) showed an increase over those for the K_2HPO_4 solution containing 0.01 M $K_4P_2O_7$. When the experiments were terminated after 3−28 days, presumably after completion of the conversion reaction, the B concentration in the solution was similar to the theoretical value (taken as the amount in the nominal composition of the starting glass), whereas the Li concentration was slightly less than theoretical value. The Li/B atomic ratio in the final solution was in the range 0.180-0.188 for all four solutions.

Based on the low concentration of Ca in the K_2HPO_4 solution containing 0 or 0.001 M $K_4P_2O_7$, it appeared that almost all the Ca^{2+} ions released from the glass reacted rapidly with the phosphate ions of the solution to precipitate a HA-type material. However, as the $K_4P_2O_7$ increased to 0.01 and 0.1 M, the concentration of Ca^{2+} remaining in solution, while low, increased with increasing $K_4P_2O_7$ concentration, indicating that all the Ca^{2+} ions did not react rapidly with the phosphate ions from the solution to precipitate a calcium phosphate material. The concentration of P in each of the four solutions decreased with increasing immersion time of the glass particles, indicating a continuous

consumption of the phosphate ions from the solution in the formation of the calcium phosphate material.

2.4.3 Microstructure of Reaction Product.

SEM images (Fig. 5) of the surfaces of the converted particles showed marked changes in the microstructure when compared to that of the starting glass particles. In general, the smooth surface typical of a dense glass changed to a porous particulate surface after conversion in the phosphate solution. After conversion in K_2HPO_4 solution containing 0 or 0.001 M $K_4P_2O_7$, the surface of the product consisted of fine, plate-like (or needle-like) particles (Fig. 5a, b), typical of HA precipitated from solution [10]. An increase of the $K_4P_2O_7$ concentration to 0.01 M resulted in a more equiaxial particle shape (Fig. 5c). The product formed in K_2HPO_4 solution containing 0.1 M $K_4P_2O_7$ had a microstructure (Fig. 5d) consisting of more rounded particles, which was markedly different from that of the HA-type material formed in the K_2HPO_4 solution without $K_4P_2O_7$ (Fig. 5a).

2.5 DISCUSSION

The results show that the presence of pyrophosphate $(P_2O_7)^{4-}$ ions in an aqueous phosphate solution (0.25 M K_2HPO_4) has a marked effect on the degradation of a calcium-lithium-borate glass and its conversion to a HA-type material. The degradation and conversion also appear to show a marked difference in behavior when the $K_4P_2O_7$ concentration in the K_2HPO_4 solution increases above 0.01-0.1 M. When the $K_4P_2O_7$ concentration is 0.01 M or lower, the degradation and conversion rate decreases with increasing $K_4P_2O_7$ concentration, and according to XRD and FTIR, the conversion

product consists of a HA-type material (Figs. 1, 2). On the other hand, for a $K_4P_2O_7$ concentration of 0.1 M, the degradation rate shows a different trend (Fig. 3), and, according to XRD and FTIR, the product does not consist predominantly of a HA-type material (Figs. 1, 2). Instead, the product consists predominantly of a pyrophosphate material consisting of $K_2CaP_2O_7.4H_2O$ and $Ca_2P_2O_7.nH_2O$, with only little HA.

Based on the results of previous work [8, 14], it is generally understood that upon immersion of a calcium–lithium–borate glass (e.g., CaLB3-15) in an aqueous phosphate solution (e.g., K_2HPO_4), Li and B dissolve to form Li^+ and BO_3^{3-} ions in the solution. At the same time, Ca^{2+} ions from the glass react with $(PO_4)^{3-}$ ions from the solution to precipitate HA. ICP-OES data for the concentration of Li, B, and Ca in the phosphate solution (Table II), coupled with the weight loss data for the glass particles (Fig. 3), are in general agreement with this degradation and conversion mechanism.

Upon addition of 0.001 M and 0.01 M $K_4P_2O_7$ to the K_2HPO_4 solution, XRD and FTIR analyses show that a HA-type product is still formed. However, the ICP-OES and weight loss data show that both the degradation of the glass particles (Table II) and the conversion to HA (Fig. 3) are markedly reduced with increasing $K_4P_2O_7$ concentration. The time for complete conversion of the particles increases from ~2 days (no $K_4P_2O_7$) to ~10 days (0.01M $K_4P_2O_7$). Assuming that all the CaO from the glass reacts with phosphate ions from the solution to form HA, then the theoretical weight loss is 73%. Figure 3 shows that the final, limiting weight loss of the particles in the K_2HPO_4 solution containing 0–0.01 M $K_4P_2O_7$ is 64%. As discussed previously [9], formation of a substituted hydroxyapatite, such as the substitution of Ca^{2+} with K^+ or $(PO_4)^{3-}$ with $(CO_3)^{2-}$ could account for a deviation from the theoretical value.

At lower $K_4P_2O_7$ concentrations (0–0.01 M), a possible explanation for the reduction in degradation rate and conversion to HA is preferential adsorption of $(P_2O_7)^{4-}$ to the surface of the particles because of their larger molecular weight, when compared to $(HPO_4)^{2-}$ ions. Upon immersion of the borate glass particles into the K_2HPO_4 solution, a calcium phosphate surface layer is presumably formed rapidly [18, 24]. Pyrophosphate ions such as $(P_2O_7)^{4-}$ and $(HP_2O_7)^{3-}$ have been reported to adsorb readily on the surfaces of HA crystals [25] and to chelate with positively charged ions such as Ca^{2+} [26]. In the present work, adsorption of pyrophosphate ions and chelation with the positively charged network modifiers Li^+ and Ca^{2+} could lead to a reduction in the degradation of the glass. The adsorption of pyrophosphate ions could also lead to a reduction in the nucleation and growth of HA-type material, resulting in a reduction in the conversion to a HA-type material, as observed (Fig. 3). For each system, the Ca content of the solution (Table II) reaches its highest value at intermediate immersion times, then it decreases at longer times. However, the Ca concentration in the solution is far smaller than the Ca content of the starting glass, indicating the Ca is essentially precipitated as a HA-type material on the particles or chelated with the $(P_2O_7)^{4-}$ ions on surface of the particles.

For the highest $K_4P_2O_7$ concentration (0.1 M) in the K_2HPO_4 solution, the weight loss data (Fig. 3b) and the concentrations of B and Li in the solution (Table II) show approximately similar trends up to an immersion time of 14 days: they increase with immersion time and reach their maximum values within 14 days. At longer times, the weight loss decreases, whereas the B and Li concentrations essentially show no further change. Essentially all the Li and B have dissolved out of the glass particles within 14 days. On the other hand, the Ca and P concentrations decrease markedly between 14 and

28 days, which indicate the precipitation of these two ions from the solution. As outlined earlier, according to XRD, the product formed after 14 days is amorphous (Fig. 4a), whereas it is crystalline after 28 days, consisting predominantly of $K_2CaP_2O_7.4H_2O$ and $Ca_2P_2O_7.nH_2O$. A possible explanation for the behavior at this higher $K_4P_2O_7$ concentration (0.1 M) is that the glass first degrades and converts to an ACP material within the first 14 days of immersion. Calcium ions are chelated with pyrophosphate $(P_2O_7)^{4-}$ ions adsorbed on the surface of the particles and in solution. Subsequently, precipitation from solution coupled with crystallization of the ACP material leads to a decrease in the weight loss and the formation of a product consisting predominantly of $K_2CaP_2O_7.4H_2O$ and $Ca_2P_2O_7.nH_2O$. XRD showed the presence of additional phases that could not be clearly identified, indicating that the final product consists of a fairly complex mixture of phases.

A schematic diagram illustrating the proposed mechanism for the conversion of the calcium–lithium–borate glass in K_2HPO_4 solution containing varying concentrations of pyrophosphate $(P_2O_7)^{4-}$ ions is shown in Fig. 6. In the K_2HPO_4 solution with no $K_4P_2O_7$, degradation of the glass, coupled with reaction between Ca^{2+} and $(PO_4)^{3-}$ ions leads to the formation of a HA-type material, as described previously [8, 14]. With the small additions of $K_4P_2O_7$ (0.01 M or smaller) to the K_2HPO_4 solution, adsorption of $(P_2O_7)^{4-}$ ions (and possibly $(HP_2O_7)^{3-}$) to the surface coupled with chelation of Ca^{2+} ions leads to a reduction in the degradation rate of the glass and its conversion to a HA-type material. However, with higher $K_4P_2O_7$ addition (0.1 M) to the K_2HPO_4 solution, an ACP material is formed which eventually converts to a crystalline pyrophosphate, consisting predominantly of $K_2CaP_2O_7.4H_2O$ and $Ca_2P_2O_7.nH_2O$.

The present results have important consequences for the use of bioactive glass in biomedical applications. Firstly, the addition of pyrophosphate ions to an aqueous phosphate solution could provide a method for controlling the degradation rate of a bioactive glass and its conversion to a HA-type material, particularly for borate glass, which has a low durability. Secondly, the presence of pyrophosphate ions in an aqueous phosphate solution should be avoided when the efficient and complete conversion of a bioactive glass to a HA-type device is required.

2.6 CONCLUSIONS

The conversion of calcium–lithium–borate glass particles (150–355 μm) to a HA-type material concentration in an aqueous phosphate solution (0.25 M K_2HPO_4) was markedly influenced by the concentration of pyrophosphate $(P_2O_7)^{4-}$ ions in the solution. In the K_2HPO_4 solution containing 0–0.01 M $K_4P_2O_7$, while the conversion rate to HA decreased with increasing $K_4P_2O_7$ concentration, XRD and FTIR showed that the fully converted particles consisted of an HA-type product. At higher $K_4P_2O_7$ concentration (0.1 M), the conversion rate of the particles also decreased, but the product did not consist of an HA-type material. Instead, the product consisted predominantly of an ACP material which eventually crystallized to a pyrophosphate product, consisting predominantly of $K_2CaP_2O_7.4H_2O$ and $Ca_2P_2O_7.nH_2O$. The results show the potential of pyrophosphate ions for influencing the conversion of a bioactive glass to HA in an aqueous phosphate solution, as well as the ability to produce a calcium pyrophosphate product predominantly by reacting a calcium– lithium–borate glass in a phosphate solution containing a sufficient concentration of pyrophosphate ions.

2.7 REFERENCES

1. Hench LL. Bioceramics. J Am Ceram Soc. 1998; 81**:**1705–28.
2. Rahaman MN, Brown RF, Bal BS, Day DE. Bioactive glasses for nonbearing applications in total joint replacement. Semin Arthroplasty. 2006; 17: 102–12.
3. Jones JR, Gentleman E, Polak J. Bioactive glass scaffolds for bone regeneration, Elements. 2007; 3: 393–9.
4. Hench LL, Splinter R. J, Allen WC, Greenlee TK Jr. Bonding mechanisms at the interface of ceramic prosthetic materials. J Biomed Mater Res. 1971; 5: 117–41.
5. Pantano CG, Clark AE, Hench LL, Multilayer corrosion films on Bioglass surfaces. J Am Ceram Soc. 1974; 57: 412–3.
6. Hench LL, Wilson J. Surface-active biomaterials. Science. 1984; 226: 630–6.
7. Ducheyne P, Qiu Q. Bioactive ceramics: the effect of surface reactivity on bone formation and bone cell function. Biomaterials. 1999; 20: 2287–303.
8. Day DE, White JE, Brown RF, McMenamin KD. Transformation of borate glasses into biologically useful materials. Glass Technol. 2003; 44: 75–81.
9. Wang Q, Huang W, Wang D, Darvell BW, Day DE, Rahaman MN. Preparation of hollow hydroxyapatite microspheres. J Mater Sci: Mater Med. 2006; 17: 641–6.
10. Conzone SD and Day DE, Preparation and properties of porous microspheres made from borate glass. J Biomed Mater Res A. 2009; 88A: 531–42.
11. Fu H, Rahaman MN, Day DE. Effect of process variables on the microstructure of hollow hydroxyapatite microspheres prepared by a glass conversion process. J Am Ceram Soc. 2010; 93: 3116–23.

12. Han X, Du M, Ma Y, Day DE. Evaluation of hydroxyapatite microspheres made from a borate glass to separate protein mixtures. J Mater Sci. 2008; 43: 5618–25.
13. Huang W, Day DE, Kittiratanapiboon K, Rahaman MN. Kinetics and mechanisms of the conversion of silicate (45S5), borate, and borosilicate glasses to hydroxyapatite in dilute phosphate solutions. J Mater Sci: Mater Med. 2006; 17: 583–96.
14. Huang W, Rahaman MN, Day DE, Li Y. Mechanisms of converting silicate, borate, and borosilicate glasses to hydroxyapatite in dilute phosphate solutions. Phys Chem. Glasses: Europ J Glass Sci Technol B. 2006; 47: 647–58.
15. Huang W, Day DE, Rahaman MN. Comparison of the formation of calcium and barium phosphates by the conversion of borate glass in dilute phosphate solution at near room temperature. J Am Ceram Soc. 2007; 90: 838–44.
16. Yao A, Wang D, Huang W, Fu Q, Rahaman MN, Day DE. In vitro bioactive characteristics of borate-based glasses with controllable degradation behavior. J Am Ceram Soc. 2007; 90: 303–6.
17. Fu Q, Rahaman MN, Day DE. Accelerated conversion of silicate bioactive glass (13-93) to hydroxyapatite in aqueous phosphate solution containing polyanions. J Am Ceram Soc. 2009; 92: 2870–6.
18. Clark AE, Hench LL. Early stages of calcium-phosphate layer formation in bioglass. J. Non-Cryst Solids. 1989; 113: 195–202.
19. Filgueiras MR, LaTorre G, Hench LL. Solution effects on the surface reaction of a bioactive glass. J Biomed Mater Res. 1993; 27: 445–53.
20. Rehman I, Bonfield W. Characterization of hydroxyapatite and carbonated apatite by photo acoustic FTIR spectroscopy. J Mater Sci: Mater Med. 1997; 8: 1–4.

21. Harcharras M, Ennaciri A, Assaaoudi H, Vibrational spectra of double diphosphates $M_2SrP_2O_7$ (M = Li,Na,K,Rb,Cs). J Can Anal Sci Spectrosc. 2001; 46: 83–8.

22. Harcharras M, Ennaciri A, Rulmont A, Gilbert B. Vibrational spectra and structures of double diphosphates $M_2CdP_2O_7$ (M = Li, Na, K, Rb, Cs). Spectrochimica Acta. 1997; A53: 345–52.

23. Sarr O, Diop L. The vibrational spectra of the crystalline tripotassium hydrogen pyrophosphates $K_3HP_2O_7.3H_2O$ and $K_3HP_2O_7$. Spectrochim Acta. 1984: A40: 1011–5.

24. Li Y, Rahaman MN, Bal BS, Day DE, Fu Q. Early stages of calcium phosphate formation on bioactive borosilicate glass in aqueous phosphate solution. J Am Ceram Soc. 2008; 91: 1528–33.

25. Christoffersen J, and Christoffersen MR. Kinetics of dissolution of calcium hydroxyapatite : IV. The effect of some biologically important inhibitors. J. Cryst Growth. 1981; 53: 42–54.

26. Christoffersen MR, Balic-Zunic T, Pehrson S, Christoffersen J. Kinetics of growth of triclinic calcium pyrophosphate dehydrate crystals. Cryst Growth Des. 2001;1: 463–6.

Table I. Composition of K_2HPO_4 solutions with varying $K_4P_2O_7$ concentration used in these experiments for converting calcium–lithium–borate (CaLB3-15) glass particles to a calcium phosphate material.

K_2HPO_4 (M)	0.25	0.25	0.25	0.25
$K_4P_2O_7$ (M)	0	0.001	0.01	0.1
Reaction time (h)	72	96	240	672

The total reaction time for each composition is also shown.

Table II. Concentration of B, Ca, Li, and P in 0.25 M K_2HPO_4 solution containing 0, 0.001 M, 0.01 M, and 0.1 M $K_4P_2O_7$ after immersion of calcium–lithium–borate (CaLB3-15) glass particles for the times shown.

	B(mg/L)	Ca(mg/L)	Li(mg/L)	P(mg/L)	Theoretical concentration of P (mg/L)
0 M $K_4P_2O_7$					7750
0h	1.3	<0.7	<0.1	7381	
1h	227	2.4	47.2	7335	
1d	2169	1.2	414	7280	
3d	2339	<0.7	427	6746	
0.001 M $K_4P_2O_7$					7810
0h	1.7	0.8	<0.1	7438	
1h	205	1.7	35.9	7337	
1d	2081	2.4	421	6972	
4d	2400	0.8	434	6802	
0.01 M $K_4P_2O_7$					8370
0h	3.8	1.2	<0.1	8300	
1h	190	5.4	39.2	8105	
1d	1148	16.3	234	7990	
10d	2275	2.5	427	7570	
0.1 M $K_4P_2O_7$					13950
0h	1.5	1.3	<0.1	13677	
1h	207	37.7	41.4	13431	
1d	1600	70.5	322	12958	
14d	2313	75.1	419	12658	
28d	2325	3.7	420	11847	
Theoretical composition (in starting glass)	2310	1070	494	0	

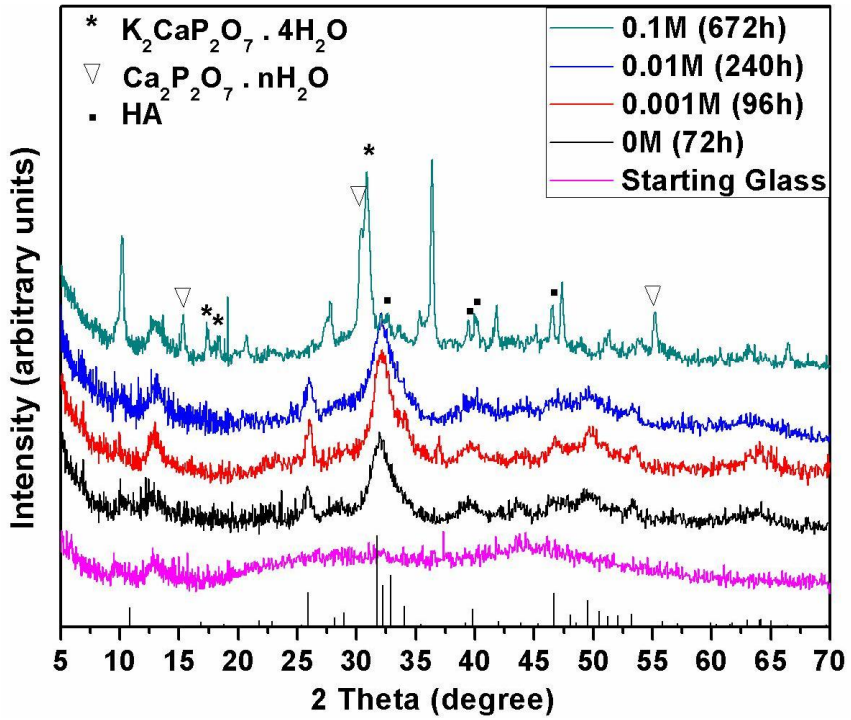

Figure 1. XRD patterns of the starting calcium–lithium–borate (CaLB3-15) glass particles and the products formed after converting the glass particles for the times shown in 0.25 M K_2HPO_4 solution containing 0, 0.001, 0.01, and 0.1 M $K_4P_2O_7$. For comparison, the pattern for a reference hydroxyapatite (JCPDS 72-1243) is also shown.

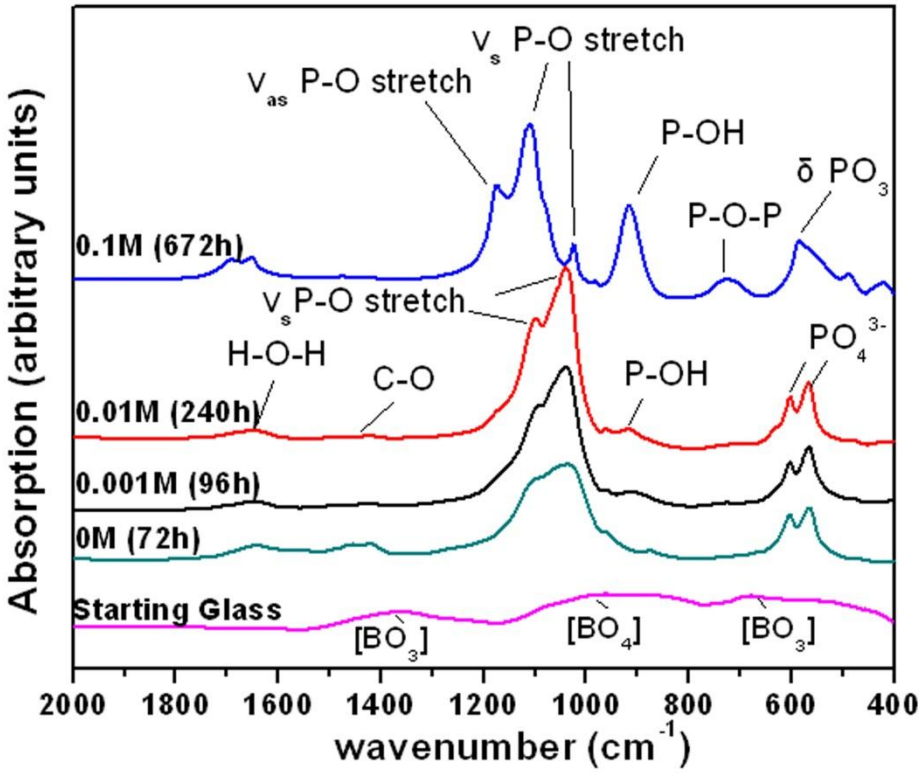

Figure 2. FTIR spectra of the starting calcium–lithium–borate (CaLB3-15) glass particles and the products formed after converting the glass particles for the times shown in 0.25 M K_2HPO_4 solution containing 0, 0.001, 0.01, and 0.1 M $K_4P_2O_7$. The main resonances in the spectra are shown.

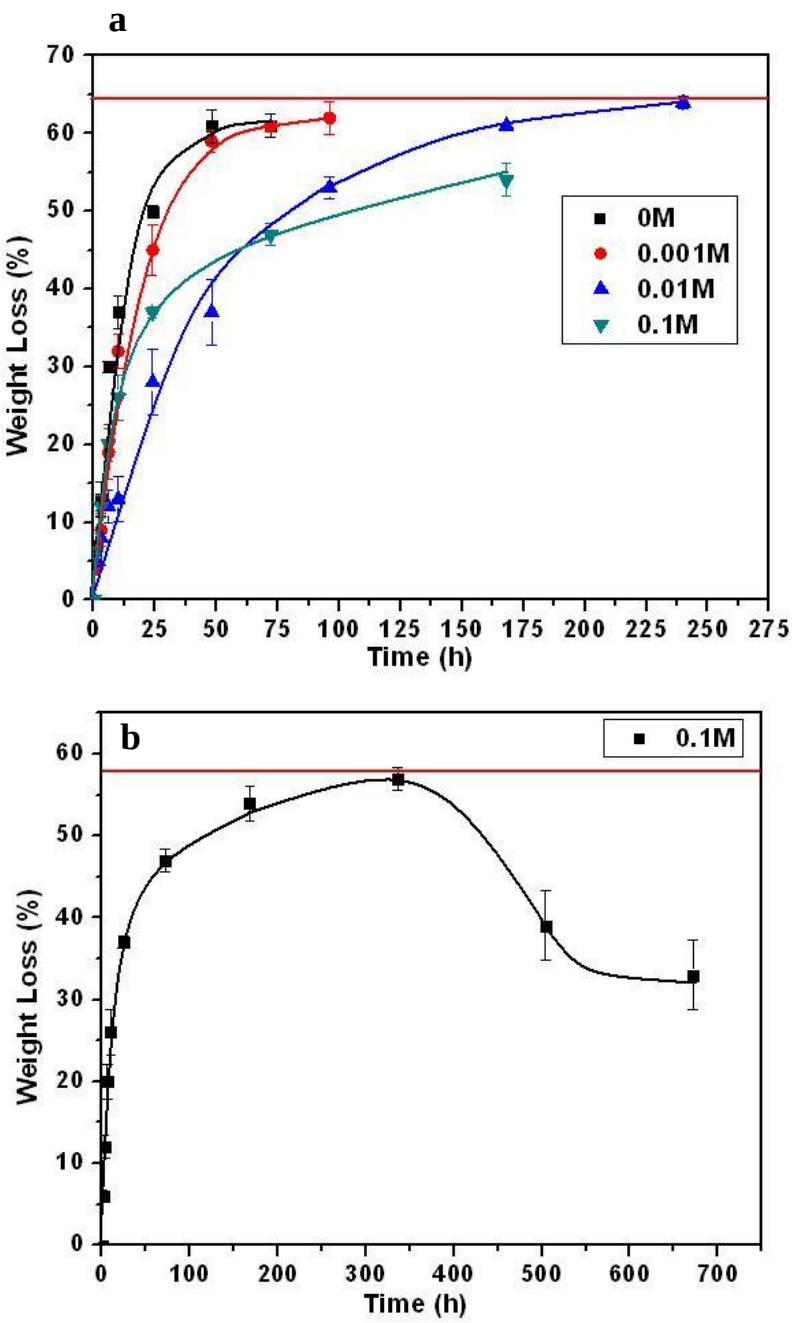

Figure 3. (a) Weight loss of calcium–lithium–borate (CaLB3-15) glass particles during conversion in 0.25 M K_2HPO_4 solution containing 0, 0.001, 0.01, and 0.1 M $K_4P_2O_7$. (b) Weight loss curve for the glass particles during conversion in 0.25 M K_2HPO_4 solution containing 0.1 M $K_4P_2O_7$, showing a maximum, followed by a decrease at longer times.

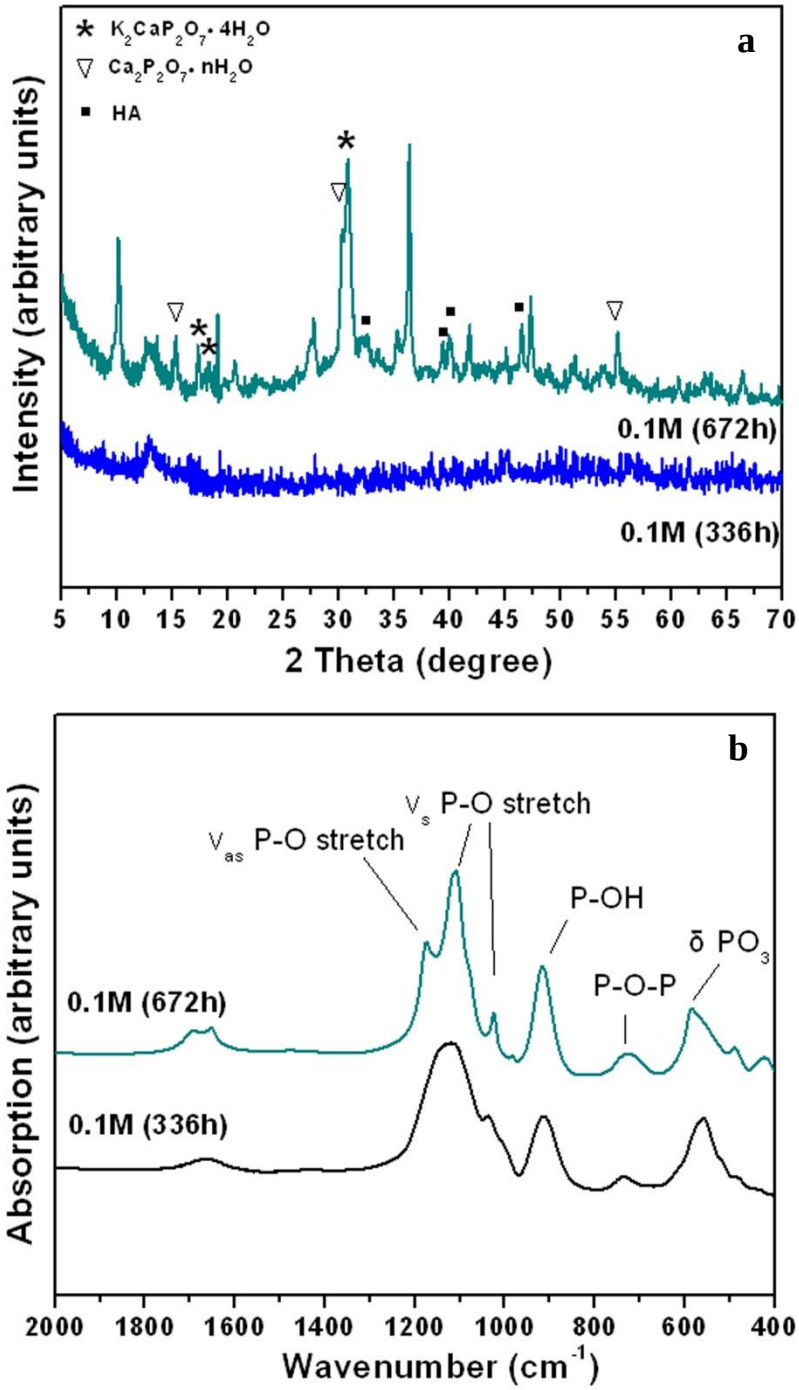

Figure 4. (a) XRD patterns and (b) FTIR spectra of the products formed by converting calcium–lithium–borate (CaLB3-15) glass particles in 0.25 M K_2HPO_4 solution containing 0.1 M $K_4P_2O_7$ for 14 days (336h) and for 28 days (672h).

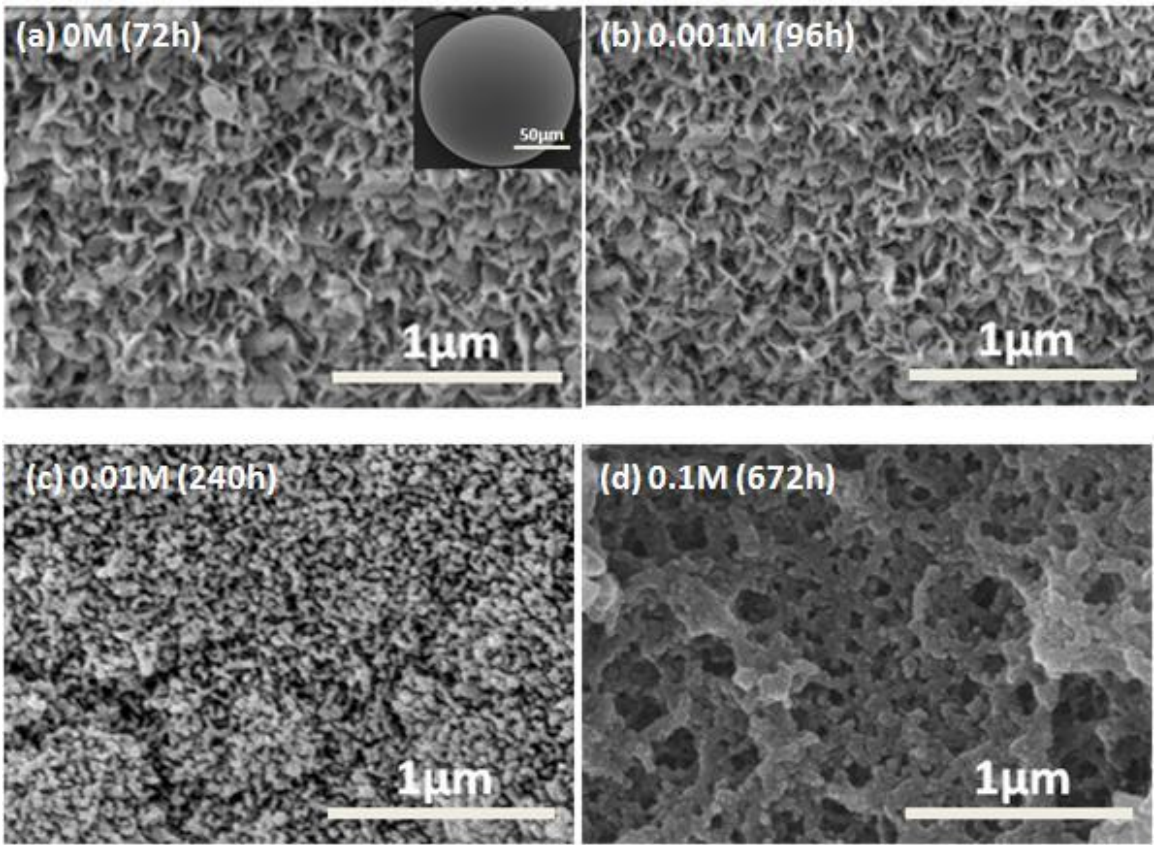

Figure 5. SEM images of the surface of the products formed by converting calcium–lithium– borate (CaLB3-15) glass particles in 0.25 M K_2HPO_4 solution containing (a) 0 M, (b) 0.001 M, (c) 0.01 M, and (d) 0.1 M $K_4P_2O_7$ for the times shown. The inset in (a) shows an SEM image of the unreacted glass surface.

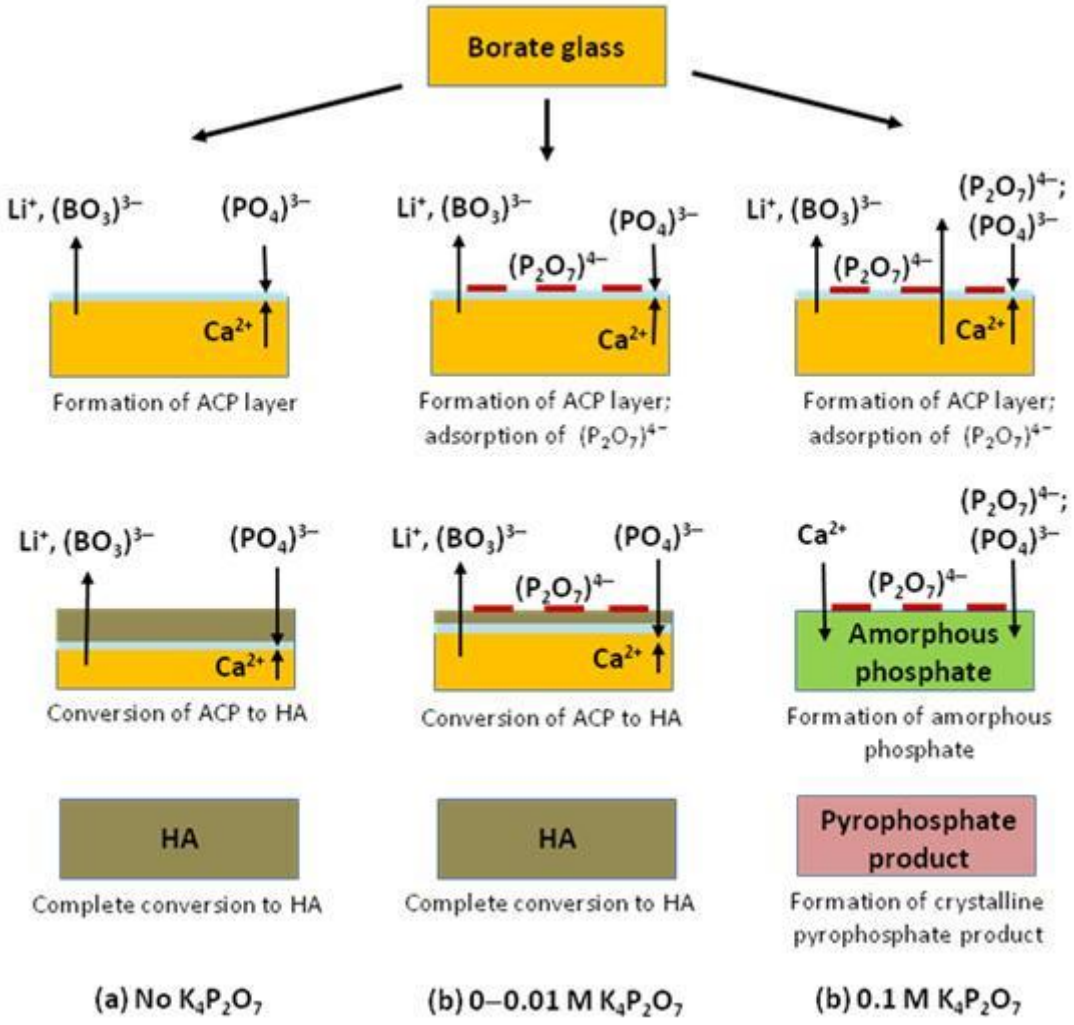

Figure 6. Schematic diagrams showing the main steps in the conversion of CaLB3-15 glass in K_2HPO_4 solution (0.25 M) containing (a) no $K_4P_2O_7$; (b) 0–0.01 M $K_4P_2O_7$; (c) 0.1 M $K_4P_2O_7$.

3. HOLLOW HYDROXYAPATITE MICROSPHERES AS A DEVICE FOR CONTROLLED DELIVERY OF PROTEINS

Hailuo Fu[1,3], Mohamed N. Rahaman[1,3], Delbert E. Day[1,3], Roger F. Brown[2,3]

[1]Department of Materials Science and Engineering, Missouri University of Science and Technology, Rolla, MO 65409, USA

[2]Department of Biological Sciences, Missouri University of Science and Technology, Rolla, MO 65409, USA

[3]Center for Bone and Tissue Repair and Regeneration, Missouri University of Science and Technology, Rolla, MO 65409, USA

3.1 ABSTRACT

Hollow hydroxyapatite (HA) microspheres were prepared by reacting solid microspheres of $Li_2O–CaO–B_2O_3$ glass (106–150 μm) in K_2HPO_4 solution, and evaluated as a controlled delivery device for a model protein, bovine serum albumin (BSA). Reaction of the glass microspheres for 2 days in 0.02 M K_2HPO_4 solution (pH = 9) at 37°C resulted in the formation of biocompatible HA microspheres with a hollow core diameter equal to 0.6 the external diameter, high surface area (~100 m^2/g), and a mesoporous shell wall (pore size ≈ 13 nm). After loading with a solution of BSA in phosphate-buffered saline (PBS) (5 mg BSA/ml), the release kinetics of BSA from the HA microspheres into a PBS medium were measured using a micro bicinchoninic acid (BCA) protein assay. Release of BSA initially increased linearly with time, but almost ceased after 24–48 h. Modification of the BSA release kinetics was achieved by modifying the microstructure of the as-prepared HA microspheres using a controlled heat

treatment (1–24 h at 600–900°C). Sustained release of BSA was achieved over 7–14 days from HA microspheres heated for 5 h at 600°C. The amount of BSA released at a given time was dependent on the concentration of BSA initially loaded into the HA microspheres. These hollow HA microspheres could provide a novel inorganic device for controlled local delivery of proteins and drugs.

3.2 INTRODUCTION

Over the past few decades, there has been considerable interest in the development of devices for controlled local delivery of proteins such as growth factors and drugs [1]. A controlled-release system consists of a biologically active agent (e.g., protein) in a carrier material (commonly a polymer or ceramic). The objective of the controlled-delivery device is to provide a means for local delivery of the protein to the target site at concentrations within the therapeutic limits and for the required duration. Since the delivery device is implanted, injected, or inserted into the body, the biocompatibility and toxicity of the carrier material must also be considered.

Natural and synthetic biodegradable polymers have found wide application as carrier materials for protein delivery [2]. The delivery systems include microspheres, hydrogels, and three-dimensional porous scaffolds [3, 4]. These polymers degrade *in vivo*, either enzymatically or non-enzymatically, to produce biocompatible or non-toxic by-products along with progressive release of the dispersed or dissolved protein. Natural polymers and their derivatives in the form of gels or sponges have been used extensively as delivery vehicles. In particular, collagen is a readily available extracellular matrix component that allows cell infiltration and remodeling, making it an attractive delivery

system for proteins [5, 6]. Biodegradable synthetic polymers, such as poly(lactic acid), PLA, and poly(glycolic acid), PGA, as well as their copolymers, poly(lactic co-glycolic acid), PLGA, are the most widely used delivery systems. In addition to being widely available, they can be prepared with well-controlled, reproducible chemical and physical properties [2–4, 7]. They are also among the few synthetic biodegradable polymers approved by the Food and Drug Administration (FDA) for *in vivo* use.

Inorganic materials which have been utilized as carriers for protein delivery consist primarily calcium phosphate materials such as β-tricalcium phosphate, $Ca_3(PO_4)_2$ and hydroxyapatite, HA, $Ca_{10}(PO_4)_6(OH)_2$ [1], and bioinert metal oxides such as silica, SiO_2 [8, 9]. The calcium phosphate materials, composed of the same elements as bone, are biocompatible and produce no systemic toxicity or immunological reactions. In addition to its chemical and structural stability, SiO_2 can be prepared near room temperature by sol-gel methods and other solution-based methods, so the protein activity can be retained. The delivery systems typically consist of nanoparticles, porous particles, granules, or porous substrates in which the protein is adsorbed or attached to the surfaces of the porous material, or encapsulated within the pores [8–11]. Hollow HA microspheres (diameter = 1,500–2,000 μm), consisting of a hollow core and a mesoporous shell, have been prepared by coating chitin microspheres with a composite layer of chitin and HA, followed by thermal decomposition of the chitin and sintering of the porous HA shell [12].

Day and Conzone [13] invented a process for preparing porous phosphate materials with high surface area by converting borate glasses with special compositions in an aqueous phosphate solution near room temperature [14, 15]. A characteristic feature

of the process is that it is pseudomorphic, so the HA product retains the same external shape and dimensions of the starting glass object. Using this process, Wang *et al*. [16] reacted solid glass microspheres (106–125 μm) with the composition (wt%) 4.7Li_2O, 13.2CaO, 82.1B_2O_3 in 0.25 M K_2HPO_4 solution for 5 days at 37°C and pH = 10.0–12.0. They found that the product consisted of hollow microspheres of a calcium phosphate material which, on heating for 4 h at 600°C, converted to HA. Huang *et al*. [17] prepared hollow HA microspheres by reacting glass microspheres with the composition 10Li_2O, 10CaO, 80B_2O_3 (wt%) for 5 days (microsphere diameter = 106–125 μm) or 14 days (microsphere diameter = 500–800 μm) under similar conditions used by Wang *et al*. [16]. They measured the surface area of the smaller HA microspheres (135 m^2/g) and the rupture strength of the larger HA microspheres (1.6 MPa), and studied the effect of heat treatment on the surface area and rupture strength. Heating the as-prepared HA microspheres for 8 h at 600°C and at 800°C resulted in a marked decrease in surface area and a sharp increase in strength.

Our previous work showed that the microstructure of hollow HA microspheres prepared by converting Li_2O–CaO–B_2O_3 glass microspheres (106–150 μm) in a K_2HPO_4 solution can be manipulated over a wide range by controlling the process variables [18]. By varying the concentration (0.02–0.25 M) and the temperature (25–60°C) of the K_2HPO_4 solution at pH = 9–12, hollow HA microspheres with a hollow core diameter to microsphere diameter (d/D) of 0.14–0.62, surface area of 78–145 m^2/g, and pore size of 8–20 nm were produced.

The objective of this work was to evaluate hollow HA microspheres prepared by the glass conversion process as a potential device for controlled delivery of proteins.

Bovine serum albumin (BSA) was used as a model protein in this work because it is one of the most widely studied proteins. The ability to fill the hollow HA microspheres with an aqueous solution of BSA, and the release kinetics of BSA from the filled microspheres into an aqueous medium were determined. The ability to manipulate the release kinetics of the BSA was studied by altering the microstructure of the shell wall of the as-prepared HA microspheres using a controlled heat treatment (1–24 h at 600–900°C).

3.3 EXPERIMENTAL PROCEDURE

3.3.1 Preparation of Hollow Hydroxyapatite (HA) Microspheres.

Hollow HA microspheres were prepared by reacting solid glass microspheres in an aqueous phosphate solution as described previously [18]. Briefly, borate glass, with the composition (wt%): 15.00CaO, 10.63Li_2O, 74.37 B_2O_3, designated CaLB3-15, was prepared by melting reagent grade $CaCO_3$, Li_2CO_3 and H_3BO_3 (Alfa Aesar, Haverhill, MA, USA) in a Pt crucible at 1,200ºC for 45 min, and quenching between cold stainless steel plates. Particles of size 106–150 μm were obtained by grinding the glass in a hardened steel mortar and pestle, and sieving through 100 and 140 mesh sieves. Microspheres were obtained by dropping the crushed particles down a vertical tube furnace at 1,000°C, as described in detail elsewhere [14].

Hollow HA microspheres were prepared by reacting the glass microspheres for 2 days in 0.02 M K_2HPO_4 solution at 37°C and pH = 9.0. These conditions were used because our previous work showed that they resulted in the formation of hollow HA microspheres with large d/D value (ratio of the hollow core diameter, d, to the sphere diameter, D), high surface area, and mesoporous shell wall [18]. In all the experiments, 1

g of glass microspheres was placed in 200 ml solution, and the system was gently stirred continuously. Upon completion of the conversion process, the HA microspheres were washed three times with distilled water, soaked in anhydrous ethanol to displace residual water, dried for at least 12 h at room temperature, then for at least 12 h at 90^{o}C, and stored in a desiccator.

These 'as-prepared' HA microspheres were subjected to a controlled thermal treatment in order to modify the microstructure of the shell wall. Microspheres were heated in a Pt crucible for 1, 5, and 24 h at temperatures between 600 and 900°C. These heat treatment temperatures were used because they are below and above the onset temperature for sintering (densification) of porous, fine-grained HA.

3.3.2 Characterization of Hollow HA Microspheres.

The phase composition of the converted microspheres was checked using X-ray diffraction, XRD (D/mas 2550 v; Rigaku; The Woodlands, TX) and Fourier transform infrared (FTIR) spectroscopy (NEXUS 670; Thermo Nicolet; Madison, WI). XRD was performed using Cu K_{α} radiation (λ = 0.15406 nm) at a scan rate of 1.8° /min in the 2θ range 20–70°. The HA microspheres were ground to a powder for the XRD and FTIR analyses. FTIR was performed in the wavenumber range of 400–4,000 cm^{-1} (resolution = 8 cm^{-1}). A mass of 2 mg of the powder was mixed with 198 mg KBr, and pressed to form pellets for the FTIR analysis.

The rupture strength of individual HA microspheres, as-prepared or heat treated, was measured in a nano-mechanical testing machine (Nano Bionix; Agilent Technologies; Oak Ridge, TN) using a procedure described in detail elsewhere [17]. Because of the difficulty of manipulating microspheres of size 106–150 μm in the testing

machine, larger spheres (diameter 200–250 μm) were tested. At least eight microspheres were measured for each group (as-prepared or heat-treated), and the rupture strength was expressed as a mean value ± standard deviation.

The microstructure of the external surface and the cross section of the as-prepared and heat-treated HA microspheres was examined in a scanning electron microscope, SEM (S-4700; Hitachi, Tokyo, Japan), at an accelerating voltage of 10 kV and working distance of 12 mm. Local composition of the external surface and across the wall of the microspheres was determined using energy dispersive X-ray (EDS) analysis in the SEM, with an electron beam spot size of 1 μm.

The specific surface area and the pore size distribution of the shell wall of the HA microspheres were measured using nitrogen adsorption (Autosorb-1; Quantachrome, Boynton Beach, FL). Prior to the measurement, a known mass of microspheres (in the range 300–500 mg) was weighed, and evacuated for 15 h at 120°C to remove adsorbed moisture. The volume of nitrogen adsorbed and desorbed at different relative gas pressures was measured and used to construct adsorption–desorption isotherms. The first five points of the adsorption isotherm, which initially followed a linear trend implying monolayer formation of adsorbate, were fitted to the Brunauer–Emmett–Teller (BET) equation for the determination of the specific surface area [19]. The pore size distribution was calculated using the Barrett–Joiner–Halenda (BJH) method applied to the desorption isotherms [20].

3.3.3 Biocompatibility of Hollow HA Microspheres.

The biocompatibility of the hollow HA microspheres was evaluated by examining their ability to support cell proliferation *in vitro*. For these experiments, thin discs of

hollow HA microspheres were formed by pouring the borate glass microspheres into a graphite die, heating the system for 1 h at 550ºC to join the glass microspheres, and then reacting the disc in 0.02M K_2HPO_4 solution to convert the glass microspheres to hollow microspheres. After sterilization by washing three times with water and ethanol, followed by heating for at least 24 h at 120ºC, the discs of hollow HA microspheres were seeded with 60,000 MC3T3-E1 cells suspended in 60 μl medium, and incubated for 4 h to permit cell attachment. The cell-seeded constructs were then transferred to a 24-well culture plate containing 2 ml of complete medium per well. All cell cultures were maintained at 37ºC in a humidified atmosphere of 5% CO_2 with the medium changed every 2 days. At selected time intervals, disks with attached cells were removed, washed, stained with Sanderson Bone Stain™, and examined in an optical microscope.

3.3.4 Loading of BSA into Hollow HA Microspheres.

The ability to load a model protein, bovine serum albumin (BSA) into the converted microspheres was studied using optical microscopy. To permit visual observation of the protein distribution within the microspheres, a fluorescein isothiocyanate-labeled BSA (referred to as FITC-BSA) (Sigma-Aldridge, St. Louis, MO) was used. A mass of 0.1 g microspheres was immersed in 5 ml of a solution consisting FITC-BSA in phosphate-buffered saline (PBS) (FITC-BSA concentration = 5 mg/ml). A small vacuum was applied to the system to remove air trapped within the microspheres, thereby assisting the incorporation of the FITC-BSA into the microspheres. When the removal of air bubbles from the microspheres had ceased (as determined visually), the microspheres loaded with FITC-BSA were dried in air at room temperature, and observed in an optical microscope.

3.3.5 Release Kinetics of BSA from Hollow HA Microspheres into PBS.

The hollow HA microspheres were loaded with a solution of BSA (without FITC labeling) using the method outlined above, removed, and immersed in PBS to determine the release of BSA from the microspheres into the PBS. In the loading step, 200 mg of the microspheres was placed in 2 ml of a PBS solution containing 5 mg/ml BSA (molecular weight = 66 kDa; Sigma-Aldrich). The BSA-loaded microspheres were removed, rinsed three times with PBS, and placed in a beaker containing 20 ml PBS. The system was kept at 37ºC, and the solution was stirred continuously. At selected time intervals, 50 µL aliquots were taken from the solution and used for determining the amount of BSA released into the solution.

The concentration of BSA in each aliquot was measured using a micro bicinchoninic acid (BCA) protein assay reagent (Product # 23240ZZ; Thermo Fisher Scientific, Rockford, IL). This assay is very sensitive to dilute concentrations of proteins and has a linear working range of 0.5–20 µg/ml for BSA [21]. The aliquots were mixed with 50 µl PBS and 100 µl of the working reagent, reacted for 2 h at 37ºC and cooled to room temperature. The absorbance of each solution was measured at 550 nm using a HP 8452A diode array spectrophotometer (BMG LABTECH Inc., Cary, NC). The concentration of BSA was determined from a standard curve calibrated from measurements of the absorbance of PBS containing known concentrations of BSA. At the completion of the BSA release experiments, the microspheres were washed three times with distilled water and dried in air at room temperature. The dried microspheres were crushed and the residual BSA in the microspheres was measured using the BCA technique described above.

3.4 RESULTS

3.4.1 Microstructure of As-prepared and Heat-treated HA Microspheres.

Figure 1 shows an optical image of the starting CaLB3-15 glass microspheres (Fig. 1a), and SEM images showing the external surface and the cross-section of a hollow HA microsphere formed by reacting the glass microspheres for 2 days in 0.02 M K_2HPO_4 solution (pH = 9) at 37°C (Figs, 1b, 1c). The HA microspheres had a hollow core diameter, relative to the external diameter of the hollow microspheres, d/D = 0.61 ± 0.03, surface area = 101 ± 5 m^2/g, and a pore size of the shell wall = 13 ± 2 nm (Table I).

XRD, FTIR, and EDS analysis (Fig. 2) confirmed that the hollow microspheres had a structure and composition corresponding to an HA-type material. The starting CaLB3-15 glass had a diffraction pattern with no measurable peaks (Fig. 2a), typical of an amorphous glass. In comparison, the patterns of the converted microspheres (as-prepared and heat treated for 5 h at 600°C) contained peaks that corresponded to those of a reference HA (JCPDS72-1243). The broad peaks in the XRD pattern of the as-prepared microspheres may indicate that the material was poorly crystallized, or consisted of nanometer-sized crystals, or a combination of both. The intensity of the peaks increased markedly for the heat-treated microspheres, presumably as a result of increased crystallization.

The FTIR spectrum of the as-prepared glass (Fig. 2b) was similar to that of a binary Li_2O-$3B_2O_3$ glass [22, 23], consisting of two broad resonances, at 600-750 cm^{-1} and 1,200 cm^{-1}, 600 cm^{-1}, which corresponded to vibrations of the trigonal BO_3 groups, and a broad resonance centered at ~975 cm^{-1} corresponding to the vibration of tetrahedral BO_4 groups. The most dominant resonances for the converted microspheres (as-prepared

or heat-treated) were the phosphate v3 resonance, centered at ~1,040 cm^{-1}, and the phosphate v4 resonance, with peaks at ~605 and 560 cm^{-1}, which are associated with crystalline HA [24, 25]. EDS analysis (Fig. 2c) showed that Ca and P were the main metallic elements present in the converted microspheres.

SEM images of the surface and cross section of the hollow HA microspheres, as-prepared and after heat treatment for 5 h at 600°C and 900°C, are shown in Fig. 3. As-prepared, the surface of the microspheres consisted of a mesoporous structure of fine, plate-like (or needle-like) HA particles (Fig. 3a). The cross section (Fig. 3b) shows that the shell wall consisted of two distinct layers: a less porous surface layer of thickness ~5 µm and a more porous inner layer. Heating for 5 h at 600°C did not produce a measurable change in the porosity of the hollow HA microspheres, but resulted in a marked change in the surface microstructure (Fig. 3c). The particles in the surface layer have a more rounded morphology, with a size <50 nm. Except for coarsening, little change in the microstructure of the inner layer of the shell wall is observed (Fig. 3d). Heating for 5 h at 900°C resulted in a porous surface layer (Fig. 3e), but the cross section of the shell wall appeared to be almost fully dense (Fig. 3f).

Figure 4 shows the effect of heating time at 600°C on the microstructure of the surface layer of the hollow HA microspheres. Heating for 1 h resulted in a fairly homogeneous microstructure of nearly rounded HA particles (or grains) (Fig. 4a, b). After 5 h, coarsening of the surface microstructure increased (Fig. 4c), but the cross section showed a more heterogeneous microstructure, consisting of a less porous layer (red arrow) between two more porous layers (Fig. 4d). For the HA microspheres heated

for 24 h, the microstructure of the surface layer appeared to be a coarsened version of that for the microspheres heated for 5 h (Fig. 4e, f).

3.4.2 Strength of Hollow HA Microspheres.

The rupture strength of the as-prepared hollow HA microspheres (200–250 μm) was 11 ± 6 MPa (Table 1). After heating for 1 h at 600°C, the rupture strength increased to 17 ± 8 MPa, while heating for 5 h at 900°C resulted in a further increase in the rupture strength (30 ± 10 MPa).

3.4.3 Biocompatibility of Hollow HA Microspheres.

Figure 5 shows optical images of MC3T3-E1 cells (stained with Sanderson Bone Stain™) on hollow HA microspheres after culture times of 2, 4, and 6 days. (The inset shows SEM images of the same constructs.) The cells seen in the micrographs appeared to attach to the HA microspheres by day 2, and increased in density with the culture duration (Figs. 5b, c). After 4 days, the cells tried to colonize the surface of the spheres. The cells were in physical contact with each other and aggregated with the neighboring cells via extensions (Fig. 5b; inset). The optical and SEM images for the 6-day culture show almost complete coverage of the scaffolds with the MC3T3-E1 cells and increased cell density (Fig. 5c; inset). Viewed as a group, the continuous increase in cell density during the 6 days culture period shows the ability of the hollow HA microspheres to support cell proliferation.

3.4.4 Loading and Distribution of BSA in Hollow HA Microspheres.

Optical images of the as-prepared hollow HA microspheres prior to loading with FITC-labeled BSA showed no fluorescence (Fig. 6a). The brightness of the image was enhanced, and the microspheres were circled to reveal their presence. In comparison, the

surfaces of the microspheres filled with the FITC-labeled BSA solution showed a high degree of fluorescence, indicating the presence of BSA (Fig. 6b). In order to show the distribution of the BSA, after filling with the BSA solution and drying, the microspheres were sectioned and observed in the microscope. The fluorescence in Fig. 6b (inset) shows that the BSA was incorporated within the hollow core of the microspheres as well as within the mesoporous shell wall.

3.4.5 Release Kinetics of BSA from Hollow HA Microspheres.

Figure 7 shows the BSA release kinetics from the BSA-loaded HA microspheres into a PBS solution, for the as-prepared microspheres and for microspheres heat treated for 5 h at 600°C or 900°C. For the as-prepared HA microspheres, the release of BSA was initially rapid (~2.0 μg/ml/h) during the first 10 h, then slowed considerably, with 95% of final amount released within 24 h, and almost ceased after 24–48 h. The total amount of BSA released into the PBS was ~22 μg/ml. Heating the as-prepared microspheres for 5 h at 600°C resulted in a marked increase in the amount and duration of the BSA released into the PBS. The amount of BSA released was comparable to that for the as-prepared microspheres during the first 48–72 h, then continued to increase, with 95% of final amount released in 7 days, and almost ceased after 14 days. The total amount of BSA released (after 14 days) was ~35 μg/ml.

For the HA microspheres heated for 5 h at 900°C, release of the BSA from the microspheres into the PBS was limited. The cumulative amount of BSA released after 3–5 h was ~2 μg/ml, and it remained at this value thereafter. The release of BSA from hollow HA microspheres heated for 5 h at 700°C was also studied. The trend in the

release kinetics was approximately similar to that for the HA microspheres heated for 5 h at 900°C, and the results are omitted for the sake of brevity.

The effect of heating the as-prepared HA microspheres for varying times (1–24 h) at 600°C on the BSA release kinetics is shown in Fig. 8. For a heating time of 1 h, the release kinetics showed a trend similar to that for the as-prepared microspheres, but the total amount of BSA released was far higher (~35 vs. ~22 μg/ml). As discussed above, an increase in the heating time to 5 h at 600°C had a marked effect on the release kinetics. When compared to the microspheres heated for 1 h, the duration of the release increased (7–14 days) but the total amount of BSA released (~35 μg/ml) was approximately the same. For a longer heating time (24 h) at 600°C, the duration of the release did not increase further. Instead the duration of the release became shorter, with 95% of the final amount released after 3 days, and BSA release almost ceased after 4–5 days. However, the total amount of BSA released (~35 μg/ml) was approximately the same as that for microspheres heated for 1 or 5 h.

Figure 9 shows the effect of varying the amount of BSA loaded into the hollow HA microspheres (1–10 mg BSA per ml of PBS) on the release kinetics. The microspheres used in these experiments were heated for 5 h at 600°C. For a BSA concentration of 1 mg/ml, the total amount of BSA released was limited (~5 μg/ml). Higher BSA loading markedly enhanced the amount of BSA released, as well as the duration of the release. The release kinetics from microspheres loaded with 10 mg/ml BSA followed the same trend as those for microspheres loaded with 5 mg/ml BSA, but

the total amount of BSA released was higher (45 μg/ml compared to 35 μg/ml) after 14 days.

3.5 DISCUSSION

The results of the present investigation show that hollow HA microspheres, prepared by a low-temperature glass conversion route, have promising potential for use as a controlled delivery device for proteins. By modifying the microstructure of the as-prepared hollow HA microspheres using a controlled heat treatment, and varying the concentration of BSA initially loaded into the microspheres, both the amount of protein (BSA) released from the microspheres into a PBS medium and the duration of the release (1–14 days) were controlled. These HA microspheres, consisting of the same ions as human bone, could provide a novel inorganic system for controlled delivery of proteins, such as growth factors and drugs.

Our previous work showed that the microstructure of hollow HA microspheres prepared by converting $Li_2O–CaO–B_2O_3$ glass microspheres in a K_2HPO_4 solution can be modified over a wide range by controlling the process variables, such as the conversion temperature, K_2HPO_4 concentration and pH of the solution [18]. In this study, a group of as-prepared HA microspheres with a mesoporous shell wall (average pore size = 13 nm), high surface area (~100 m^2/g), and a hollow core diameter, *d*, equal to 0.6 the external diameter, *D*, of the microspheres, was evaluated as a delivery device for a model protein, BSA. Based on their ability to support the proliferation of MC3T3-E1 cells, the as-prepared HA microspheres prepared by this glass conversion route were shown to be biocompatible (Fig. 5).

The present study showed that the microstructure of the as-prepared HA microspheres can be further modified by a controlled heat treatment at temperatures between approximately 600 and 900°C. Modification of the microstructure by heat treatment resulted in the ability to markedly influence the release of BSA from the microspheres into a PBS. Both the amount of BSA released as well as the duration of the release was influenced by the heat treatment. The microstructural changes produced by the heat treatment and, hence, the ability to control the BSA release kinetics, were dependent on the time–temperature schedule used in the heat treatment.

Upon heating the as-prepared hollow HA microspheres, surface diffusion presumably dominated at lower temperatures (e.g., approximately 600°C or below), resulting in rounding of the high surface area plate-like (or needle-like) particles present in the microspheres, as well as coarsening of the pores and particles (Figs. 3a–3d). These processes are driven by the need of the system to reduce its surface free energy [26]. At these lower temperatures, there is rearrangement of the porosity but little or no reduction in the total porosity of the shell wall. At higher temperatures, other types of matter transport processes become more dominant, resulting in actual densification of the shell wall (reduction in the porosity). At 900°C, densification dominated to the extent that the shell wall became almost fully dense, although some porosity remained on the microsphere surface (Fig. 3e, 3f).

Using an FITC-labeled BSA, it was clearly shown that the hollow HA microspheres can be loaded with BSA by immersing the microspheres in a solution of BSA in PBS and applying a small vacuum to replace the entrapped air with the solution

(Fig. 6). Furthermore, it was shown that the BSA loaded into the microspheres was distributed both in the pores of the shell wall and in the hollow core.

The release of BSA from the as-prepared HA microspheres into a PBS medium was rapid, and essentially ceased after 24–48 h (Fig. 7). The cumulative amount of BSA in the medium when the release of BSA ceased was ~22 μg/ml. Little release of BSA was found for the HA microspheres heated for 5 h at 900°C. As described earlier, SEM observation showed that the shell wall for this group of HA microspheres was dense (Fig. 3f), so presumably no BSA was loaded into the microspheres. The little BSA released was presumably due to BSA adsorbed on the surface of the microspheres.

Heating the as-prepared HA microspheres for varying times (1–24 h) at 600°C provided the most favorable conditions for manipulating the amount and duration of the BSA released from the microspheres (Fig. 8). Presumably, the transition from coarsening of the microstructure to densification of the shell wall occurred above this temperature, and the heating time provided an additional variable to modify the microstructure. With the smallest heating time (1 h), the amount of BSA released at any time was far higher than that for the as-prepared HA microspheres, but the duration of release was approximately the same (24–48 h). Coarsening apparently resulted in a fairly homogeneous surface layer (Fig. 4a, b). The larger pores presumably allowed more BSA to be loaded into the microspheres, as well as faster release through the microsphere wall. When heated for longer time (5h), rearrangement of the porosity during the coarsening process presumably resulted in the formation of a less porous layer (Fig. 4d; arrow) within the coarsened surface layer. This resulted in a more sustained release of BSA, over a period of 7-14 days. With a longer heat treatment (24h), the release of BSA from the

microspheres was initially faster that for the microspheres heated for 5 h, but the duration of the release was shorter (4-5 days). For the 24 h heating, the microstructure of the surface layer of the microspheres (Fig. 4f) appeared to be a coarsened version of that for the microspheres heated for 5 h (Fig. 4d); this resulted in faster release kinetics because of the easier migration of the BSA molecules through the larger pores. Although the duration of the BSA release was different, Fig. 8 showed that the cumulative amount of BSA released (32–35 μg/ml) was approximately independent of the heating time at 600°C. The coarsening of the microstructure at nearly constant pore volume coupled with the small difference in surface area (Table I) resulted in approximately the same amount of BSA loaded into the microspheres and released into the PBS.

The amount of BSA released from the hollow HA microspheres can also be varied by changing the concentration of BSA initially loaded into the microspheres (Fig. 9). At any time, the cumulative amount of BSA released into the PBS increased with the amount of BSA initially loaded into the microspheres. Furthermore for BSA concentrations of 5 and 10 μg/ml loaded into the microspheres, the release kinetics showed the same trend, indicating that the mechanism of BSA release was the same for these two concentrations (Table II).

As described earlier, release of BSA from the as-prepared or heat-treated HA microspheres effectively ceased within 1–14 days. Taking the amount released after 14 days as the final value, the data for the fractional amount of BSA released (α) as a function of time (t) were fitted by a least-squares regression analysis using software (Fig. 10). For the microspheres heated for 5 h at 600°C (Fig. 10a), the fractional release data could be well fitted by a power-law equation:

$$\alpha = kt^n \quad (1)$$

where k and n are constants, with the values $k = 0.26$ and $n = 0.25$ for this group (Table III). The coefficient of determination, R^2, which represents the goodness of the fit to the data, was equal to 0.94. The fractional release data for different concentrations of BSA loaded into the microspheres (5 and 10 mg/ml) lie on the same curve, indicating that the release mechanism was independent of the concentration.

Figure 10b shows that the BSA release from the as-prepared HA microspheres and the microspheres heated for 1 h at 600°C could be well fitted by a different power-law equation:

$$\alpha = \frac{kt^n}{c + t^n} \quad (2)$$

where the constants $k = 0.96$; $c = 4.08$, and $n = 1.43$ ($R^2 = 0.95$). The fractional release data for these two groups lie on the same curve, indicating the same BSA release mechanism. Table III summarizes the constants in Eqs. 1 and 2 for the different groups of HA microspheres.

Equation 1 was introduced to describe the general release of drugs and other solutes by diffusion from non-swellable polymer devices in the shape of slabs, spheres, cylinders, and discs [27]. The exponent n is characteristic of the shape of the device, with $n = 0.43$ for spheres of the same size. In the present work, using hollow HA microspheres with an external diameter in the range 106–150 μm, which were heated for 5 h at 600°C, the release data can be well fitted by Eq. 1 but the value of the exponent ($n = 0.25$) is smaller than the predicted value of 0.43. In comparison, the BSA release from the as-prepared HA microspheres and the microspheres heated for 1 h at 600°C cannot be well

fitted by Equation 1; this may indicate that the release is not controlled by a diffusion process, and that the release mechanism for these two groups of microspheres is different from that for the microspheres heated for 5 h at 600°C.

The amount of BSA loaded into the HA microspheres was determined from the final cumulative amount released into the PBS, plus the amount remaining in the microspheres. For the as-prepared HA microspheres, the total BSA loading was ~50 mg per gram of HA microspheres. The cumulative amount released was ~22 mg per gram of HA microspheres, indicating that ~40% of the total amount of BSA initially loaded into the HA microspheres was released into the PBS. In the case of the HA microspheres heated at 600°C, the total amount of BSA loaded into the HA microspheres was 115~126 mg per gram HA, of which ~35 mg (~30%) was released into the PBS.

The results described above showed that only 30–40% of the BSA initially loaded into the HA microspheres was released into the PBS. The factors that limit the release of larger amounts of BSA into the PBS are not clear. However, it should be recalled that loading of the BSA solution into the hollow HA microspheres was assisted by a small pressure gradient, resulting from the application of a small vacuum to the system to remove the air from within the hollow HA microspheres. On the other hand, the release of the BSA into the PBS was driven by the concentration gradient of BSA between the HA microspheres and the PBS. As the concentration gradient decreased with time, the release of BSA became slower, and eventually ceased.

The structure (conformation) of the BSA molecule is the subject of some controversy, but based on hydrodynamic experiments, BSA is reported to take up the shape of an oblate ellipsoid with dimensions of 14 nm and 4 nm along the long and short

axis, respectively [28]. The average pore size of the shell wall of the as-prepared HA microspheres was 13 ± 2 nm, approximately equal to the long dimension of the BSA molecules. As indicated above, during the loading step, the application of a small vacuum to the system produced a pressure difference between the surface and the interior of the hollow microspheres as the air was removed from the microspheres. This pressure difference, coupled with some alignment of the ellipsoidal BSA molecules during liquid flow, presumably facilitated the migration of the BSA molecules into the pores of the shell wall and into the hollow core.

After the microspheres are filled, release of the BSA into a surrounding PBS medium (Fig.11) is controlled by their ability to diffuse through the pores of the microsphere wall down the BSA concentration gradient between the interior of the microspheres and the surrounding medium. Interaction between the functional groups of the BSA and the pore surfaces of the hollow HA microspheres could also influence the BSA release. The pH value of the PBS was 7.2, while the isoelectric point BSA is reported as 4.7, with a net surface potential of –18 mV at pH = 7.0 [28]. The isoelectric point of hydroxyapatite depends on a few factors, such as preparation method and composition, but it has been reported in the range of 7.4–8.0 [29]. Therefore, at pH = 7.2 (the pH of the PBS), the HA surface should be almost neutral or should carry only a small positive surface charge. Electrostatic interaction between the oppositely-charged HA surface and the BSA molecules could enhance adsorption, limiting the amount of BSA released.

3.6 CONCLUSION

Hollow hydroxyapatite (HA) microspheres (106–150 μm) with a hollow core diameter equal to 0.6 the external diameter and a mesoporous shell wall were prepared by a low temperature glass conversion route and evaluated as a device for controlled delivery of a model protein, bovine serum albumin (BSA). Both the hollow core and the mesopores of the shell wall were loaded with a solution of BSA. Release of the BSA from the as-prepared HA microspheres increased linearly time, and ceased after 24–48 h. The amount of BSA released from the microspheres and the duration of the release was varied by heat treating the as-prepared HA microspheres to modify their microstructure. For HA microspheres heated for 5 h at 600°C, 30–40% of the BSA initially loaded into the microspheres was released over 7–14 days. In general, the present results show promising potential for the application of these hollow HA microspheres as a device for controlled local delivery of proteins such as growth factors and drugs.

3.7 ACKNOWLEDGEMENT: This work was supported by the National Institute of Dental and Craniofacial Research, National Institutes of Health, Grant # 1R15DE018251-01.

3.8 REFERENCES

1. Mallapragada SK, Narasimhan B**.** Drug delivery systems. In van Recaum AF, editor. Handbook of biomaterials evaluation. 2nd ed. Philadelphis: Taylor & Francis; 1999. P.425–37.
2. Sinha VR, Trehan A. Biodegradable microspheres for protein delivery. J Control Release. 2003;90:261–80.
3. Tabata Y. Tissue regeneration based on growth factor release. Tissue Eng. 2003;9 (Suppl. 1):S5–S15.
4. Chen RR, Mooney DJ. Polymeric growth factor delivery strategies for tissue engineering. Pharm Res. 2003;20:1103–12.
5. Ma S, Chen G, Reddi AH. Collaboration between collagenous matrix and osteogenin is required for bone induction. Ann NY Acad Sci. 1990;580:525–35.
6. McPherson JM. The utility of collagen-based vehicles in delivery of growth factors for hard and soft tissue wound repair. Clin Mater. 1992;9:225–34.
7. Cleek RL, Ting KC, Eskin SG, Mikos AG. Microparticles of poly(DL-lactic-co-glycolic acid)/poly (ethylene glycol) blends for controlled drug delivery. J Control Release. 1997;48:259–68.
8. Ono I, Ohura T, Murata M, Yamaguchi H, Ohnuma Y, Kuboki Y. A Study on bone induction in hydroxyapatite combined with bone morphogenetic protein. Plast Reconstr Surg. 1992;90:870–9.

9. Ripamonti U, Ma S, Van den Heever B, Reddi AH. Osteogenin, a bone morphogenetic protein, adsorbed on porous hydroxyapatite substrata, induces rapid bones differentiation in calvarial defects of adult primates. Plast Reconstr Surg. 1992;90:382–93.
10. Ripamonti U. Osteoinduction in Porous Hydroxyapatite implanted in heterotopic sites of different animal models. Biomaterials. 1996;17:31–5.
11. Matsumoto T, Okazaki M, Inoue M, Yamaguchi S, Kusunose T, Toyonaga T, et al. Hydroxyapatite particles as a controlled release carrier of protein. Biomaterials. 2004;25:3807–12.
12. Peng Q, Ming L, Jiang C X, Feng B, Qu SX, Weng J. Preparation and characterization of hydroxyapatite microspheres with hollow core and mesoporous shell. Key Eng Mater. 2006;309–311:65–8.
13. Day DE, Conzone SA. Method for preparing porous shells or gels from glass particles. US Patent No. 6,358,531, March 19, 2002.
14. Day DE, White JE, Bown RF, McMenamin KD. Transformation of borate glasses into biologically useful materials. Glass Technol. 2003;44:75–81.
15. Conzone SD, Day DE. Preparation and properties of porous microspheres made from borate glass. J. Biomed. Mater Res Part A. 2009;88:531–42.
16. Wang Q, Huang W, Wang D, Darvell BW, Day DE, Rahaman MN. Preparation of hollow hydroxyapatite microspheres. J Mater Sci: Mater Med. 2006;17:641–6.

17. Huang W, Rahaman MN, Day DE, Miller BA. Strength of hollow microspheres prepared by a glassc process. J Mater Sci: Mater Med. 2009;20:123–9.

18. Fu H, Rahaman MN, Day DE. Effect of process variables on the microstructure of hollow hydroxyapatite microspheres prepared by a glass conversion process. J Am Ceram Soc. 2010;93:3116–23.

19. Coleman NJ, Hench LL. A Gel-derived mesoporous silica reference materials for surface analysis by gas sorption, 1, textural features. Ceram Int. 2000;26:171–8.

20. Barrett EP, Joyney LG, Halenda PP. The determination of pore volume and area distributions in porous substances I: computations from nitrogen isotherms. J Am Chem Soc. 1951;73:373–80.

21. Smith PK. Measurement of protein using bicinchoninic acid. Anal Biochem. 1985;150:76–85.

22. Verhoef AH, DenHartog HW. Infrared spectroscopy of network and cation dynamics in binary and mixed alkali borate glasses. J Non-Cryst Solids. 1995;182:221–34.

23. Verhoef AH, DenHartog HW. Structure and dynamics of alkali borate glasses: a molecular dynamics study. J Non-Cryst Solids. 1995;182:235–47.

24. Clark AE, Hench LL. Early stages of calcium-phosphate layer formation in Bioglass. J Non-Cryst Solids. 1989;113:195–202.

25. Filgueiras MR, LaTorre G, Hench LL. Solution effects on the surface reaction of a bioactive glass. J Biomed Mater Res. 1993;27:445–53.

26. Rahaman M N. Sintering of Ceramics. Boca Raton: CRC Press; 2007. p.388.

27. Ritger PL, Peppas NA. A simple equation for description of solute release I. Fickian and non-Fickian release from non-swellable devices in the form of slabs, spheres, cylinders or discs. J Control Release. 1987;5:23–36.
28. Peters T. Serum Albumin. Adv Protein Chem. 1985;37:161–245.
29. Rahaman MN. Ceramic Processing. Boca Raton: CRC Press; 2006. p.473.

Table I. Characteristics of as-prepared hollow HA microspheres formed by reacting $Li_2O–CaO–B_2O_3$ glass microspheres (106–150 μm) in K_2HPO_4 solution, and after heat treatment under the temperature/time conditions shown

Sample	*d*/*D*	Surface area (m^2/g)	Rupture strength* (MPa)
As-prepared	0.61 ± 0.03	102	11 ± 6
600°C/1 h	0.61 ± 0.03	21	17 ± 8
600°C/5 h	0.62 ± 0.03	19	–
600°C/24 h	0.66 ± 0.02	14	23 ± 14
700°C/5 h	0.73± 0.02	7	–
900°C/5 h	0.80± 0.02	2	30 ± 10

The ratio of hollow core diameter to microsphere diameter, *d*/*D*; specific surface area, and rupture strength are shown.

*Measured for HA microspheres of size 200–250 μm prepared under the same conditions.

Table II. Data for release of BSA from hollow HA microspheres into a medium of PBS.

Sample	BSA loading (mg BSA/g HA)	BSA released (mg BSA/g HA)	BSA released/ BSA loaded (%)	Duration (days)
As-prepared	56	22	44	1–2
600°C/1 h	126	35	30	1–2
600°C/5 h	119	35	30	7–14
600°C/24 h	115	32	30	4–5
700°C/5 h	19	2	–	<1
900°C/5 h	<5	2	–	<1

Table III. Parameters of equations used to fit the BSA release data from the as-prepared HA microspheres and the HA microspheres heat-treated HA at 600°C for the times shown.

HA microspheres	Loading concentration of BSA (mg/ml)	Equation	Parameters
As-prepared	5	$\alpha = kt^n/(c + t^n)$	k = 0.96; n = 1.43; c = 4.08; (R^2 = 0.95)
600°C/1 h	5		
600°C/5 h	5	$\alpha = kt^n$	k = 0.26 ; n = 0.25 (R^2 = 0.94)
600°C/5 h	10		
600°C/24 h	5	$\alpha = kt^n/(c + t^n)$	k =1.20; n = 0.55; c=2.40; (R^2 = 0.96)

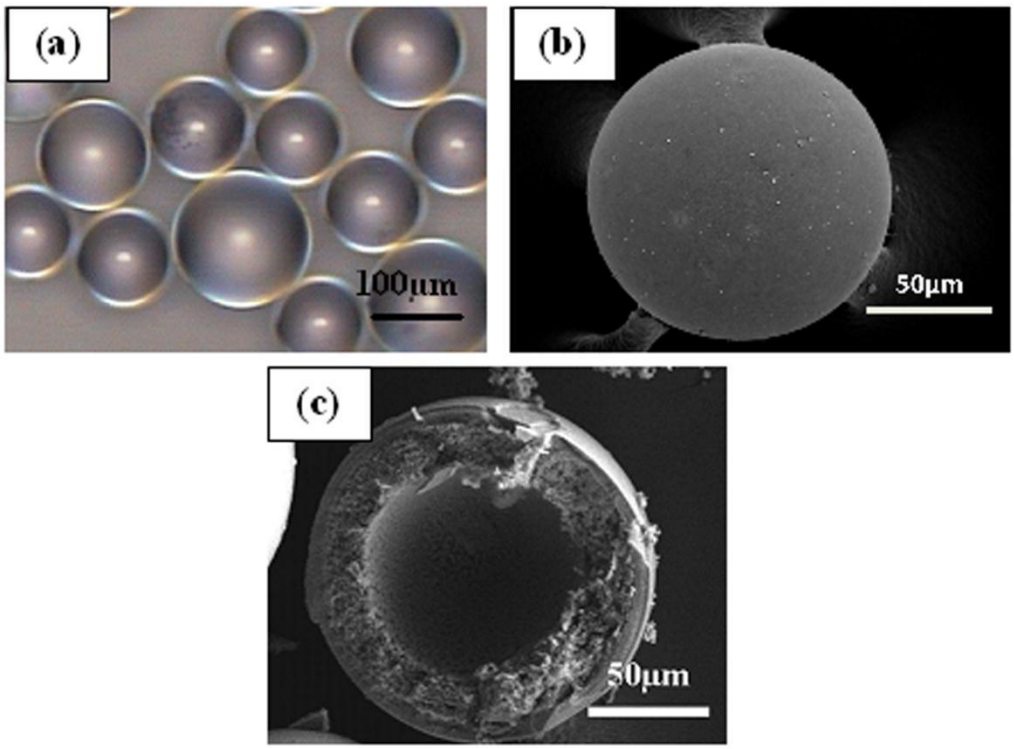

Figure 1. (a) Optical image of starting glass (CaLB3-15) microspheres, and SEM images of (b) external surface of hollow HA microsphere prepared by converting the glass microspheres for 48 h in 0.02M K_2HPO_4 solution at 37°C and pH = 9, (c) cross section of hollow HA microsphere.

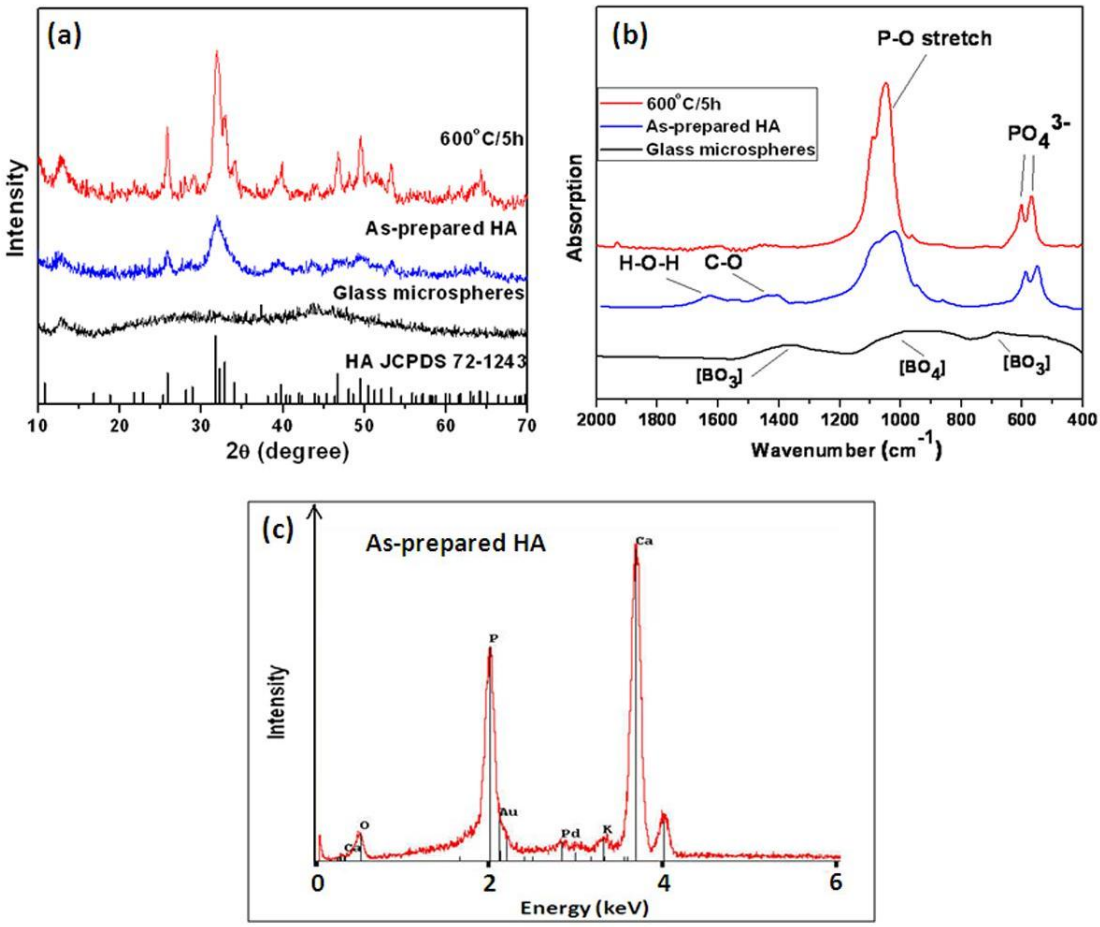

Figure 2. (a) XRD patterns and (b) FTIR spectra of the starting glass microspheres, the as-prepared hollow HA microspheres, and the hollow HA microspheres heated for 5 h at 600°C; (c) EDS spectrum of the as-prepared hollow HA microspheres.

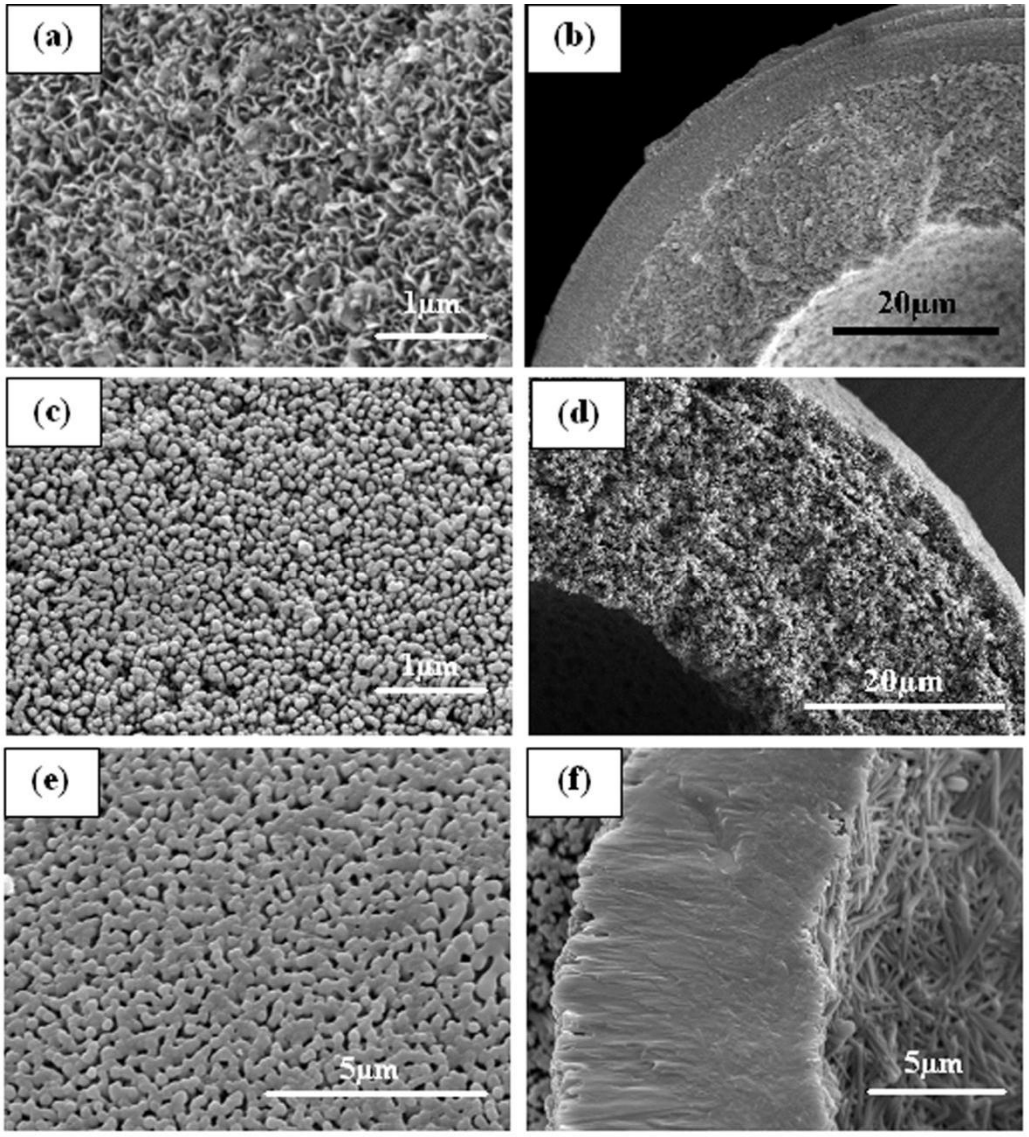

Figure 3. SEM images of the surface (*left*) and cross section (*right*) of the shell wall of hollow HA microspheres: (a, b) as-prepared; (c, d) heated for 5 h at 600°C; (e, f) heated for 5 h at 900°C.

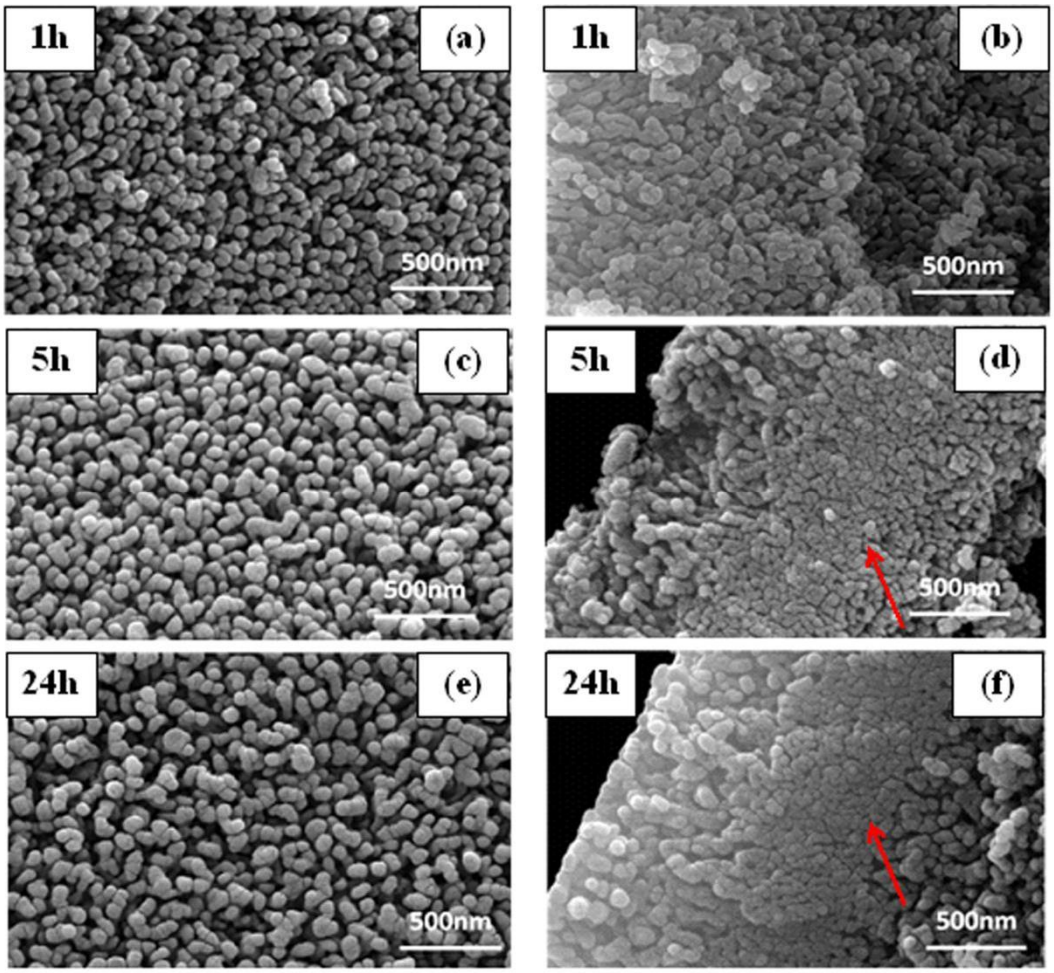

Figure 4. SEM images of the surface (*left*) and cross section (*right*) of the surface layer of the hollow HA microspheres after heat treatment at 600°C for (a, b) 1 h; (c, d) 5h; (e, f) 24 h, showing coarsening of the pores and particles, and the formation of less porous layer (*arrow*) within the surface layer.

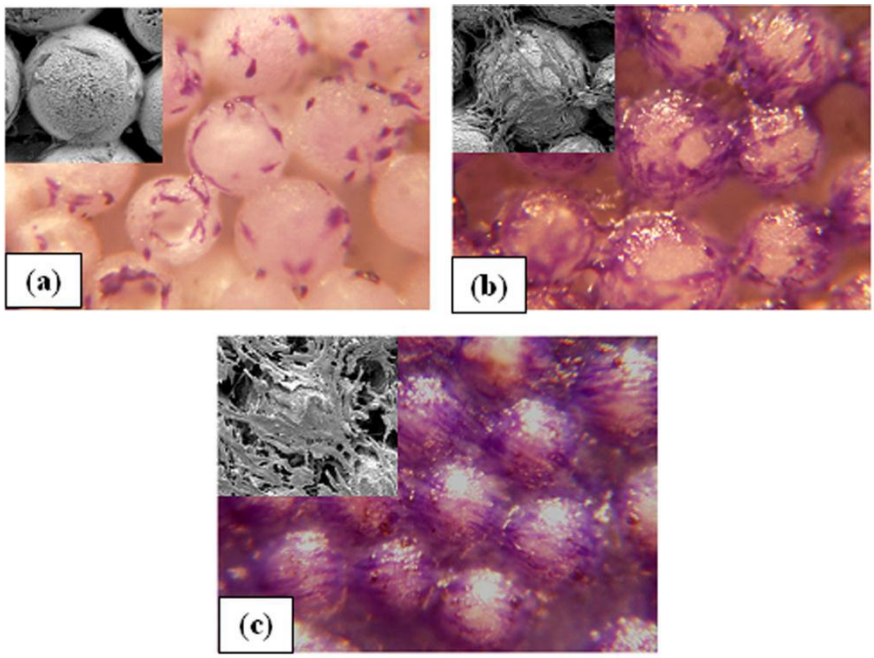

Figure 5. Optical images and SEM images (*inset*) of MC3T3-E1 cell morphology on hollow HA microsphere(106–150μm) after culturing for (a) 2, (b) 4 and (c) 6 days.

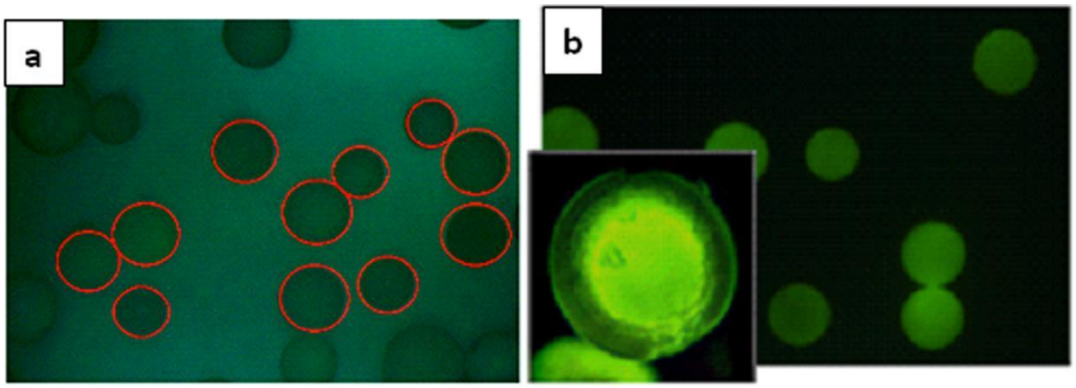

Figure 6. Optical images of the surface of (a) as-prepared HA microspheres (brightness enhanced to show microspheres (circles)), and (b) HA microspheres loaded with fluorescent FITC-labeled BSA. (Inset: cross section of microspheres loaded with FITC-labeled BSA.) (Diameter of microspheres = 106–150 µm)

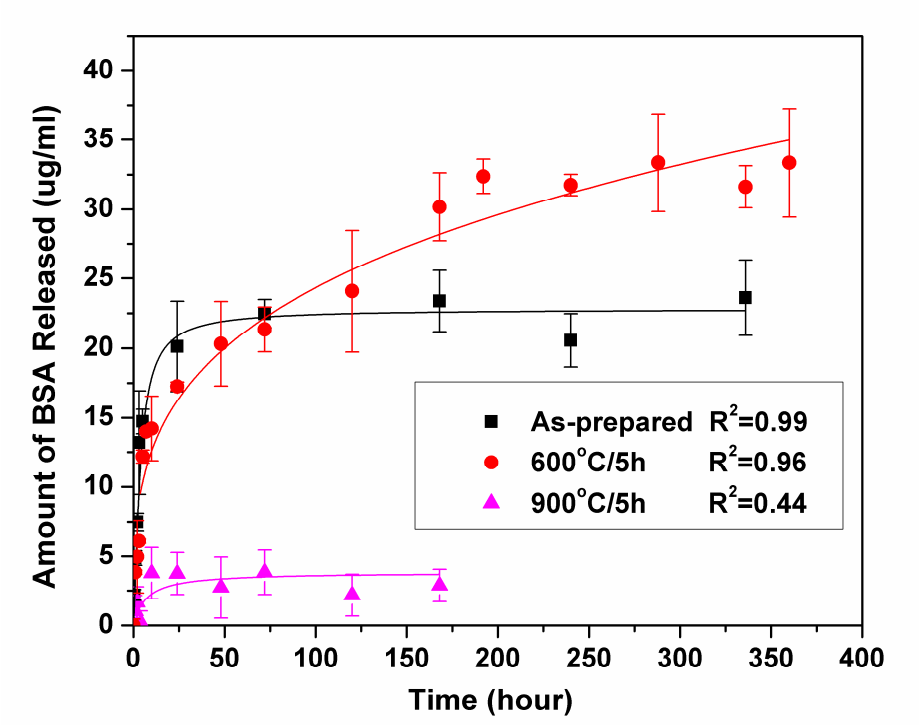

Figure 7. Amount of BSA released from hollow HA microspheres into PBS, for the as-prepared HA microspheres, and after heat treatment under the conditions shown. (The R^2 value for each fitted curve is also shown.)

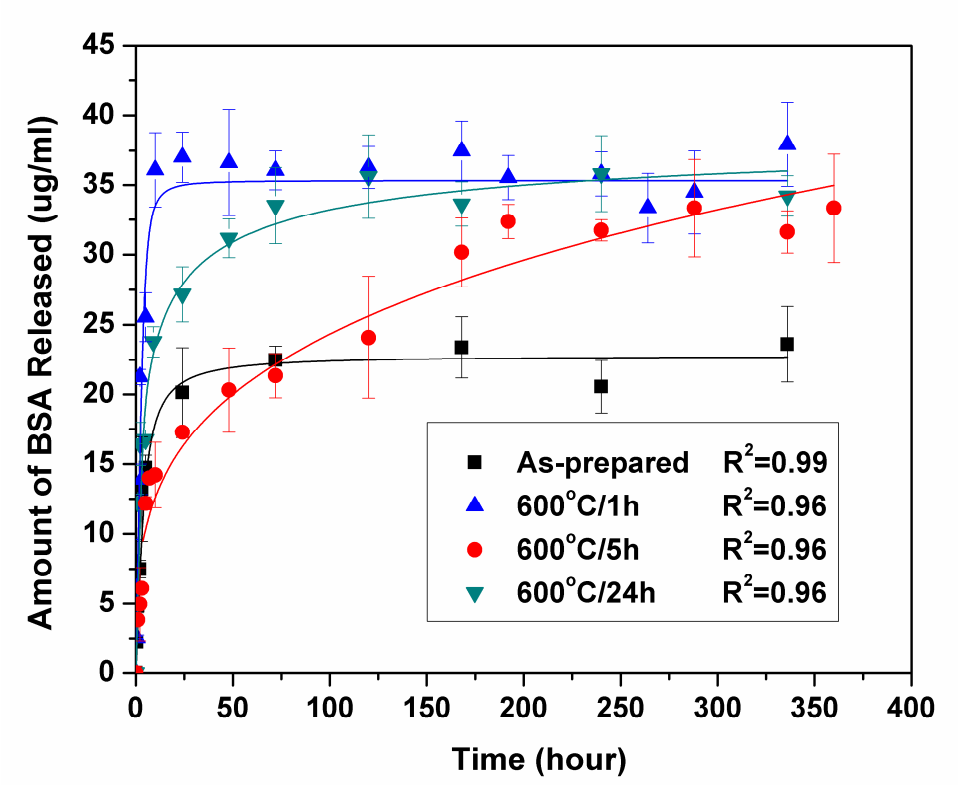

Figure 8. Amount of BSA released from hollow HA microspheres heat treated at 600°C for the times shown (1–24 h). The data for BSA released from the as-prepared HA microspheres are shown for comparison. (The R^2 value for each fitted curve is also shown.)

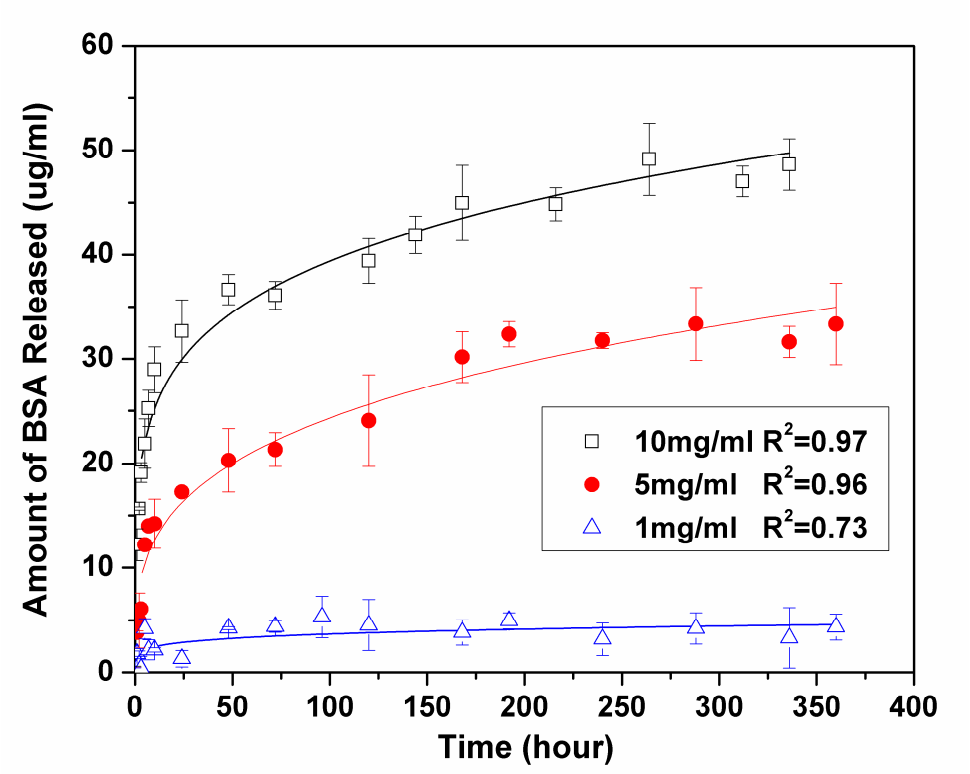

Figure 9. Amount of BSA released from hollow HA microspheres heat treated at 600°C for 5h, for different concentrations of BSA loaded into the microspheres. (The R^2 value for each fitted curve is also shown.)

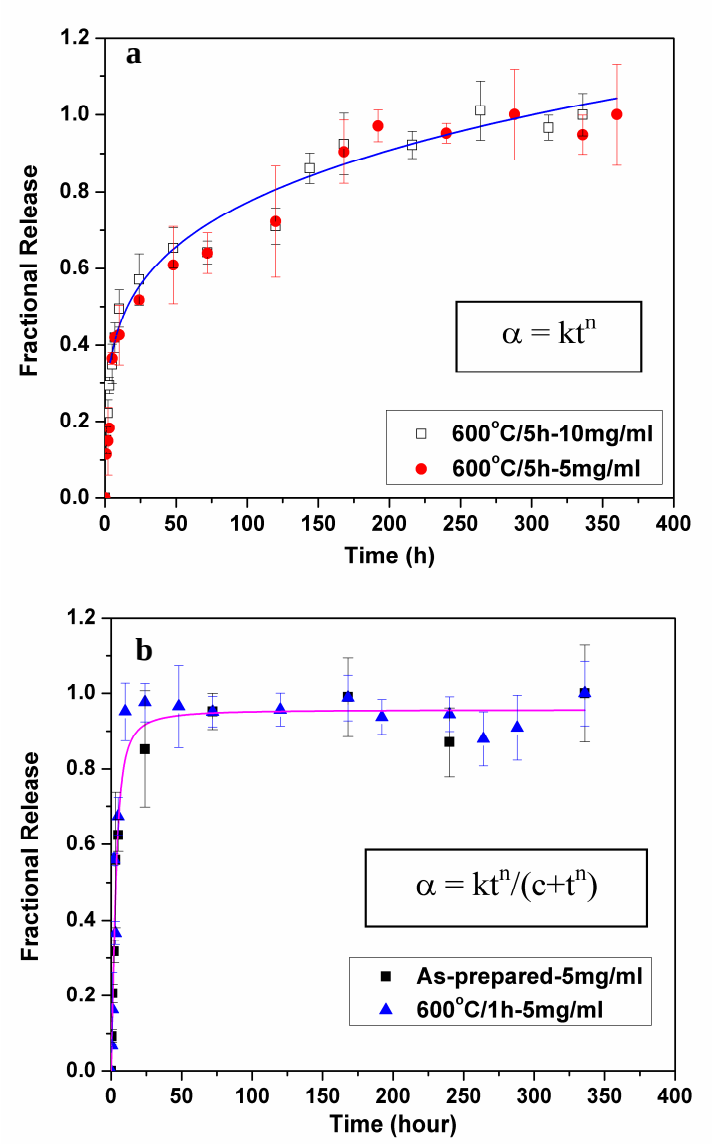

Figure 10. Least-squares regression fit to the data for the BSA release (as a fraction of the final amount released) vs. time: (a) Release from microspheres heated for 5 h at 600°C for two different BSA loading (5 and 10 mg/ml); (b) Release from the as-prepared HA spheres and the microspheres heated for 1 h at 600°C (BSA loading = 5 mg/ml).

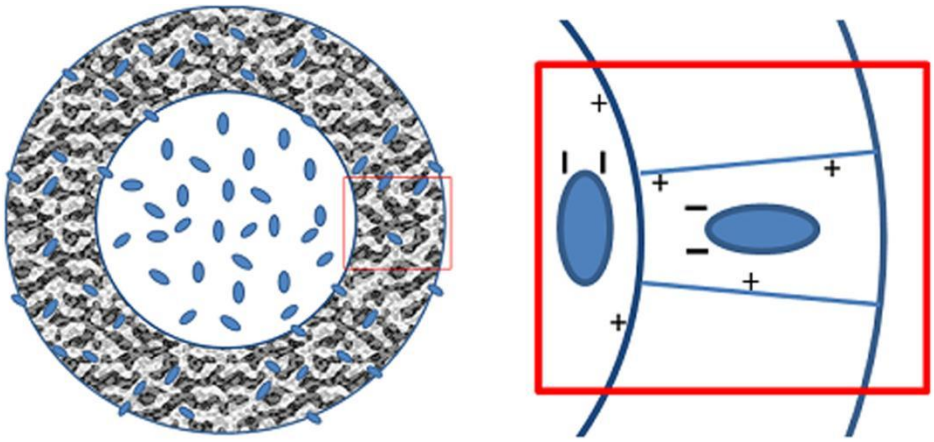

Figure 11. Qualitative model illustrating the release of BSA from hollow HA microspheres into PBS medium. (*Left*): Cross section of HA microsphere showing BSA molecules (ellipsoids) located in the hollow core and mesoporous shell wall; (*Right*): Magnified view of an idealized pore in the shell wall and BSA molecules (ellipsoids). At the pH value of the PBS (7.2), the HA surface should have a small positive (+) charge (isoelectric point = 7.4–8.0), while the BSA molecules should have a negative (–) charge (isoelectric point ≈ 4.7).

4. EVALUATION OF BSA PROTEIN RELEASE FROM HOLLOW HA MICROSPHERES INTO PEG HYDROGEL

Hailuo Fu[1], Mohamed N. Rahaman[1], Roger Brown[2], Delbert E. Day[1]

[1]Department of Materials Science and Engineering, Missouri University of Science and Technology, Rolla, MO 65409, USA

[2]Department of Biological Sciences; Missouri University of Science and Technology, Rolla, MO 65409, USA

4.1 ABSTRACT

Hollow hydroxyapatite (HA) microspheres with a mesoporous shell wall can provide a unique inorganic system for bone regeneration by simultaneously functioning as a device for local delivery of growth factors or drugs and as an osteoconductive matrix. In our previous work, the characteristics of the hollow HA microspheres and the release of a model protein (bovine serum albumin, BSA) from the microspheres into phosphate-buffered saline (PBS) were studied. In the present work, the release of BSA from similar HA microspheres into poly (ethylene glycol), PEG, hydrogel, used to mimic the extracellular matrix, was evaluated. BSA-loaded HA microspheres were placed in PEG solution which was rapidly gelled using ultraviolet radiation. The release of the BSA into PEG hydrogel, measured using spectrophotometry, was dependent on the initial BSA loading and on the HA microstructure, and was far slower than into PBS. A total of 35–40% of the BSA initially loaded into the microspheres was released into PEG over ~14 days. The results indicate that these hollow HA microspheres have promising potential as an osteoconductive device for local delivery of proteins or drugs in bone regeneration and in the treatment of bone diseases.

Keywords: protein release; hydroxyapatite microspheres; bovine serum albumin; poly(ethylene glycol) hydrogel; controlled release

4.2 INTRODUCTION

The regeneration of bone lost as a result of trauma, bacterial infection of prosthetic implants, and diseases is a major problem in orthopaedic surgery. Local delivery of protein growth factors is often required for tissue regeneration [1,2], while local delivery of high doses of antibiotics is desirable in treating bone infections [3,4]. An ideal system for bone regeneration should simultaneously function as a controlled local delivery device for growth factors or drugs and as an osteoconductive matrix to support bone formation.

Poly (methyl methacrylate) (PMMA) cement is widely used clinically as a carrier material for antibiotics in the treatment of bone infections [4]. However, PMMA is not biodegradable, and provides a surface upon which secondary bacterial infection can occur. Consequently, PMMA must be removed upon completion of the treatment in a further procedure. There has been considerable effort over the last three decades to develop alternative carrier materials to PMMA. Biodegradable polymers, natural or synthetic, are attractive because they reduce the potential risk of secondary infection and the avoidance of a second surgical procedure to remove foreign material. While collagen is the most widely used biodegradable carrier system for growth factors and antibiotics [5,6], the synthetic polymers, such as poly(lactic acid), PLA, and poly(glycolic acid), PGA, and their copolymers, poly(lactic co-glycolic acid), PLGA, have received considerable interest. In addition to being widely available, they can be prepared with

well-controlled, reproducible chemical and physical properties [7–10]. They are also among the few synthetic biodegradable polymers approved by the Food and Drug Administration (FDA) for in vivo use.

Inorganic biomaterials have been investigated as alternatives to the above-mentioned polymeric carrier materials in the repair of hard tissues because they can more closely mimic the physical and chemical properties of bone [11,12]. Calcium sulfate hemihydrate, $CaSO_4.0.5H_2O$ (plaster of Paris, POP), has been widely used as a biodegradable inorganic carrier, but POP has a limited ability to stimulate bone regeneration, high resorption rate, and rapid elution in vitro; in addition, its low mechanical strength prevents its application in load-bearing sites [13−15]. The calcium phosphates such as hydroxyapatite (HA), $Ca_{10}(PO_4)_6(OH)_2$, and beta-tricalcium phosphate (β-TCP), $Ca_3(PO_4)_2$, are attractive because they can provide an osteoconductive matrix for bone regeneration plus a matrix to fill a bone defect [16–18]. The delivery systems typically consist of porous particles, granules, or substrates in which the protein is adsorbed or attached to the surfaces of the porous material, or encapsulated within the pores [19–22]. A disadvantage of those materials is that the release rate of growth factors or antibiotics can be rapid.

Inorganic–organic composites have been receiving increasing interest because they can take advantage of the properties of the different components to better control the release rate of growth factors and antibiotics. The composite carriers often include a microporous HA which provides for greater adsorption of growth factors or drugs, in addition to its osteoconductive properties [23]. Recently, composites of borate glass particles and chitosan loaded with teicoplanin have shown promising results for

simultaneously eradicating bone infection (osteomyelitis) and regenerating bone in a rabbit tibial model [24,25].

In our previous work [26], hollow HA microspheres were prepared using a novel glass conversion process [27], and their characteristics were investigated. The microspheres consisted of a hollow core and a high surface area, mesoporous shell of fine HA particles. Subsequent work showed that a model protein, bovine serum albumin (BSA) can be loaded into the microspheres and that the release rate of the BSA into a phosphate buffered saline (PBS) can be controlled by modifying the microstructure of the shell wall by a controlled heat treatment [28].

This work is a continuation of our previous work to evaluate release of BSA from hollow HA microspheres into a surrounding medium of poly (ethylene glycol), PEG, hydrogel. Hydrogels provide a mimicked environment of the extracellular matrix [29–31], and they have been widely used as a scaffold in tissue engineering. While it is not biodegradable, PEG is used as model photopolymerizable hydrogel. As described previously, BSA was used as a model protein [28]. HA microspheres loaded with BSA were placed in a PEG solution and following photopolymerization with UV radiation, the release of BSA into the PEG was determined as a function of time.

4.3 EXPERIMENTAL PROCEDURE

4.3.1 Preparation and Characteristics of Hollow HA Microspheres.

The preparation of hollow HA microspheres by a glass conversion process is described in detail elsewhere [26]. Two groups of microspheres were used in this work: (1) as-prepared microspheres, formed by reacting borate glass microspheres (106–150

μm) with the composition 15CaO, 10.6 Li_2O, 74.4 B_2O_3 (wt%) (designated CaLB3-15) for 2 days in 0.02 M K_2HPO_4 solution at 37°C, followed by drying for at least 24 h at 90°C, and (2) heat-treated microspheres formed by heating the as-prepared HA microspheres for 5 h at 600°C. The characteristics of the two groups of microspheres are summarized in Table I. These two groups of HA microspheres were used because they showed a large difference in BSA release kinetics into PBS in our previous work [28].

For ease of measuring the BSA release in the present work, the hollow HA microspheres were lightly bonded at their contact points to form thin discs (4.5 mm in diameter × 1.5 mm) with a mass of 10 mg each. The discs were prepared by pouring the borate glass microspheres into a graphite die, heating the system for 1 h at 560°C to lightly bond the glass microspheres at their contact points, and reacting the disc under the conditions described above to convert the glass into hollow HA microspheres.

4.3.2 Loading BSA into Hollow HA Microspheres.

Fluorescein isothiocyanate-labeled bovine serum albumin, referred to as FITC-BSA (molecular weight = 66 kDa; Sigma-Aldrich, St. Louis, MO) was used in order to permit visual observation and spectrophotometric measurement of the BSA released from the disc of microspheres. Ten disks of hollow HA microspheres (mass =10 mg each) were immersed in 2 ml of a solution consisting of 5 mg of FITC-BSA per ml of PBS. A small vacuum was applied to the system to remove air trapped within the microspheres, thereby assisting the incorporation of the FITC-BSA into the microspheres. When the removal of air bubbles from the microspheres had ceased (as determined visually), the discs loaded with FITC-BSA were washed with deionized water twice and dried in air at room temperature in the dark.

4.3.3 Measurement of BSA Release Kinetics From Hollow HA Microspheres into PEG Hydrogel.

Each disc of hollow HA microspheres, loaded with FITC-BSA as described above, was immersed in a solution (1 or 2 ml) of poly(ethylene glycol diacrylate), (molecular weight = 3.4 kDa; Laysan Bio Inc., Arab, AL) in a 12- or 24-well plate. The system was placed for 5 minutes under an ultraviolet lamp (365 nm; Glo-Mark Systems, NY) to crosslink the polymer to form a gel (referred to as PEG hydrogel), sealed with a plate sealer, and stored at room temperature in the dark. At selected times, the samples were removed from the dark, and optical images of the fluorescent FITC-BSA were taken. The amount of FITC-BSA released into the PEG hydrogel, at specific distances from the circumference of the HA disc, was also measured in a BMG FLUORstar Optima plate reader using an excitation wavelength of 490 nm and an emission wavelength of 520 nm. Each well of a 12-well plate contained an HA disc in 2 ml PEG hydrogel; at each selected time, the amount of BSA at different positions in each well was measured in the BMG FLUORstar Optima plate reader using 96-well plate reading program. The concentration of FITC-BSA was determined from a calibration curve determined from measurements of the fluorescent intensity of PEG containing known concentrations of FITC-BSA.

4.4 RESULTS

4.4.1 Microstructure of HA Microspheres.

Figure 1a shows an optical image of a disc (4.5 mm in diameter × 1.5 mm) composed of hollow HA microspheres; an SEM image (Fig. 1b) shows that the HA microspheres were bonded at their contact points. The disc is estimated to have a porosity of ~40%, based on the dense random packing of spheres. SEM images of the surface and

cross section of the two groups of hollow HA microspheres used in this work, as-prepared and heat treated for 5 h at 600°C, are shown in Fig. 2. As-prepared, the surface of the microspheres consisted of a mesoporous structure of fine, plate-like (or needle-like) HA particles (Fig. 2a-inset), while the cross section (Fig. 2a) shows that the shell wall consisted of two distinct layers differing in porosity. The heat treatment for 5 h at 600°C did not produce a measurable change in the porosity of the hollow HA microspheres, but resulted in a marked change in the surface microstructure (Fig. 2b-inset). The particles in the surface layer have a more rounded morphology, with a size <50 nm. Except for coarsening, little change in the microstructure of the inner layer of the shell wall was observed (Fig. 2b). The characteristics of the as-prepared and heat-treated HA microspheres used in this work are presented in Table 1.

4.4.2 Release Kinetics of BSA from Hollow HA Microspheres into PEG Hydrogel.

Figure 3 shows the BSA release kinetics from the HA microspheres loaded with FITC-BSA into a surrounding medium of PEG hydrogel, for the as-prepared and heat-treated HA microspheres. The figure also shows a schematic diagram of the HA microspheres (disc) and the position (center of the hydrogel) at which the BSA concentration was determined. Initially, for the first 4–5 days, there was no difference in the amount of BSA released from both groups of HA microspheres. After this initial period, the BSA released from the as-prepared microspheres slowed considerably, and almost ceased after 5–7 days. The total amount of BSA released was ~25 μg per ml of PEG. In comparison, release of BSA from the heat-treated microspheres continued up to

~14 days, after which time it slowed markedly. The total amount of BSA released after 14 days was ~37μg/ml.

Optical fluorescent images, taken at different times, of the PEG medium surrounding a disc of heat treated HA microspheres loaded with FITC-BSA are shown in Fig. 4. The intensity of green color is an indication of the amount of the FITC-BSA released. As shown, little fluorescence can be observed in the first 1–2 h, but the intensity of the green color becomes very noticeable after 3–4 h, and increased at longer times. The images provide visual evidence for the release of FITC-BSA from the HA microspheres into the PEG hydrogel.

The amount of BSA released into the PEG at three different distances from the edge of the HA disc is shown in Fig. 5 as a function of time. The disc was composed of the heat-treated HA microspheres, and the BSA concentration in the PEG hydrogel was measured near the edge of the disc (position A); 4.5 mm from the edge (B), and 13.5 mm from the edge (C). The BSA concentration at these 3 positions showed a markedly different dependence on time. Near the edge of the disc (A), the BSA concentration in the PEG increased rapidly in the first 2 days, remained nearly constant (~38 μg/ml) during days 2–5, then decreased gradually in the next 3 days to ~35 μg/ml, and remained nearly stable at this concentration for up to 2 weeks. At position B, the BSA concentration increased continuously, with a decreasing slope, and reached a value of ~32 μg/ml after the two-week duration. The BSA concentration at position C initially increased far more slowly than that at B in the first 2–3 days, but then showed an almost linear increase with time in the next 8–10 days, after which the concentration increased slowly to ~33 μg/ml by day 14.

4.5 DISCUSSION

The present system, consisting of protein-loaded hollow HA microspheres dispersed in a hydrogel, can provide an approach for controlled local delivery of growth factors or drugs and an osteoconductive matrix for bone regeneration in a single device. The in vitro results obtained in the present study for BSA release from the hollow HA microspheres in a PEG hydrogel show considerable promise for the eventual use of these hollow HA microspheres in bone repair applications.

The PEG hydrogel, as described earlier, provides a mimicked environment of the extracellular matrix. When compared to the results from our previous work for the release of BSA from similar HA microspheres into PBS [28], the present results for BSA release into the PEG hydrogel showed similarities and differences (Fig. 3). For the same group of HA microspheres, the BSA release into the PEG was far slower initially. However, later in the process when BSA release essentially ceased, the total amount released into the PEG was approximately the same as that into PBS. For example, the BSA release from the as-prepared HA microspheres into PBS increased rapidly and ceased within 1–2 days. In comparison, the release into the PEG increased more slowly and ceased after ~7 days. The total amount of BSA released into the PEG (~25 μg/ml) was approximately the same as that released into PBS. For the heat-treated HA microspheres (600°C/5h), the BSA release into the PEG was initially slower than that into the PBS; however, after ~7 days the release into the PEG continued to increase at approximately the same rate as that into the PBS. The total amount of BSA released from the heat-treated microspheres into the PEG or the PBS was ~37 μg/ml.

Because of the ease of diffusion in a liquid, the release of the BSA into the PBS is expected to be controlled by diffusion through the mesoporous shell wall of the HA microspheres and presumably, by desorption from the pore surface of the HA microspheres. In comparison, the BSA release into the PEG is expected to be controlled by the diffusion/desorption process in the PBS system as well as by diffusion through the PEG hydrogel. The relationship between the diffusion coefficient of a solute in a gel (D_g) and the diffusion coefficient of the solute in a liquid (D_l) has been described by the equation [32]:

$$D_g / D_l = \left(1 - \frac{r_s}{\varsigma}\right) \exp\left[-y\left(\frac{\varphi}{1-\varphi}\right)\right] \quad (1)$$

where r_s is the radius of the solute, ζ is the scaling correlation length between crosslinks, $y > 0$ is a parameter related to the critical volume required for a successful translational movement of the solute molecule and the average free volume per molecule of the liquid, and φ ($0 < \varphi < 1$) is the volume fraction of polymer in hydrogel. Since the solute transport within a hydrogel occurs primarily within the water-filled regions delineated by the polymer chains, ζ must be larger than r_s to provide enough space for the movement of the solute, that is $r_s/\zeta < 1$, and $0 < (1 - r_s/\zeta) < 1$. The term $\exp[-y\,\varphi/(1-\varphi)]$ is always less than 1 since $y > 0$ and $0 < \varphi < 1$. Therefore, Equation (1) predicts that $D_g/D_0 < 1$, and the diffusion rate in the PEG hydrogel is always smaller than the diffusion rate in the PBS solution.

Since the release of the BSA into the PEG hydrogel is controlled by diffusion through the mesoporous shell wall of the HA microspheres and by diffusion through the PEG, the amount of BSA released into the PEG should depend on the distance from the

HA disc as well as the time. Figure 5 shows that release of BSA close to the edge of the HA disc was initially rapid, reaching a value of ~35 μg/ml after day 1; however, the total amount of BSA released at this position changed by less than ±5% between day 1 and day 7, and remained nearly constant at longer times. This indicated that after day 1, the amount of BSA released near the edge of the HA disc is approximately constant. Therefore, after day 1, the diffusion away from the edge of the HA disc is approximately balanced by the diffusion of BSA out of the HA microspheres. In comparison, the amount of BSA at position B (4.5 mm from the edge of the HA disc) increased approximately as $t^{1/2}$, where t is the time, while the amount of BSA at position C (13.5 mm from the edge of the HA disc) increased approximately linearly with t.

As described above, after day 1 the BSA concentration near the edge of the disc of hollow microspheres (position A) remained approximately constant as a function of time (Fig. 5), while the concentration at position B (4.5 mm from the edge of the disc) and position C (13.5 mm from the edge of the disc) increased with time as the BSA molecules diffused down the concentration gradient (from A to C). The diffusion coefficient of the BSA molecules in the PEG hydrogel can be estimated from the measured time-dependent concentrations at B and C. By approximating the system to a semi-infinite source with a constant concentration C_o for $x< 0$ in contact with a semi-infinite system, such that $C = 0$ for $x > 0$ at $t = 0$, the solution to Fick's second law is [33]:

$$C = C_0 erfc\left[\frac{x}{2(Dt)^{1/2}}\right] \qquad (2)$$

where D is the diffusion coefficient and *erfc* is the error-function complement. By plotting the argument of the complementary error function, *argerfc* (C/C_o), versus x, D is

found from the slope = $1/[2(Dt)^{1/2}]$. Figure 6 shows the plots for t = 48 h and t = 96 h, from which D was found to be 1.7 mm^2/h (48 h) and 2.3mm^2/h (96 h).

In the present study, the hollow HA microspheres were bonded at their contact points into small discs (Fig. 1) for ease of manipulation and for ease of measuring the BSA release from the microspheres into the PEG hydrogel by a spectrophotometric method. However, it is expected that the loose microspheres will also provide an attractive system for biomedical applications. For example, loose HA microspheres loaded with a growth factor can be packed into a bone defect to regenerate bone by osteoconduction and osteoinduction. In addition, the HA microspheres can fill the defect and integrate with new bone. Growth factor-loaded HA microspheres can also be dispersed in a biodegradable hydrogel can be injected into a bone defect and hardened in situ by ultraviolet radiation or by thermal methods. The present in vitro study showed that these hollow HA microspheres can serve as a device for controlled delivery of BSA into a PEG hydrogel that was used to mimic the extracellular matrix. Current work is aimed at investigating the release of an actual growth factor (TGF-β) from the HA microspheres in vitro, and the use of TGF-loaded HA microspheres for repairing bone defects in vivo.

4.6 CONCLUSION

In vitro evaluation of BSA release from hollow HA microspheres into a PEG hydrogel provided experimental support for the potential use of the HA microspheres as an osteoconductive device for controlled local delivery of proteins such as growth factors and drugs. The BSA release kinetics into the PEG hydrogel was far slower than the release from similar HA microspheres into phosphate-buffered saline (PBS). However,

the final amount of BSA released into the PEG was approximately the same as that released into PBS. The BSA release kinetics into the PEG was dependent on the microstructure of the shell wall of the HA microspheres. Approximately 40% of the BSA initially loaded into the HA microspheres was released from as-prepared HA microspheres after ~7 days when release of the BSA ceased. In comparison, BSA release from heat-treated HA microspheres (600°C/5h) increased continuously, and reached a total value of 37% after 14 days.

4.7 ACKNOWLEDGEMENT: This work was supported by the National Institute of Dental and Craniofacial Research, National Institutes of Health, Grant # 1R15DE018251-01.

4.8 REFERENCES

[1] J.E. Babensee, L.V. McIntire, A.G. Mikos, Pharmaceut. Res. 17 (2000) 497.

[2] Y. Tabata, Tissue Eng. 9 (2003) S5.

[3] P.D.P. Lew, P.F.A. Waldvogel, Lancet 364 (2004) 369.

[4] A.D. Hanssen, Clin. Orthop. Rel. Res. 437 (2005) 91.

[5] S. Ma, G. Chen, A.H. Reddi, Ann. NY Acad. Sci. 580 (1990) 524.

[6] J.M. McPherson, Clin. Mater. 9 (1992) 225.

[7] M. El-Husseiny, S. Patel, R.J. MacFarlane, F.S. Haddad, J. Bone Joint. Surg. Br. 93 (2011) 151.

[8] V.R. Sinha, A. Trehan, J. Control. Release 90 (2003) 261.

[9] R.R. Chen, D.J. Mooney, Pharmaceut. Res. 20 (2003) 1103.

[10] R.L. Cleek, K.C. Ting, S.G. Eskin, A.G. Mikos, J. Control. Release 48 (1997) 259.

[11] N. Roveri, B. Palazzo, in: C. Kumar (Ed.), Tissue, cell and organ engineering, Weinheim, Wiley-VCH, 2006.

[12] A. Tampieri, G. Celotti, E. Landi, Anal. Bioanal. Chem. 381 (2005) 568.

[13] W. Chang, M. Colangeli, S, Colangeli, C. Di Bella, E. Gozzi, D. Donati, Acta Orthop. Belg. 73 (2007) 238.

[14] S.M. Sanicola, S.F. Albert, J. Foot Ankle Surg. 44 (2005) 121.

[15] M.A. Rauschmann, T.A. Wichelhaus, V. Stirnal, E. Dingeldein, L. Zichner, R. Schnettler, V. Alt, Biomaterials 26 (2005) 2677.

[16] S.J. Kalita, A. Bhardwaj, H.A. Bhat, Mater. Sci. Eng. C 27 (2007) 441.

[17] A.I. Villacampa, J.M. García-Ruiz, J. Cryst. Growth 211 (2000) 111.

[18] M. Vallet-Regi, A. Rámila, R.P. Del Real, J. Pérez-Pariente, Chem. Mat. 13 (2001) 308.

[19] I. Ono, T. Ohura, M. Murata, H. Yamaguchi, Y. Ohnuma, Y. Kuboki, Plast. Reconstr. Surg. 90 (1992) 870.

[20] U. Ripamonti, S. Ma, B. van den Heever, A.H. Reddi, Plast. Reconstr. Surg. 90 (1992) 382.

[21] U. Ripamonti, Biomaterials 17 (1996) 31.

[22] T. Matsumoto, M. Okazaki, M. Inoue, S. Yamaguchi, T. Kusunose, T. Toyonaga, Y. Hamada, J. Takahashi, Biomaterials 25 (2004) 3807.

[23] F. Chai, J.C. Hornez, N. Blanchemain, C. Neut, M. Descamps, H.F. Hildebrand, Biomol. Eng. 24 (2007) 510.

[24] X. Zhang, W.T. Jia, Y. Gu, W. Xiao, X. Liu, D. Wang, C.Q. Zhang, W. Huang, M.N. Rahaman, D.E. Day, N. Zhou, Biomaterials 31 (2010) 5865.

[25] W.T. Jia, X. Zhang, S.H. Luo, X. Liu X, W.H. Huang, M.N. Rahaman, D.E. Day, C.Q. Zhang, Z.P. Xie, J.Q. Wang, Acta Biomater. 6 (2010) 812.

[26] H. Fu, M.N. Rahaman, D.E. Day, Q. Fu, J. Am. Ceram. Soc. 93 (2010) 3116.

[27] D.E. Day, S.A. Conzone, US Patent No. 6,358,531, March 19, 2002.

[28] H. Fu, M.N. Rahaman, D.E. Day, R.F. Brown, J. Mater. Sci. Mater. Med. 22 (2010) 579.

[29] K.Y. Lee, D.J. Mooney, Chem. Rev. 101 (2001) 1869.

[30] H.R. Oxley, P.H. Corkhill, J.H. Fitton, B.J. Tighe, Biomaterials 14 (1993) 1064.

[31] N.A. Peppas, Y. Huang, M. Torres-Lugo, J.H. Ward, J. Zhang, Annu. Rev. Biomed. Eng. 2 (2000) 9.

[32] S.R. Lustig, N.A. Peppas, J. Appl. Polym. Sci. 36 (1988) 735.

[33] J. Crank, The mathematics of diffusion, 2nd ed., Oxford (UK), Oxford University Press, 1975.

Table I. Characteristics of as-prepared hollow HA microspheres formed by reacting $Li_2O–CaO–B_2O_3$ glass microspheres (106–150 μm) in K_2HPO_4 solution, and after heat treatment under the temperature/time conditions shown. The ratio of hollow core diameter to microsphere diameter, *d*/*D*; specific surface area and rupture strength are shown.

Sample	*d*/*D*	Surface area (m^2/g)	Rupture strength* (MPa)
As-prepared	0.61 ± 0.03	102	11 ± 6
600°C/5 h	0.62 ± 0.03	19	19 ± 11

*Measured for HA microspheres of size 200–250 μm prepared under the same conditions.

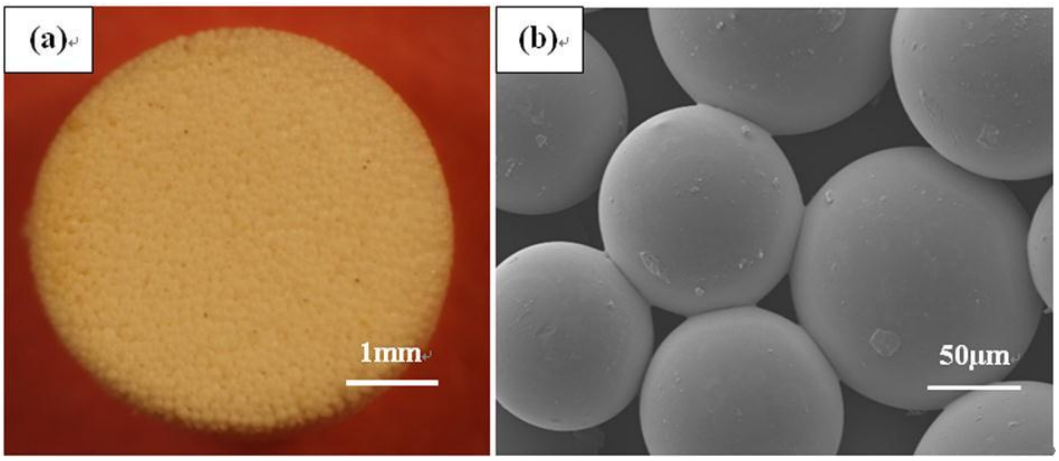

Figure 1. Microstructure of thin disk consisting of hollow HA microspheres bonded at their contact points. (a) optical image of thin disk with hollow HA microspheres; (b) higher magnification SEM image showing the hollow HA microspheres bonded at their contact points.

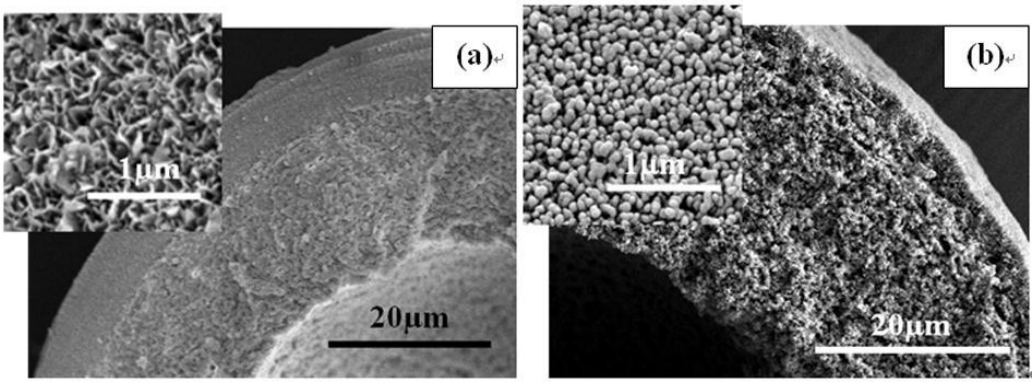

Figure 2. SEM images of the cross section and surface (*insert*) of the shell wall of hollow HA microspheres: (a) as-prepared; (b) heated for 5 h at 600°C.

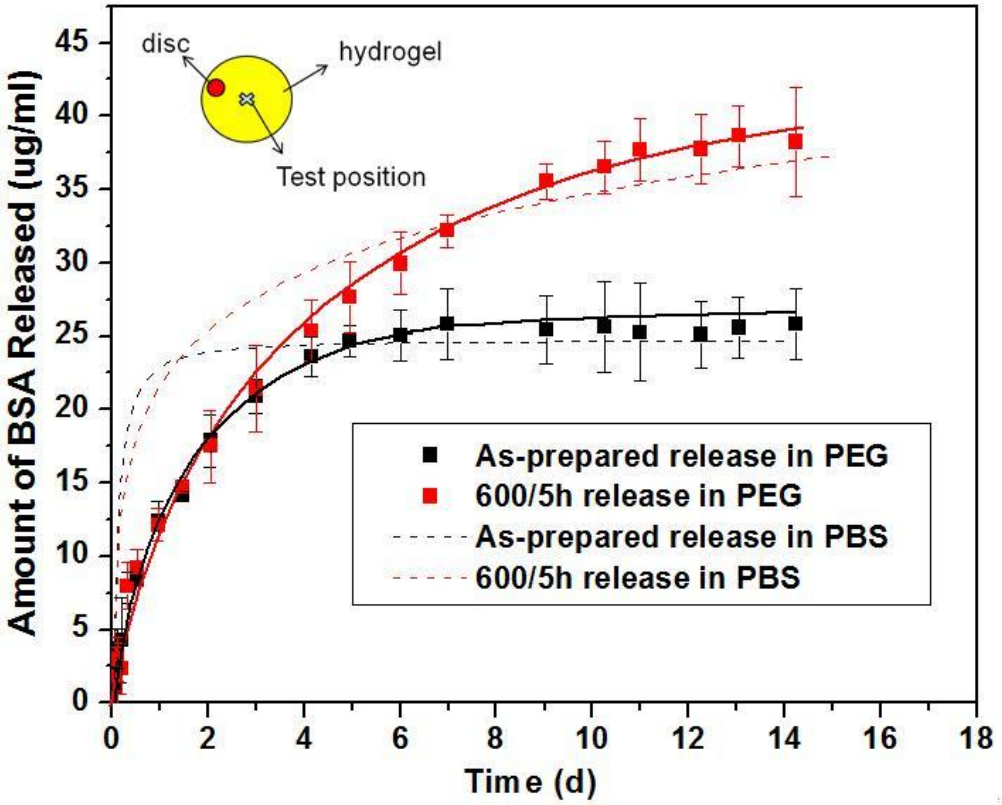

Figure 3. Release of BSA from a disc of hollow HA microspheres into PEG hydrogel as a function to time measured at the position indicated, approximately 4.5 mm from the edge of the disc. For comparison, the BSA release from similar HA microspheres into phosphate-buffered saline (PBS), taken from Ref. 28, is also shown (dashed lines).

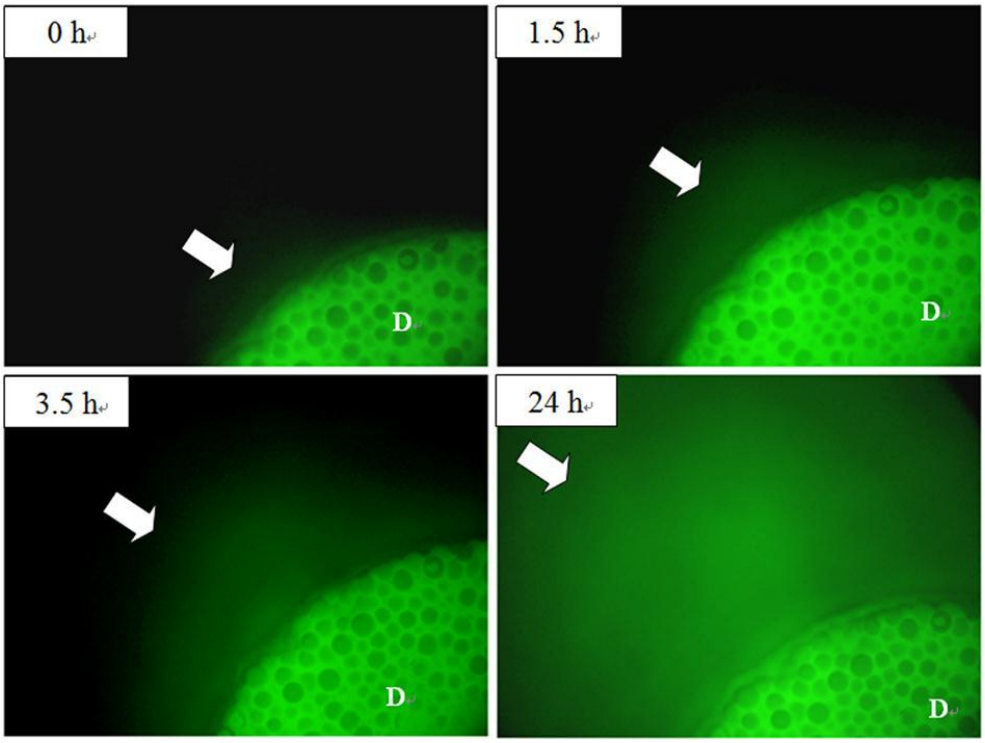

Figure 4. Optical images of BSA released from hollow HA microspheres (600°C/5 h) into PEG hydrogel at different times. The intensity of the green fluorescence is an indication of the concentration of BSA released.

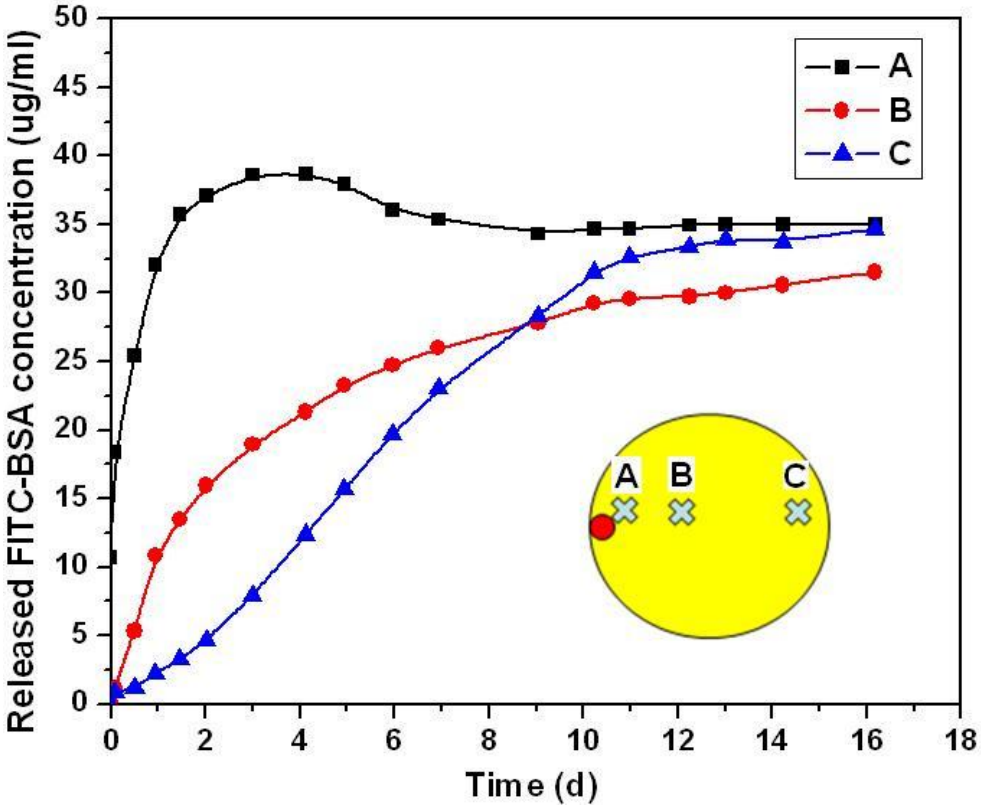

Figure 5. Amount of BSA released from disc of hollow HA microspheres (600°C/5 h) into PEG hydrogel at the different positions shown (A: near the edge of the HA disc; B: 4.5 mm from the A position; C: 13.5 mm from the A position).

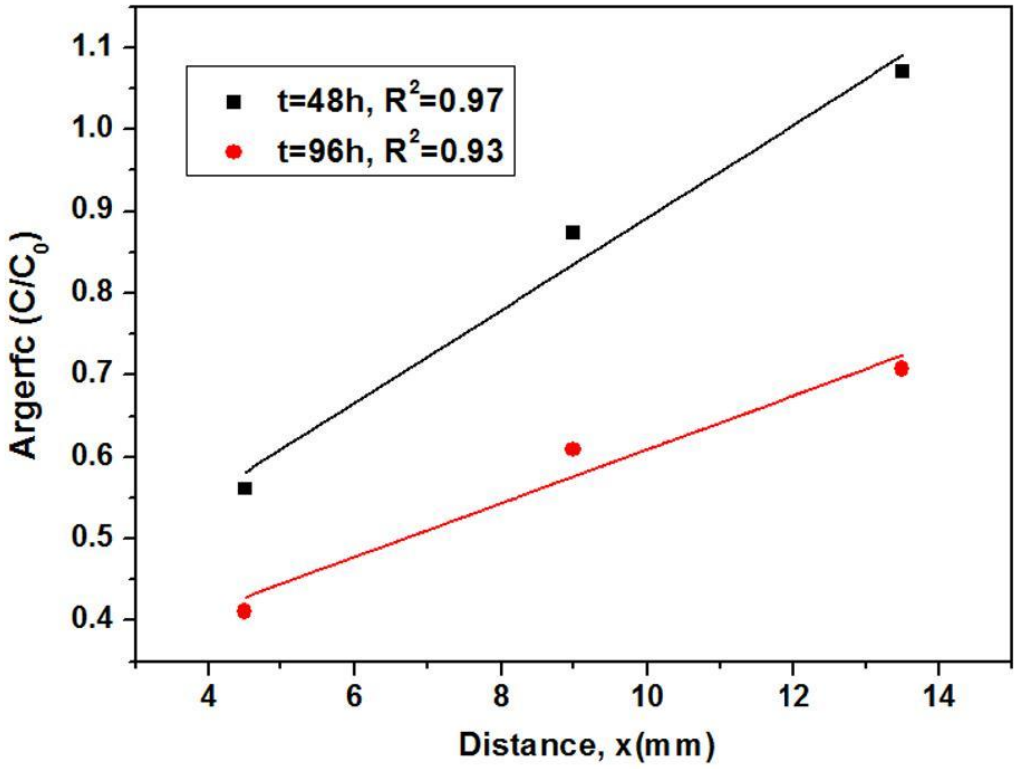

Figure 6. Plot of the argument of the complementary error function, *argerfc* (C/C_o), vs. distance (x) from the edge of the HA disc, for the BSA release data from the disc of HA microspheres (600°C/5 h) into PEG hydrogel after t = 48 h and t = 96 h. The diffusion coefficient for the BSA molecules in the hydrogel was determined from the slope of each plot. (The coefficient of determination, R^2, is shown for each plot.)

5. EVALUATION OF BONE REGENERATION IN IMPLANTS COMPOSED OF HOLLOW HA MICROSPHERES LOADED WITH TGF-β1 IN A RAT CALVARIAL DEFECT MODEL

Hailuo Fu[1,3], Mohamed N. Rahaman[1,3], Roger Brown[2,3], Delbert E. Day[1,3]

[1]Department of Materials Science and Engineering, Missouri University of Science and Technology, Rolla, MO 65409, USA

[2]Department of Biological Sciences, Missouri University of Science and Technology, Rolla, MO 65409, USA

[3]Center for Bone and Tissue Repair and Regeneration, Missouri University of Science and Technology, Rolla, MO 65409, USA

5.1 ABSTRACT

Scaffolds for bone regeneration should ideally serve simultaneously as an osteoconductive matrix and as a device for local growth factor delivery. In this work, implants composed of hollow hydroxyapatite (HA) microspheres with a mesoporous shell wall were created and evaluated for their ability to regenerate bone in non-healing rat calvarial defects. Three-dimensional (3D) scaffolds composed of hollow HA microspheres (Group 1) were created by thermally bonding borate glass microspheres (106–150 μm) into a porous 3D construct, conversion in an aqueous phosphate solution at 37°C, and thermal treatment (5 h at 600°C). For comparison, individual hollow HA microspheres (Group 2) were created using the same process but without thermal bonding of the glass microspheres. Bone regeneration increased significantly in Group 1 and Group 2 implants with increase in the implantation time from 6 to 12 weeks; bone regeneration was significantly higher (23%) in Group 2 (individual HA microspheres)

than in Group 1 (HA scaffold) (15%) after 12 weeks. Loading with TGF–β1 (5μg/defect) enhanced bone regeneration in both Group 1 and Group 2 implants after 6 weeks, but had little effect after 12 weeks. Group 1 and Group 2 implants composed of hollow HA microspheres of larger size (150–250 μm) showed better ability to regenerate bone. Based on these results, implants composed of hollow HA microspheres show promising potential as an osteoconductive matrix for local growth factor delivery in bone regeneration.

Keywords: bone regeneration; hollow hydroxyapatite microspheres; scaffolds; rat calvarial defect model; transforming growth factor–β1.

5.2 INTRODUCTION

Bone repair is a complex cascade of biological events controlled by numerous cytokines and growth factors that provide signals at local injury sites, allowing progenitors and inflammatory cells to migrate and trigger healing processes. An ideal implant for bone regeneration should therefore function simultaneously as an osteoconductive matrix and a device for local growth factor delivery. The success of this strategy is highly dependent on the properties of the scaffold material (such as biocompatibility, osteoconductivity, and degradation rate) and on the scaffold architecture (such as porosity, pore size, and surface morphology.

Calcium phosphates such as hydroxyapatite (HA), $Ca_{10}(PO_4)_6(OH)_2$, and beta-tricalcium phosphate (β-TCP), $Ca_3(PO_4)_2$, composed of the same ions as the main mineral constituent of bone, are attractive implant materials for bone regeneration because they are biocompatible, osteoconductive, and produce no systemic toxicity or immunological

reactions [1–3]. These calcium phosphates also have a high affinity for proteins, such as the growth factors bone morphogenetic protein-2 (BMP-2) and transforming growth factor-β (TGF-β) [4] which are known to stimulate the proliferation and differentiation of osteoprogenitor cells [5]. Consequently, they can provide attractive carrier materials for growth factors and stem cells without a surface chemical modification that is sometimes required for polymers [6].

Methods used to produce synthetic HA include precipitation [7], hydrothermal [8], hydrolysis [9], mechanochemical [7], and sol–gel [10]. Commonly, synthetic HA implants are formed by first preparing nano- or micro-sized HA particles and then forming them into different morphologies or architectures. HA in the form of porous scaffolds, substrates, or granules has been widely researched and used for biomedical applications, such as periodontal, oral, and maxillofacial surgery, and skeletal reconstruction [11]. As a substrate for growth factor delivery, the growth factor is commonly adsorbed or attached to the surfaces of the porous HA material [1–3, 12]. Macroporous HA scaffolds have limited ability to serve as devices for local growth factor delivery because of their low surface area; nano- or micro-sized HA particles, porous granules, or porous substrates with higher surface area provide more effective devices.

Hollow HA microspheres with a mesoporous, high surface area shell wall can potentially provide greater capacity for more sustained release because the growth factor can be incorporated in the mesoporous porous shell as well as within the hollow core. While release of the growth factor from the shell could presumably be controlled by desorption, release of the growth factor from the hollow core could be controlled by

diffusion through the mesoporous shell, which provides an additional mechanism for more sustained release.

Hollow HA microspheres with high surface area (>100 m^2/g) and a mesoporous shell wall have been prepared by a glass conversion process, in which borate glass microspheres are converted in an aqueous phosphate solution near room temperature [13–15]. Hollow HA spheres of small diameter (~500 nm) have been prepared by a solution-based method [16], in which calcium and phosphate ions were reacted in a solution and aged at 60°C or 100°C for 1–7 days. Hollow HA spheres of larger diameter (1.5–2 mm) have been prepared by coating chitin microspheres with a composite layer of chitin and HA, followed by thermal decomposition of the chitin and sintering of the porous HA shell [17]. In our previous work, hollow HA microspheres (diameter in the range 106–250 μm) were prepared by a glass conversion process described above, and their microstructures were characterized in detail [18]. In subsequent work, the ability of the hollow HA microspheres to serve as a device for controlled delivery of a model protein (bovine serum albumin) was evaluated [19].

The objective of the present work was to evaluate the ability of implants composed of hollow hydroxyapatite (HA) microspheres with a mesoporous shell wall to regenerate bone in non-healing rat calvarial defects. Implants composed of (1) hollow HA microspheres (106–150 μm) thermally bonded into a porous three-dimensional (3D) construct, or (2) individual hollow HA microspheres were evaluated after implantation for 6 and 12 weeks. The effects of loading the implants with TGF-β1 and increasing the size of the HA microspheres in the implants on bone regeneration were studied.

5.3 MATERIAL AND METHODS

5.3.1 Fabrication of Constructs Composed of Hollow HA Microspheres.

Two groups of implants were created and evaluated in the present work. Group 1 implants consisted of porous scaffolds in which hollow HA microspheres were bonded at their contact points into a 3D network. In comparison, Group 2 implants were composed of individual hollow HA microspheres. Group 1 implants were prepared by thermally bonding solid borate glass microspheres into a porous 3D network, reacting the 3D construct in an aqueous phosphate solution to convert the glass microspheres into hollow HA microspheres, and finally thermally treating the converted construct to improve its strength. Group 2 implants were prepared using the same process but without thermally bonding the starting glass microspheres.

The starting borate glass (composition in wt%: 15CaO, 10.63 Li_2O, 74.37 B_2O_3; designated CaLB3-15) was prepared by melting Reagent grade $CaCO_3$, Li_2CO_3 and H_3BO_3 (Alfa Aesar, Haverhill, MA, USA) in a Pt crucible at 1200ºC for 45 min, and quenching the melt between cold stainless steel plates to prevent crystallization of the glass. Particles of size 106–150μm and 150–250μm were obtained by grinding the glass using a Spex mill (Model 8500, Spex SamplePrep LLC, Metuchen, N.J. USA), and sieving the ground particles through 140, 100, and 60 mesh stainless steel sieves. The glass particles were formed into microspheres by allowing then to fall vertically through a heated tube furnace, as described in detail elsewhere [14]. Porous constructs with the shape of a cylinder (6 mm in diameter × 5 mm) for mechanical property evaluation, and with the shape of a disc (4.6 mm in diameter × 1.5 mm) for implantation, were prepared by pouring the glass microspheres into graphite molds, and sintering the system for 1 h at

560°C. The sintering conditions were selected on the basis of data for the glass transition and crystallization temperatures of the glass obtained from differential thermal analysis (DTA), coupled with trial and error. DTA (model DTA-7; Perkin-Elmer Corporation, Norwalk, CT, USA) was carried by heating the glass powder in air at 10°C/min to 1000°C.

Constructs composed of hollow HA microspheres were obtained by reacting the glass constructs for 7 days in 0.02 M K_2HPO_4 solution at 37°C and with a starting pH of 9.0. The converted constructs were washed three times with distilled water, then twice with ethanol, and dried overnight at room temperature. The dried constructs were heated for 5 h at 600°C to improve their strength.

5.3.2 Characterization of As-fabricated HA Constructs and Microspheres.

The microstructure of the surface and cross section of the 3D scaffolds and individual HA microspheres was examined using scanning electron microscopy, SEM (S4700; Hitachi, Tokyo, Japan) at an accelerating voltage of 10 kV and a working distance of 12 mm. Liquid extrusion porosimetry (Model LEP-100-A; Porous Materials Inc., Ithaca, NY) and the Archimedes method were used to measure the porosity and pore size distribution of the macropores in the 3D scaffolds. The HA microsphere shell in the 3D scaffolds had similar mesoporosity to the shell in the individual HA microspheres, which was characterized in previous work [18].

3D scaffolds (6 mm in diameter × 5 mm) composed of hollow HA microspheres were tested in compression at a rate of 0.5 mm/min in a mechanical testing machine (Model 4204, Instron Corp., High Wycombe, UK) to determine their strength. Five

samples were tested, and the compressive strength was expressed as a mean ± standard deviation.

5.3.3 Response of Cells to HA Scaffolds.

The biocompatibility of the as-fabricated HA scaffolds was assessed by evaluating their ability to support the proliferation of cells in vitro. Murine MLO-A5 cells, an established post-osteoblast/pre-osteocyte cell line kindly provided by Professor Lynda F. Bonewald, University of Missouri-Kansas City, were cultured in α-MEM supplemented with 5% fetal calf serum (FCS) and 5% newborn calf serum (NCS) plus 100 U/ml penicillin on a collagen-coated plate (rat tail collagen type I; 0.15 mg/ml). All cell cultures were maintained at 37 ℃ in a humidified atmosphere of 5% CO_2 with the medium changed every 2 days.

MLO-A5 cells (30,000 cells) were seeded on disc-shaped scaffolds (6 mm × 2 mm) and cultured in normal medium. The medium was replaced every 2 days. After incubation for 2, 4, and 6 days, the scaffolds were washed gently twice with PBS, and the cells were lysed using two freeze–thaw cycles (–80/37 ℃) with 500 μl of 1% Triton X-100 in PBS. Aliquots of the lysate were placed in a 96-well plate for spectrophotometric measurement of alkaline phosphatase (ALP) activity with p-nitrophenyl phosphate (p-NPP) substrate as described elsewhere [20]. The values of ALP activity were normalized with respect to the total protein content obtained from the same cell lysate and expressed as nanomoles of pNP formed per microgram of protein per min. Total protein content was determined using a micro-BCA Protein Assay kit (Pierce Biotechnologies, Rockford, IL), following the manufacturer's recommended procedure.

5.3.4 RhTGF-β1 Loading and Release.

Scaffolds (discs) composed of hollow HA microspheres were loaded with transforming growth factor β-1 (TGF-β1; Peprotech), and used to study the release kinetics of TGF-β1 in phosphate-buffered saline (PBS). Each scaffold (10 mg) was placed on a Teflon sheet and 20 µl of 1% solution of bovine serum albumin (BSA) was placed on the scaffold. The system was dried overnight to produce a BSA coating on the pore surface of the scaffold. The BSA-coated scaffold was loaded with TGF-β1 by dropping 10 µl of TGF-β1 solution (concentration = 5 ng per µl of solution) on the scaffold and applying a small vacuum to the system to replace the air in the HA microspheres with the TGF-β1 solution. After drying, the TGF-loaded scaffold was placed in PBS (2 scaffolds in 2 ml PBS). The samples were incubated while shaking at 37^{o}C and at selected times (10 h, 1 d, 2 d, 3 d, 5 d, 7 d), 50 µl of the PBS was removed for testing. Control samples containing a known amount of TGF-β1 in a buffer were also incubated at 37^{o}C. The amount of TGF-β1 present in the release buffer was determined by an enzyme-linked immunosorbent assay (ELISA) kit. The concentrations of the unknown samples were quantified relative to a TGF-β1 standard curve run on the same plate.

5.3.5 Animals and Surgery.

All animal experimental procedures were approved by the Missouri University of Science and Technology Animal Care and Use Committee, in compliance with the NIH Guide for Care and House of Laboratory Animals (1985). Thirty Sprague Dawley rats (3 months old; 350 ± 30g) were housed in the animal care facility and acclimated to diet, water, and housing. The rats were anesthetized with an intramuscularly injected mixture

of ketamine and xylazine (0.15 μl per 100 g). The surgical area was shaved, scrubbed with 70% ethanol, and then draped. With sterile instruments and aseptic technique, a cranial skin incision was sharply made in an anterior to posterior direction along the midline. The subcutaneous tissue, musculature and periosteum were dissected and reflected to expose the calvarium. Bilateral full-thickness defects 4.6 mm in diameter were created in the central area of each parietal bone using a 4.6 mm outer diameter trephine attached to an electric drill. The sites were constantly irrigated with sterile PBS to prevent overheating of the bone margins and to remove the bone debris.

The calvarial defects were implanted with 6 groups composed of hollow HA microspheres:

(1) 3D scaffolds (discs) composed of 106–150 μm microspheres;

(2) individual microspheres (106–150 μm);

(3) 3D scaffolds (discs) composed of 106–150 μm microspheres loaded with TGF-β1 (5 μg/defect);

(4) individual microspheres (106–150 μm) loaded with TGF-β1 (5 μg/defect);

(5) 3D scaffold (disc) composed of 150–250 μm microspheres;

(6) individual microspheres (150–250 μm)

The defects were randomly implanted with 5 implants per group, but mixing of implants with or without TGF-β1 in the same animal was avoided. Defects left empty served as negative control. Each animal received an intramuscular injection of ~200 μl penicillin and ~200 μl buprenorphine post-surgery. The animals were monitored daily for condition of the surgical wound, food intake, activity and clinical signs of infection. After 6 or 12

weeks, the animals were sacrificed by CO_2 inhalation, and the calvarial defect sites with surrounding bone and soft tissue were harvested.

5.3.6 Histology.

The calvarial samples consisting of the defect sites with surrounding bone and soft tissue were washed with PBS solution and fixed in 10% formalin solution for 5 days. The fixed tissue samples were each cut into two parts; half of each sample was for paraffin embedding and the other half for methyl methacrylate embedding. The samples for paraffin sections were decalcified for 4 weeks in ethylenediaminetetraacetic acid (EDTA) (14 wt%) under mild agitation on a rocking plate. After the samples were dehydrated in ethanol and embedded in paraffin using standard histological techniques, 5 μm thick sections were cut and stained with hematoxylin and eosin (H&E). The undecalcified samples were dehydrated through a graded series of ethanol solutions, and embedded in methyl methacrylate. Sections were ground to a thickness of 30–40μm using a micro grinding system (EXAKT 400CS, Norderstedt, Germany), and stained using the von Kossa technique to observe mineralization.

5.3.7 Histomorphometric Analysis.

Stained sections were examined in a transmitted light microscope (Model BX51; Olympus America, Center Valley, PA) fitted with a digital color camera (Model DP71; Olympus). Images were analyzed on a computer using the Image J software. Sections stained with H&E were used to analyze the percentage of new bone formed within the defect. The newly formed bone was identified by outlining the edge of the defect, with the presence of original and new bone being identified by lamellar and woven bone, respectively. The total defect area was measured from one edge of the old calvarial bone,

including the entire implant and tissue within it, to the other edge of the old bone. The newly formed bone within this area was then outlined and measured; the amount of new bone was expressed as a percentage of the total defect area.

5.3.8 Statistical Analysis.

Measurements (n = 5) of percentage new bone were expressed as a mean ± standard deviation. Analysis for differences between groups was performed using one-way analysis of variance (ANOVA) with Tukey's post hoc test; differences were considered significant for $p < 0.05$.

5.4 RESULTS

5.4.1 Microstructure and Properties of Implants.

The DTA pattern (Fig. 1) of the starting borate glass used to prepare the HA implants showed an onset of the glass transition at ~525°C, and two crystallization events with onset temperatures of ~645°C and ~700°C, respectively. Since one objective of the scaffold fabrication process was to bond the glass spheres into a 3D network by viscous flow sintering without crystallization of the glass, the DTA pattern indicated a sintering temperature in the range 525–645°C. Experiments showed that sintering for 1 h at 560°C provided adequate scaffold strength for subsequent use without measurable crystallization of the glass; consequently, these sintering conditions were used to prepare 3D constructs of the glass microspheres.

Figure 2 shows SEM images of a 3D construct composed of thermally-bonded borate glass microspheres (Fig. 2a, b) and a scaffold composed of hollow HA microspheres formed by converting the glass construct in K_2HPO_4 solution (Fig. 2c, d).

The diameter of the starting glass microspheres was 150–250μm. The conversion of the glass microspheres to HA was pseudomorphic, with little change in the external dimensions of the glass microspheres (or the 3D construct), and the HA microspheres remained bonded together in a 3D network. The cross section confirmed that the HA microspheres in the 3D constructs were hollow. (Because each HA microsphere is sectioned at a different depth along its diameter, the hollow core diameter can vary in the planar section). Images of hollow HA microspheres formed under the same conditions showed that the ratio of the hollow core diameter to the external diameter was 0.61 ± 0.03. High magnification SEM images (Fig. 2e, f) showed that the shell of the hollow HA microspheres was mesoporous, with a microstructure similar to that of individual HA microspheres formed under the same conversion conditions.

The SEM images (Fig. 2) showed that the porosity in the 3D scaffold consisted of macropores between the HA microspheres (arrows) and mesopores in the HA shell, in addition to the porosity in the hollow cores of the microspheres. The volume of the macropores determined by the Archimedes method were 34 ± 3% for scaffolds composed of 106–150 μm microspheres, and 38 ± 4% for those composed of 150–250 μm microspheres. Porosimetry showed that scaffolds composed of 106–150 μm microspheres had pore sizes in the range 10 – 100 μm, with an average of 65 μm (Fig. 3); in comparison, scaffolds composed of 150–250 μm microspheres had pore sizes in the range 30–150 μm, with an average of 100 μm. The shell of the hollow HA microspheres was ~60% porous, with pores of average size = 10 nm (measured using nitrogen adsorption).

The compressive strength of the 3D scaffolds was 1.6 ± 0.4 MPa. For comparison, the rupture strength of the individual hollow HA microspheres, determined in previous

work, was 17 ± 8 MPa. The characteristics of the 3D scaffolds and individual HA microspheres are summarized in Table I.

5.4.2 Biocompatibility of HA Scaffolds.

Results of the quantitative assay of total protein and alkaline phosphatase (ALP) activity in MLO-A5 cell lysates recovered from the hollow HA scaffolds after incubation times of 2, 4, and 6 days are shown in Fig. 4. The amount of protein recovered from the scaffolds showed an increase in cell proliferation during the 6 day incubation, a finding that complements SEM images of the cell morphology on the scaffolds (results not shown). The ALP activity increased during the 6 day incubation, which indicated that the cells were able to carry out an osteogenic function in the scaffolds. In general, the increase in cell proliferation and ALP activity during the six-day incubation confirmed the biocompatibility of the HA scaffolds created in this work.

5.4.3 Release of TGF-β1 from Hollow HA Microspheres.

Figure 5 shows the release of TGF-β1 from 3D scaffolds composed of hollow HA microspheres (106–150 μm) into PBS. The release was initially rapid, with ~25% of the TGF-β1 initially loaded into the scaffold released during the first 12 hours. This initial burst release was followed a slower, more sustained release over the next 2 days, after which the release almost ceased. After 7 days, the total amount of TGF-β1 released into the PBS was ~30% of the original amount loaded into the microspheres.

5.4.4 Bone Regeneration.

H&E and von Kossa stained sections of HA implants composed of 3D scaffolds (Group 1) and individual microspheres (Group 2), as well as for Group 1 and Group 2 implants loaded with TGF–β1 (5μg/defect) are shown in Fig. 6 after implantation for 6

weeks in rat calvarial defects. (The size of HA microsphere in these implants was 106–150 μm.) For Group 1 and Group 2 scaffolds (without TGF-β1), bone regeneration was limited mainly to the edges of the implants, with some bone bridging along the top and bottom of the implants (Fig. 6A1–C1; A3–C3). The majority of the defect was filled with fibrous connective tissue (light blue in H&E stained sections). Total bone regeneration in Group 2 (individual microspheres) (12%) was significantly higher than in Group 1 (3D scaffold) (3%) (Fig. 7).

Bone regeneration was significantly enhanced in both implant groups loaded with TGF-β1 after the six-week implantation (Fig. 6A2–C2; A4–C4); bone regeneration increased from 3% to 9% in Group 1 and from 12% to 19% in Group 2 (Fig. 7). For both groups, new bone formation was observed at the edges, with bone bridging along the top and bottom of the implants, as well as within the implant. In Group 1 implants (3D scaffolds), most new bone formed along the top and bottom of the implants, with a smaller amount of new bone infiltrating the edges of the implant. In comparison, for Group 2 (individual microspheres), most new bone formed within the implant, and new bone infiltrated 1–2 mm into the edges of the implant. Some HA microspheres were surrounded by newly formed bone, and tightly connected with new bone (Fig. 6C2). Blood vessels were observed in the tissue between the HA microspheres (Fig. 6C2, C4; arrows). H&E and von Kossa stained sections of empty defects after implantation for 6 weeks are shown in Fig. 6A5, B5. The defect was almost filled with soft connective tissue, and bone regeneration was observed only at the edge of the defects along the native dura mater.

Bone regeneration increased significantly in Group 1 and Group 2 implants (without TGF–β1) as the implantation time increased from 6 to 12 weeks (Fig. 8A1, B1; A3, B3). New bone infiltrated the implants from the edges and also formed on the dural (bottom) side of the implants. Increase of the implantation time from 6 to 12 weeks resulted in an increase in bone regeneration from 3 to 14% for Group 1 (3D scaffolds) and from 12% to 23% for Group 2 (individual microspheres) (see Fig. 7). For Group 1 and Group 2 implants loaded with TGF-β1, the percent new bone regeneration was not significantly different from that for the corresponding implants without loading TGF-β1 after the twelve-week implantation. In comparison, new bone formation in the empty defects (Fig. 8A5, B5) was limited to ~1mm from the edge of the defect, and the thickness of the new bone in the stained section was only ~200 μm.

Bone regeneration in the Group 1 and Group 2 implants increased significantly as the diameter of the HA microspheres in the implants was increased from 106–150 μm to 150–250 μm (Fig. 9, 10). Twelve weeks postimplantation, bone regeneration increased from 14% to 25% in the Group 1 implants (3D scaffolds) and from 23% to 35% with the increase in the size of the HA microspheres. Bone growth was enhanced at the edges and on the dural side of both groups of implants composed of the larger HA microspheres (Fig. 9B, D).

5.5 DISCUSSION

The results indicate that porous 3D scaffolds composed of hollow HA microspheres with a mesoporous shell wall or the individual HA microspheres themselves can provide a promising matrix for bone regeneration. In addition to being

biocompatible, the 3D scaffolds or individual microspheres can simultaneously provide the functions of an osteoconductive matrix and a device for local growth factor delivery.

Three-dimensional scaffolds composed of hollow HA microspheres or individual hollow HA microspheres were created using a glass conversion technique [15], resulting in a unique combination of characteristics that cannot be readily achieved by known methods. By thermally bonding solid borate glass microspheres into the desired macroporous architecture and 3D geometry, the glass constructs were converted into 3D scaffolds composed of hollow HA microspheres with the same external geometry and macroporosity as the original glass construct (Fig. 2). In addition to a matrix of interconnected macropores to support bone ingrowth and integration with surrounding tissue, the 3D scaffolds consisted of high surface area, nanostructured HA known to be favorable for protein adsorption [21], osteogenic cell differentiation, and nutrient transport [22]. The hollow core combined with the high surface area, mesoporous shell of the HA microspheres provided mechanisms for growth factor loading and release. Except for the absence of a well-defined 3D geometry, individual hollow HA microspheres provided the benefits of the 3D scaffolds in addition to the potential benefit of implantation into irregular-shaped defects.

The rat calvarial defect model, a standard assay for evaluating new bone formation in a non-healing defect, was used in the present work to evaluate bone regeneration in the implants. The 3D scaffold maintained its structural integrity throughout the twelve-week implantation period (Fig. 8B2, B4), indicating its ability to maintain the shape of the defect. The individual HA microspheres were also well contained in the defect sites. H&E stained sections (Fig. 6) showed significant cellular

infiltration throughout all the implants, as well as significant extracellular matrix formation, indicating good scaffolding properties of the implants. However, new bone formation (NB) in the defects was observed mainly at the edge of the implants adjacent to the host bone (HB) and at the bottom (dural) side of the implants (Fig. 6). This pattern of bone regeneration presumably resulted from contact of the edge of the implant with the host bone, making this area easily accessible to osteogenic cells and blood supply, and from contact of the bottom of the implant with the dura mater which also contains osteogenic cells.

The results showed that when implanted in rat calvarial defects for 6 or 12 weeks, the individual HA microspheres had a greater capacity to support bone regeneration than the 3D scaffolds composed of HA microspheres with the same diameter; this trend was independent of the HA microsphere diameters used in this work (106–150 μm or 150–250 μm) (Fig. 7, 10). The lower bone formation in the 3D scaffolds was presumably limited by the pore size and pore interconnectivity of the scaffold which contained a large fraction of pores smaller than 100 μm (particularly for the 3D scaffold composed of 106–150 μm microspheres) (Fig. 3; Table I). It is known that osteoblasts require pores larger than ~100 μm for bone formation [23–25]. Enlarging the macropore size of the 3D scaffold is necessary to better support bone regeneration. In comparison, implants composed of individual HA microspheres showed a greater capacity to support bone regeneration, which might be attributed to the ease with which the microspheres could adjust their positions in response to a stress, thereby enabling changes in the pore sizes to accommodate cell infiltration.

TGF-β1 was chosen as a model growth factor to evaluate the drug release function of the 3D scaffolds and individual HA microspheres because it has been reported to promote bone growth when delivered locally or administered systematically [26, 27]. Our results showed that loading the implants with TGF-β1 significantly enhanced bone regeneration at 6 weeks (Fig. 7), which is consistent with the observations of those studies. The enhancement of bone regeneration by TGF-β1 loading was observed for both the 3D scaffolds and the individual HA microspheres.

Although the volume of new bone continued to increase significantly in all groups except for the individual HA microspheres loaded with TGF-β1, the difference in bone regeneration between corresponding groups with or without TGF-β1 loading became insignificant 12 weeks postimplantation (Fig. 7). We postulated that this was due to the non-optimized release profile of TGF-β1 from the HA microspheres. Our in vitro results (Fig. 5) showed a significant burst release of TGF–β1 in the first 12 hours, and ~30% of the TGF-β1 initially loaded in the microspheres was released within 2 days. However, after 2 days, the release of TGF-β1 almost ceased, although ~70% of the initial TGF-β1 was still retained by the implants. HA is known for its high affinity for various proteins [28], and the release of adsorbed proteins is often dependent on the resorption of HA in the in vivo environment [29, 30]. In the present work, measureable resorption of HA was not observed within the twelve-week implantation period. It is therefore likely that TGF-β1 was not continuously released into the bone defect, which could account for the absence of a significant difference in bone regeneration after 12 weeks. We are currently modifying the HA microspheres to provide more sustained release of growth factors, after which bone regeneration in the system will be further investigated.

5.6 CONCLUSION

Three-dimensional (3D) scaffolds composed of hollow hydroxyapatite (HA) microspheres with mesoporous shell wall and individual hollow HA microspheres were created by a glass conversion process and evaluated for their ability to regenerate bone in rat calvarial defects. Bone regeneration increased significantly in both groups of implants with an increase in implantation time from 6 to 12 weeks. Bone regeneration was significantly higher in the implants composed of individual HA microspheres than in the 3D scaffolds after both implantation times. Loading the implants with TGF-β (5 μg/defect) significantly enhanced bone regeneration in both groups of implants 6 weeks postimplantation, but showed little effect in enhancing bone regeneration 12 weeks postimplantation. Increasing the HA microsphere diameter in the implants from 106–150 μm to 150–250 μm resulted in a significant increase in bone regeneration. Individual hollow HA microspheres or 3D scaffolds composed of hollow HA microspheres loaded with a suitable growth factor are promising implants for bone regeneration.

5.7 ACKNOWLEDGEMENT: This work was supported by the National Institute of Dental and Craniofacial Research, National Institutes of Health, Grant # 1R15DE018251-01, and by the Center for Bone and Tissue Repair and Regeneration, Missouri S&T.

5.8 REFERENCES

1. Giannoudis P, Dinopoulos H, Tsiridis E. Bone substitutes: an update. Injury 2005;36:20–7.
2. LeGeros RZ. Properties of osteoconductive biomaterials: calcium phosphates. Clin Orthop Relat Res 2002;395:81–98.
3. Bucholz R. Nonallograft osteoconductive bone graft substitutes. Clin Orthop Relat Res 2002; 395:44–52
4. Ruhé P, Kroese-Deutman H, Wolke J, Spauwen P, Jansen J. Bone inductive properties of rhBMP-2 loaded porous calcium phosphate cement implants in cranial defects in rabbits. Biomaterials 2004;25:2123–32.
5. Lieberman JR, Daluiski, A, Einhorn TA. The role of growth factors in the repair of bone. J Bone Jt Surg Am 2002;84:1032–44.
6. Hing K. Bioceramic bone graft substitutes: influence of porosity and chemistry. Int J Appl Ceram Technol 2005;2:184–99.
7. Saeri MR, Afshar A, Ghorbani M, Ehsani N, Sorrell CC. The wet precipitation process of hydroxyapatite. Mater Lett 2003;57:4064–9.
8. Masahiro Y, Hiroyuki S, Kengo O, Koji I. Hydrothermal synthesis of biocompatible whiskers. J Mater Sci 1994;29:3399-402.
9. Shih WJ, Chen YF, Wang MC, Hon MH. Crystal growth and morphology of the nano-sized hydroxyapatite powders synthesized from $CaHPO_4.2H_2O$ and $CaCO_3$ by hydrolysis method. J Cryst Growth, 2004;270:211–8.
10. Kim IS, Kumta PN. Sol-gel synthesis and characterization of nanostructured hydroxyapatite, Mater Sci Eng B 2004;111:232–6.

11. Orlovskii VP, Komlev VS, Barinov SM. Hydroxyapatite and hydroxyapatite-based ceramics. Inorg Mater 2002;38:973–84.

12. Schek R, Wilke E, Hollister S, Krebsbach P. Combined use of designed scaffolds and adenoviral gene therapy for skeletal tissue engineering, Biomaterials 2006;27:1160–6.

13. Day DE, Conzone SA. Method for preparing porous shells or gels from glass particles. US Patent No. 6,358,531; March 19, 2002.

14. Day DE, White JE, Bown RF, McMenamin KD. Transformation of borate glasses into biologically useful materials. Glass Technol 2003;44:75–81.

15. Conzone SD, Day DE. Preparation and properties of porous microspheres made from borate glass. J Biomed Mater Res Part A 2009; 88:531–42.

16. Xia W, Grandfield K, Schwenke A, Engqvist H. Synthesis and release of trace elements form hollow and porous hydroxyapatite spheres. Nanotechnology 2011;22:305610.

17. Peng Q, Ming L, Jiang CX, Feng B, Qu SX, Weng J. Preparation and characterization of hydroxyapatite microspheres with hollow core and mesoporous shell. Key Eng Mater 2006; 309–311:65–8.

18. Fu H, Rahaman MN, Day DE. Effect of process variables on the microstructure of hollow hydroxyapatite microspheres prepared by a glass conversion process. J Am Ceram Soc 2010; 93:3116–23.

19. Fu H, Rahaman MN, Day DE, Brown RF. Hollow hydroxyapatite microspheres as a device for controlled delivery of proteins. J Mater Sci Mater Med 2011;22:579–91.

20. Barragan-Adjemian C, Nicolella D, Dusevich V, Dallas MR, Eick JD, Bonewald LF. Mechanism by which MLO-A5 late osteoblasts/early osteocytes mineralize in culture: Similarities with mineralization of lamellar bone. Calcif Tissue Int 2006;79:340–53.

21. Lin T, Su C, Chang C. Stereomorphologic observation of bone tissue response to hydroxyapatite using SEM with the EDTA-KOH method. J Biomed Mater Res 1997;36:91–7.

22. Kawai N, Niwa S, Sato M, Sato Y, Suwa Y, Ichihara I. Bone formation by cells from femurs cultured among three-dimensionally arranged hydroxyapatite granules. J Biomed Mater Res 1997;37:1–8.

23. Tsuruga E, Takita H, Itoh H, Wakisaka Y, Kuboki Y. Pore size of porous hydroxyapatite as the cell-substratum controls BMP-induced osteogenesis. J Biochem 1997; 121:317–24.

24. Freyman TM, Yannas IV, Gibson LJ. Cellular materials as porous scaffolds for tissue engineering. Prog Mater Sci 2001;46:273–82.

25. Cao Y, Mitchell G, Messina A, Price L, Thompson E, Penington A, et al. The influence of architecture on degradation and tissue ingrowth into three-dimensional poly(lactic–co-glycolic acid) scaffolds in vitro and in vivo. Biomaterials 2006;27:2854–64.

26. Lind M, Schumacker B, Soballe K, Keller J, Melsen F, Bunger C. Transforming growth factor-β enhances fracture healing in rabbit tibiae. Acta Orthop Scand 1993;64:553–6.

27. Beck LS, Amento EP, Xu Y, DeGuzman L, Lee WP, Nguyen T, Gillett NA. TGF-β1 induces bone closure of skull defects: Temporal dynamics of bone formation in defects exposed to rhTGF-β1. J Bone Miner Res 1993;8:753–61.

28. Wen HB, Hippensteel EA, Li P. Protein adsorption property of a biomimetic apatite coating. Key Eng Mater 2005;284–286:403–6.

29. Piskounova S, Forsgren J, Brohede U, Engqvist H, Stromme M. In vitro characterization of bioactive titanium dioxide/hydroxyapatite surfaces functionalized with BMP-2. J Biomed Mater Res B 2009;91:780–7.

30. Suárez-González D, Barnhart K, Migneco F, Flanagan C, Hollister SJ, Murphy WL. Controllable mineral coatings on PCL scaffolds as carriers for growth factor release. Biomaterials 2012;33:713–21.

Table I. Porosity and pore size of macropores in 3D scaffolds composed of hollow HA microspheres.

Microsphere diameter (μm)	Interconnected macroporosity (%)	% of macropores of size >100 μm
106–150	34 ± 3	10
150–250	38 ± 4	35

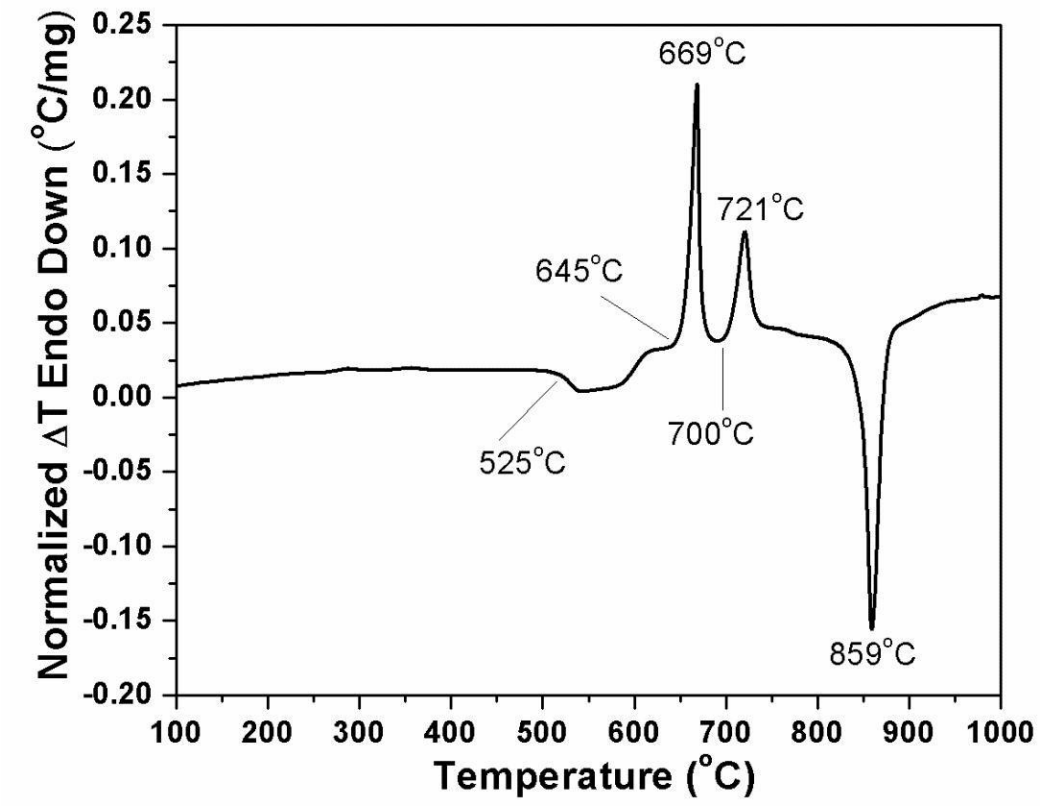

Figure 1. DTA pattern of borate (CaLB3-15) glass microspheres used for the creation of scaffolds of hollow HA microspheres by the glass conversion process.

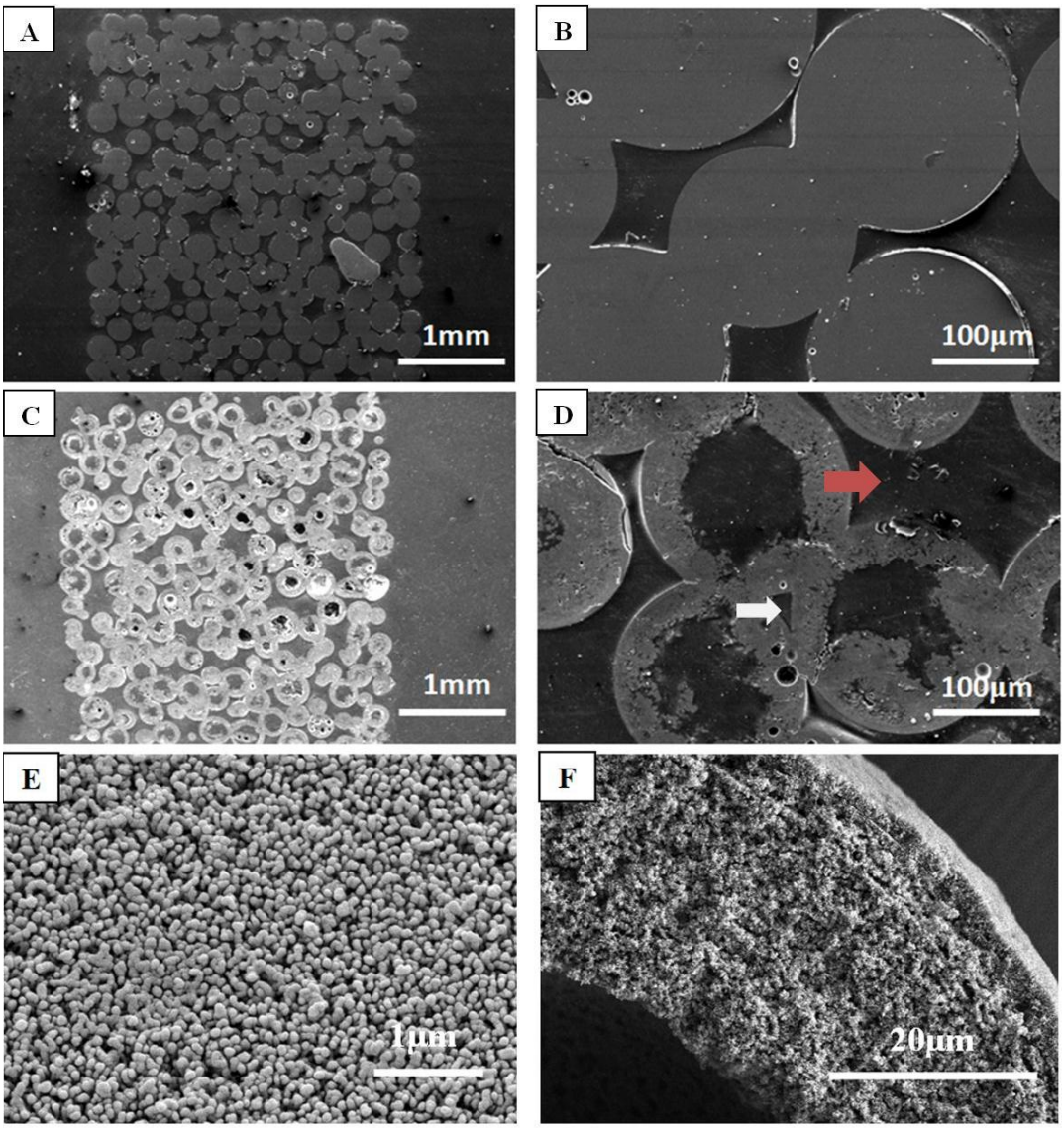

Figure 2. (A,B) Cross sections of 3D construct composed borate glass microspheres (150–250 µm); (C,D) cross sections of 3D scaffolds composed of hollow HA microspheres (150–250 µm) formed by the glass conversion process; SEM images of the surface (E) and the cross section (F) of the shell wall of the hollow HA microspheres.

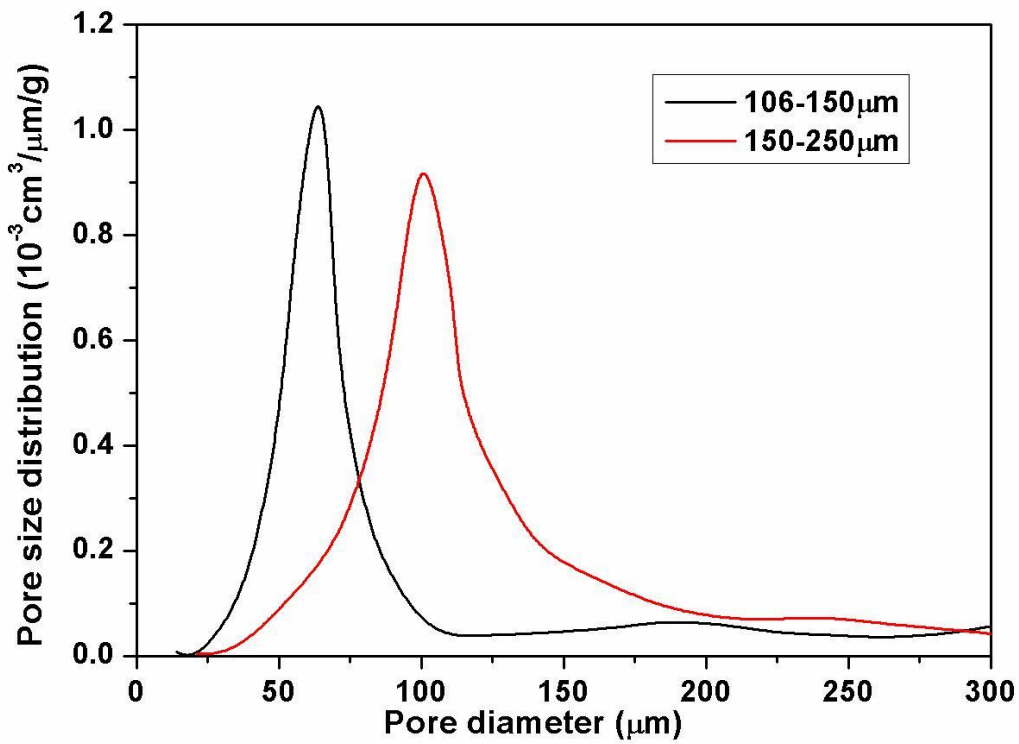

Figure 3. Size distribution of macropores in 3D scaffolds composed of hollow HA microspheres of diameter 106–150 μm and 150–250 μm, as determined by liquid extrusion porosimetry.

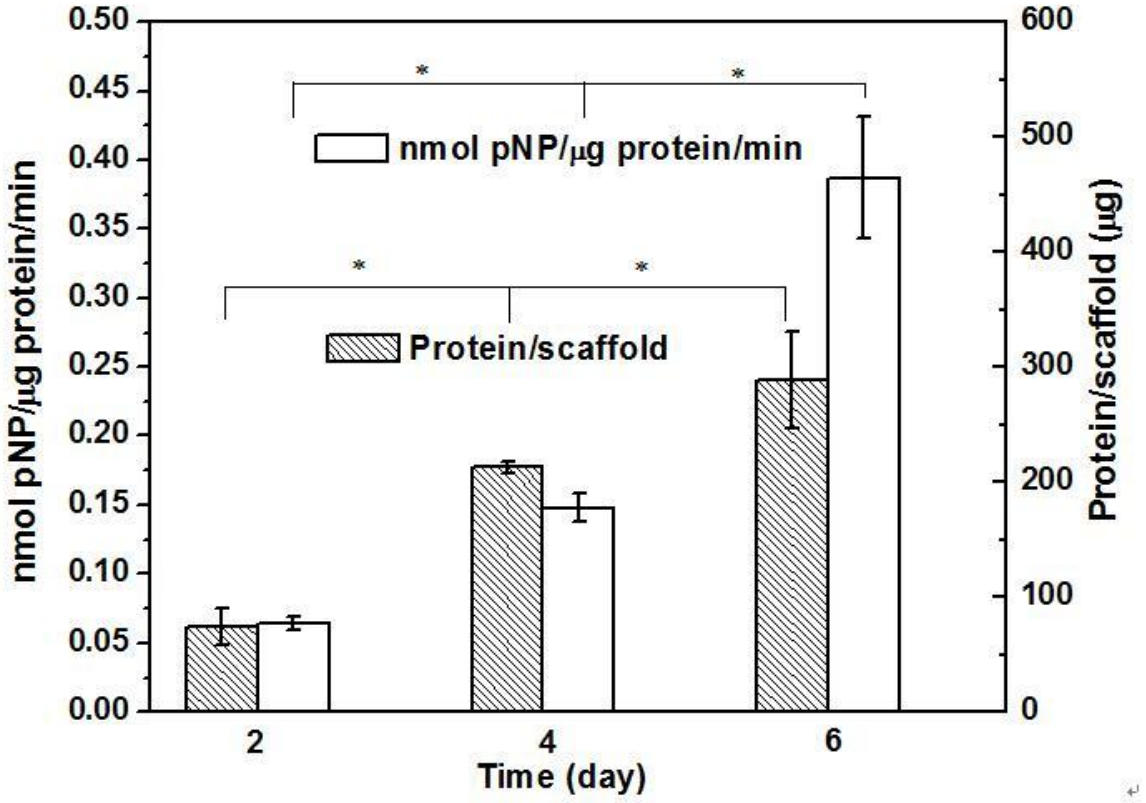

Figure 4. Protein amount and alkaline phosphatase activity of MLO-A5 cells cultured for 2, 4, and 6 days on scaffold (disc) composed of hollow HA microspheres. Mean ± SD; n=3. (*significant difference between groups; $p<0.05$.)

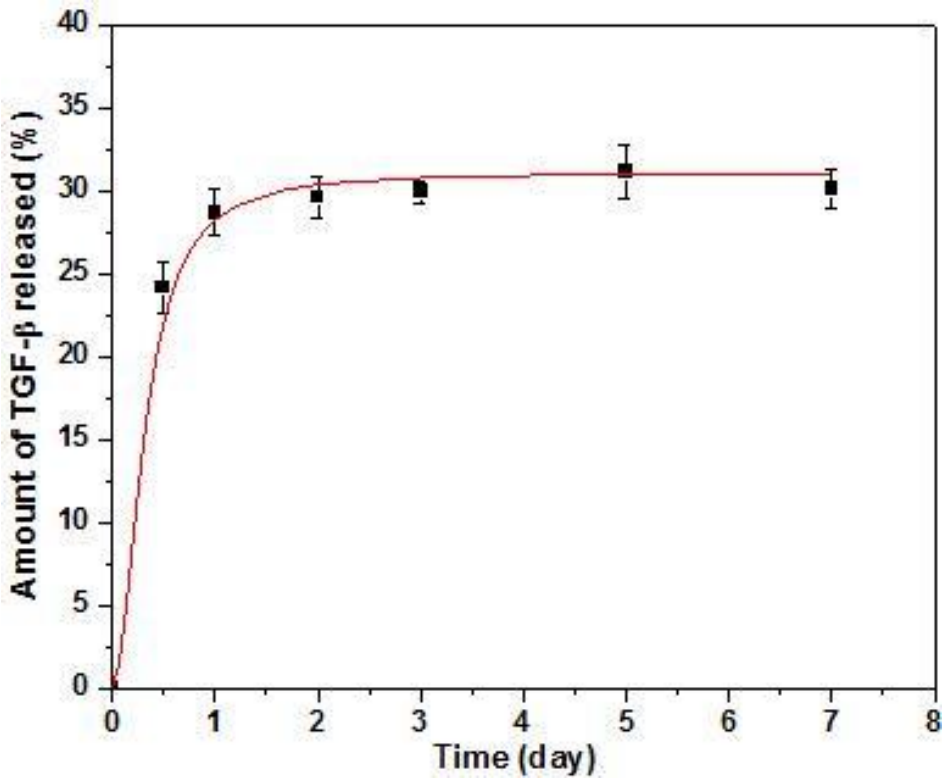

Figure 5. Amount of TGF-β1 released from 3D scaffolds (discs) composed of hollow HA microspheres (diameter = 106–150μm) into PBS as a function of time.

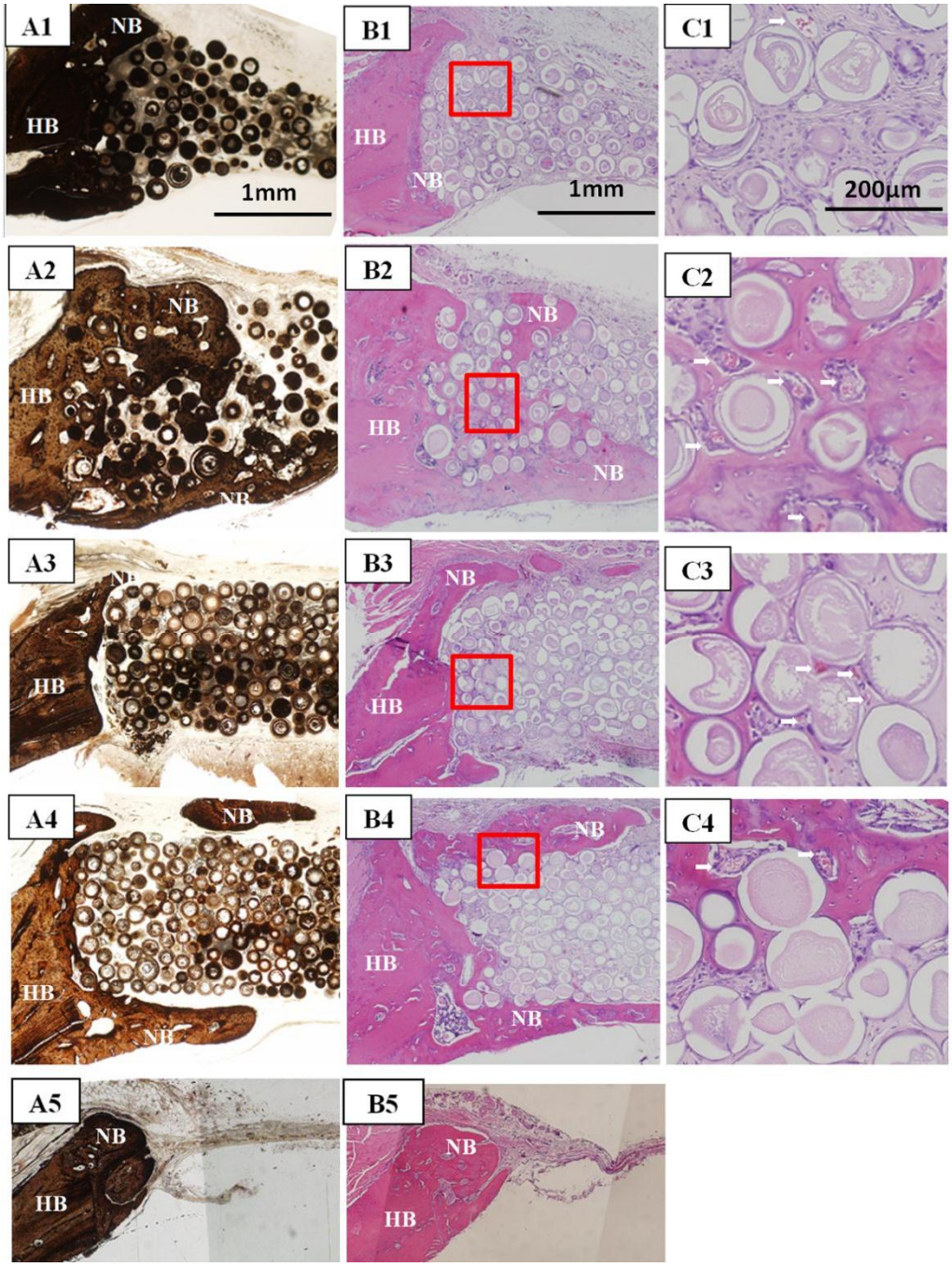

Figure 6. Von Kossa stained sections (A1–A4) and H&E stained sections (B1–C4) of implants composed of hollow HA microspheres (106–150 µm) after 6 weeks in rat calvarial defects: individual hollow HA microspheres (Group 2) without TGF-β1 (A1–C1) and with TGF-β1 (A2–C2); 3D scaffolds (Group 1) without TGF-β1 (A3–C3) and with TGF-β1 (A4–C4); von Kossa and H&E stained sections of the empty defects (A5, B5) are shown for comparison.

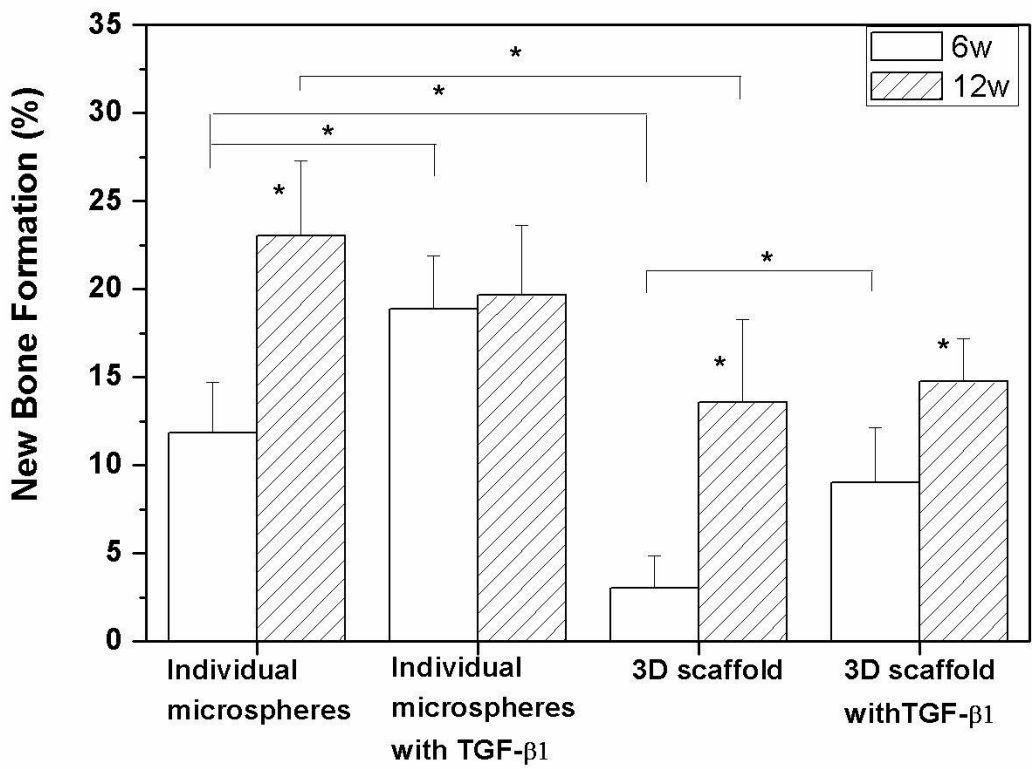

Figure 7. Percent new bone formation in implants composed of hollow HA microspheres (106–150 μm) after 6 and 12 weeks in rat calvarial defects. (Mean ± SD; n=5. *significant difference between groups; $p<0.05$).

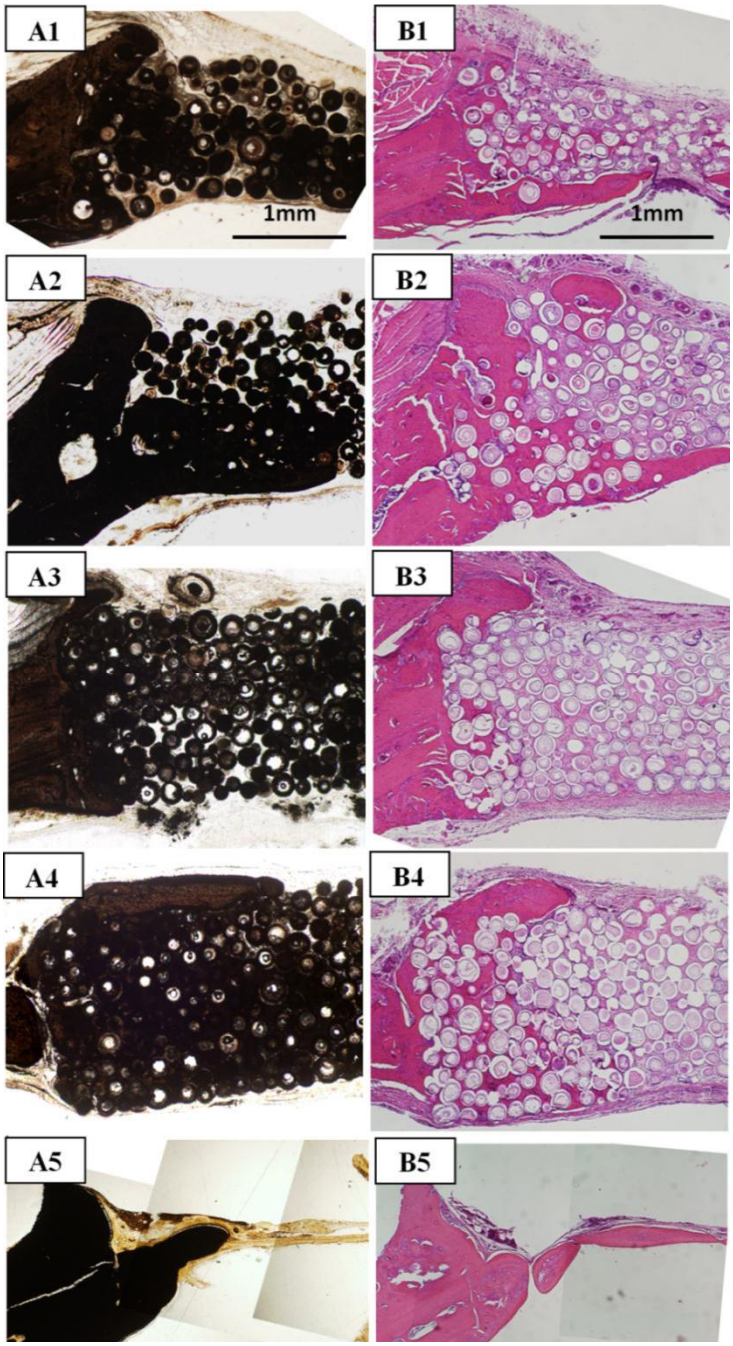

Figure 8. (*Left*) von Kossa and (*right*) H&E stained sections of implants composed of hollow HA microspheres (106–150 μm) after 12 weeks in rat calvarial defects: individual hollow HA microspheres (Group 2) without TGF-β1 (A1,B1) and with TGF-β1 (A2, B2); 3D scaffolds (Group 1) without TGF-β1 (A3,B3) and with TGF-β1 (A4,B4); stained sections of the empty defects are shown for comparison (A5,B5).

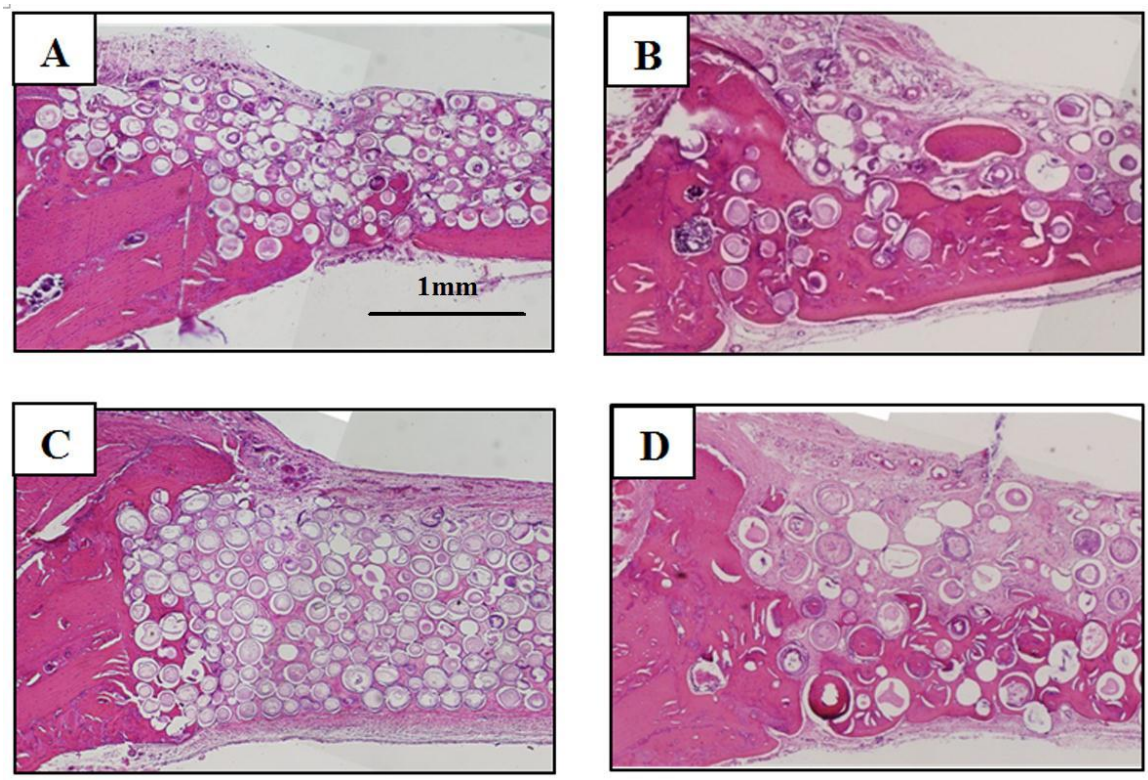

Figure 9. H&E stained sections of implants composed of hollow HA microspheres with two different microsphere diameter: individual microspheres of diameter 106–150 µm (A) and 150–250µm (B); 3D scaffold composed of microspheres of diameter 106–150 µm (C) and 150–250 µm (D).

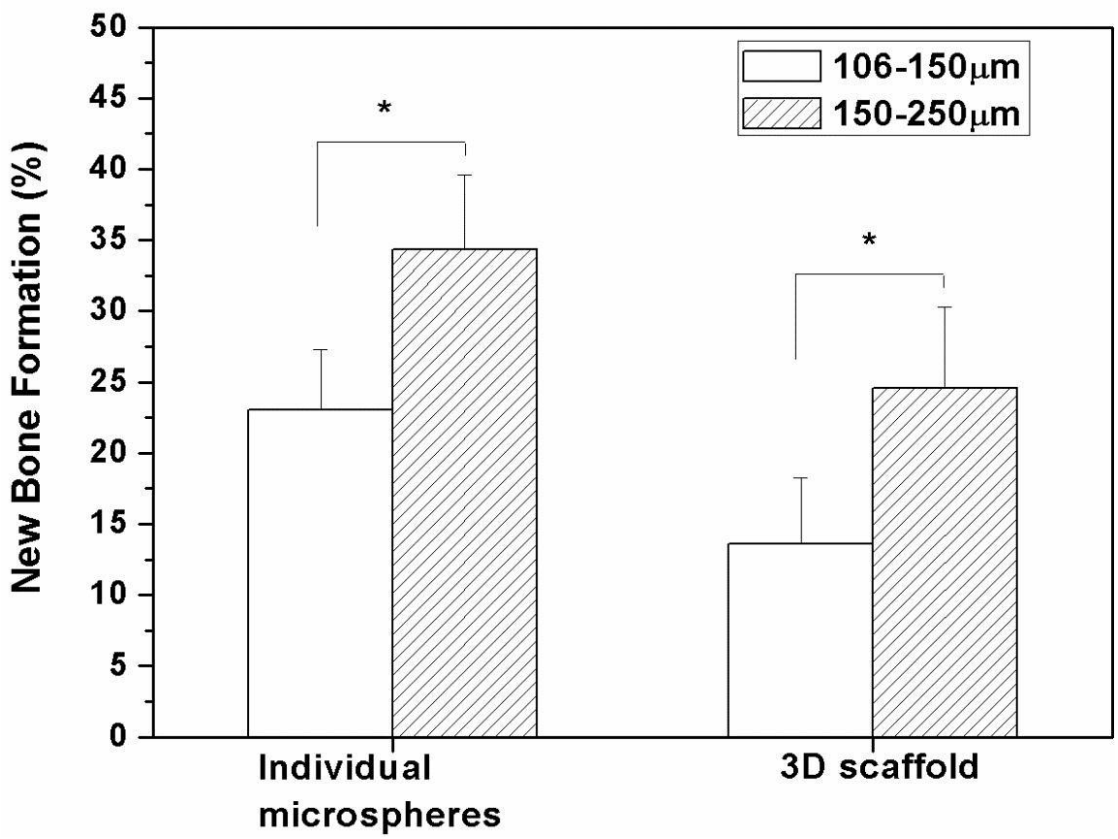

Figure 10. Percent new bone formation in implants composed of hollow HA microspheres of diameter 106–150 μm or 150–250 μm after 12 weeks in rat calvarial defects. (Mean ± SD; n=5. *significant difference between groups; $p<0.05$).

6. SUMMARY OF MAIN RESEARCH RESULTS

Hollow hydroxyapatite (HA) microspheres with a high surface area, mesoporous shell wall were prepared by converting borate glass microspheres with the composition (wt%): 15CaO, 10.63Li_2O, 74.37 B_2O_3, designated CaLB3-15, in dipotassium phosphate (K_2HPO_4) solution. Microspheres with an external diameter of 106–150 μm were used in most of the experiments, but microspheres of diameter 150–250 μm were also used.

The process parameters controlling the structural characteristics (hollow core diameter; pore size of the shell wall; surface area) of the as-prepared hollow HA microspheres were comprehensively investigated using an approach based on statistical design of experiments. Microspheres with larger hollow core size (ratio of the hollow core diameter to the external diameter of the sphere, $d/D \approx 0.6$) were obtained at lower temperature (25°C) or with low K_2HPO_4 concentration (0.02 M). In comparison, microspheres with high surface area (~140 m^2/g) were obtained at higher K_2HPO_4 concentration (0.25 M). The pH value of the K_2HPO_4 solution (9 or 12) had little effect on the characteristics of the HA microspheres. Potassium pyrophosphate ($K_4P_2O_7$), present as an impurity in the K_2HPO_4, can markedly reduce the conversion rate of the borate glass microspheres to HA in the K_2HPO_4 solution. In general, these experiments showed how hollow HA microspheres can be prepared reliably and reproducibly with the desired characteristics using the glass conversion process.

The structural characteristics of the as-prepared hollow HA microspheres can be modified by a subsequent thermal treatment (heating the microspheres for 0−24 hours at 500−900°C). Typically, heating at 500−600°C resulted in coarsening of the HA particles

and pores in the shell wall of the hollow HA microspheres, with a consequent reduction in the surface area; however, there was no measurable change in the total porosity of the shell wall. In comparison, heating at 900°C resulted in densification of the shell wall, resulting in hollow HA microspheres with dense shells.

A model protein, bovine serum albumin (BSA), was used to evaluate the ability of the hollow HA microspheres to serve as a device for controlled delivery of a protein in vitro. After loading, the BSA was shown to be present in both the mesoporous shell wall and in the hollow core of the HA microspheres. The release rate of BSA from the hollow HA microspheres into phosphate-buffered saline (BSA) was controlled by the structure of the mesoporous shell wall and by the concentration of BSA initially loaded into the microspheres. The duration of BSA released from the HA microspheres into PBS varied from 1–2 days for the as-prepared HA microspheres to 7–14 days for the HA microspheres heated for 5 hours at 600^{o}C. The total amount of BSA released into PBS was 30−40% of the BSA initially loaded into the microspheres.

Release of BSA from the hollow HA microspheres into a medium composed of poly(ethylene glycol), PEG, was also evaluated. In this case, the PEG was used to provide a mimicked environment of the extracellular matrix (ECM). When compared to the release into PBS, a more sustained release of BSA was observed in the PEG, but the total amount of BSA released into the PEG was approximately the same. Approximately 40% of the BSA initially loaded into the HA microspheres was released from the as-prepared HA microspheres after ~7 days when release of the BSA ceased. In comparison, BSA release from the heat-treated HA microspheres (600°C/5h) increased continuously, and reached a total value of 37% after 14 days.

In vitro cell culture confirmed that the hollow HA microspheres prepared in this work are biocompatible. The ability of hollow HA microspheres to support bone regeneration in a standard bone defect model (non-healing rat calvarial defects) was evaluated. Individual HA microspheres or three-dimensional (3D) scaffolds composed of hollow HA microspheres bonded at their contact points were evaluated. Bone regeneration increased significantly in both groups of implants with an increase in implantation time from 6 to 12 weeks. Bone regeneration was significantly higher in the implants composed of individual HA microspheres than in the 3D scaffolds after both implantation times. Loading the implants with TGF-β (5 μg/defect) significantly enhanced bone regeneration in both groups of implants 6 weeks postimplantation, but showed little effect in enhancing bone regeneration 12 weeks postimplantation. Increasing the HA microsphere diameter of the implants from 106–150 μm to 150–250 μm resulted in a significant increase in bone regeneration. These results indicate that individual hollow HA microspheres or 3D scaffolds composed of hollow HA microspheres loaded with a suitable growth factor could provide promising implants for bone regeneration.

7. ADDITIONAL WORK AND SUGGESTIONS FOR FUTURE WORK

In addition to the five manuscripts that formed the body of this PhD dissertation, additional work was performed recently which further supports the potential of the hollow HA microspheres in bone regeneration. These recent results could provide a basis for future work in this area.

7.1 HOLLOW HA MICROSPHERES LOADED WITH BMP-2 ACCELERATE BONE REGENERATION IN RAT CALVARIAL DEFECTS

As described previously (Paper 5 of this thesis), hollow HA microspheres loaded with TGF-β1 were evaluated for their ability to support bone regeneration in non-healing rat calvarial defects. In recent work, the microspheres were loaded with bone morphogenetic protein-2 (BMP-2), a more potent growth factor for bone regeneration, and evaluated in the same animal model. The surgical and histological procedures were similar to those described previously (Paper 5) and, for the sake of brevity, they will not be repeated in detail.

Briefly, two groups of implants were evaluated: (1) as-prepared hollow HA microspheres loaded with BMP-2 (Shenandoah Biotechnology Inc., PA, USA) (1 µg/defect), and (2) as-prepared hollow HA microspheres (without BMP-2) (control group). Scaffolds composed of individual HA microspheres (106–150µm) were used; 4 scaffolds for each group were implanted in rat calvarial defects for 6 weeks. The 2 groups of implants were not mixed in the same animal.

Figure 1 shows H&E and von Kossa stained sections of bone defects 6 weeks postimplantation. Implants without BMP-2 showed limited ability to regenerate bone

after the six-week implantation (Fig. 1-A, B), and the new bone formed mainly at the edges of the implants. In comparison, the HA microspheres loaded with BMP-2 showed a far greater ability to regenerate bone (Fig. 1-C, D); a large quantity of new bone (NB) infiltrated the implants and bridged the entire defect.

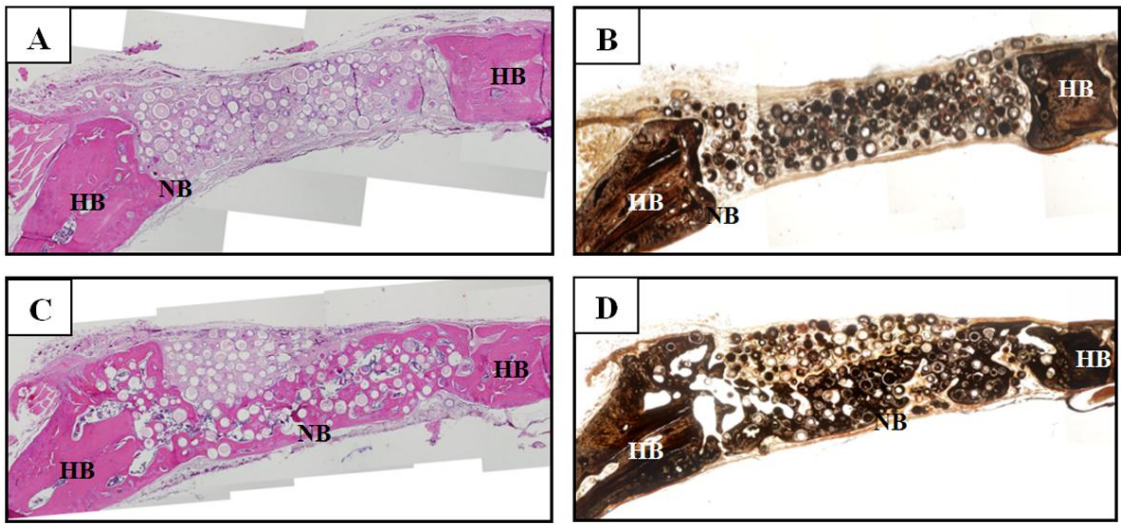

Figure 1. (*Left*) H&E and (*right*) von Kossa stained sections of implants composed of hollow HA microspheres (106–150 μm) after 6 weeks in rat calvarial defects: individual hollow HA microspheres without BMP-2 (A, B) and with BMP-2 (C, D).

Figure 2 shows the percentage new bone formed in the two groups of implants; for comparison, results for individual HA microspheres (heat treated for 5 hours at 600^{o}C) loaded with TGF-β1 (5 μg/defect) and implanted for 6 weeks (taken from Paper 5 of this thesis) are also shown. Loading the hollow HA microspheres with BMP-2 significantly enhanced bone formation when compared to the microspheres without BMP-2. Furthermore, bone regeneration in the microspheres loaded with BMP-2 (~36%) was significantly higher than bone regeneration (~19%) in the microspheres loaded with TGF-β1.

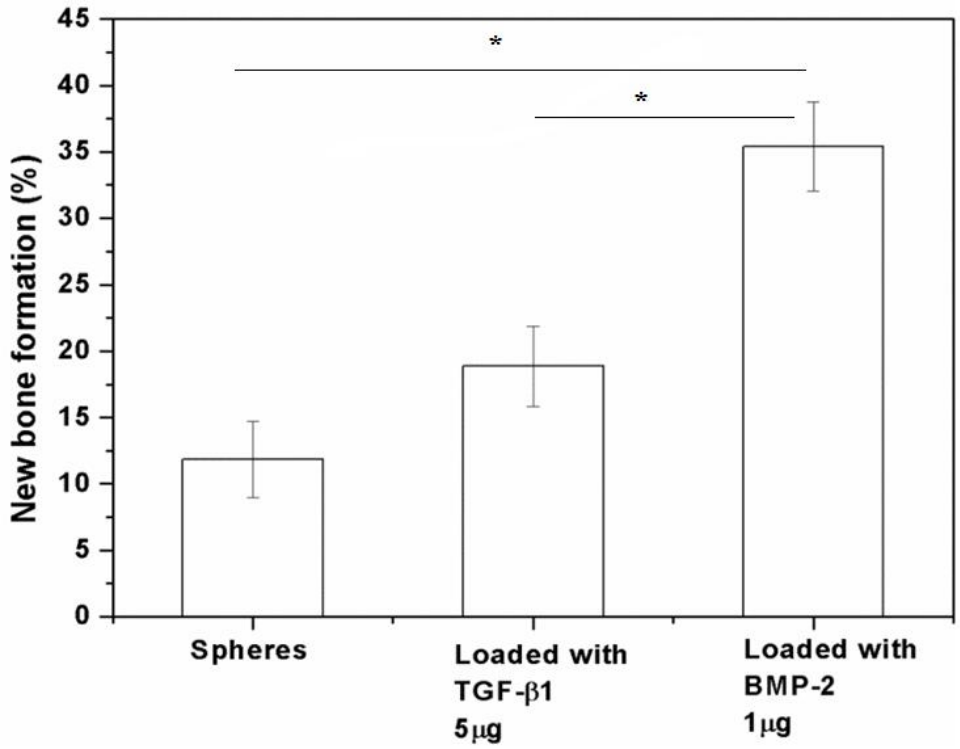

Figure 2. Percent new bone formation in implants composed of individual hollow HA microspheres (diameter 106–150 μm) after 6 weeks in rat calvarial defects: The groups consisted of hollow HA microspheres without growth factor (spheres), loaded with TGF-β1 (5 μg/defect), or loaded with BMP-2 (1 μg/defect). (Mean ± SD; n=5. *significant difference between groups; $p<0.05$).

7.2 USE OF POLYMER COATING TO MODIFY THE RELEASE RATE OF GROWTH FACTOR (TGF-β1) FROM HOLLOW HA MICROSPHERES

In the experiments described previously in this thesis, the hollow HA microspheres or 3D scaffolds composed of hollow HA microspheres were used as prepared or after heat treatment (typically 5 hours at 600^{o}C). The use of a polymer coating on the hollow HA microspheres was investigated as an approach to further control the release rate of a growth factor from the microspheres.

Three-dimensional scaffolds (discs), composed of hollow HA microspheres (106−150 μm), each with a mass of ~10 mg, were used in the experiments. The discs

were first coated with a 1% BSA solution in PBS and loaded with 10 μl TGF-β1 solution (50 ng TGF-β1 for each disc). The 3D scaffolds loaded TGF-β1 were then coated with a layer of poly(DL-lactic acid), PLA, by twice dipping the discs in a PLA solution and drying in air for 10 minutes. The PLA solution was prepared by dissolving PLA (Inherent viscosity = 0.55−0.75dl/g; Birmingham Polymers, Inc.) in chloroform. The concentration of the PLA was varied from 12.5 mg/ml to 50 mg/ml to vary the thickness of the PLA coating on the hollow HA microspheres. The coated discs were placed in PBS (2 discs in 2 ml PBS) and incubated, while shaking, at 37^{o}C. At periodic intervals, 50 μl PBS was removed for testing. Control samples containing a known amount of TGF-β1 in buffer were also incubated at 37^{o}C. The amount of The TGF-β1 present in the release buffer was determined by an enzyme-linked immunosorbent assay (ELISA). Concentrations of the unknown samples were quantified relative to a TGF-β1 standard curve run on the same plate.

The cumulative amount of TGF-β1 released from the disc composed of hollow HA microspheres was measured as a function of time (Fig. 3). Release of TGF-β1 from the uncoated disc was initially rapid, and almost ceased after 2 days; approximately 30% of the TGF-β1 initially loaded into microspheres was released into the medium after the two-day period. The presence of the PLA coating on the hollow HA microspheres resulted in a reduction in the release rate and to a more sustained release of TGF-β1; the release rate decreased and the duration of the release increased with the thickness of the PLA coating. For the thickest coating used, formed from the PLA solution with the highest concentration (50 mg PLA per ml), release of TGF-β1 was extended to over 2 weeks. The total amount of TGF-β1 released after the two-week period was ~24%.

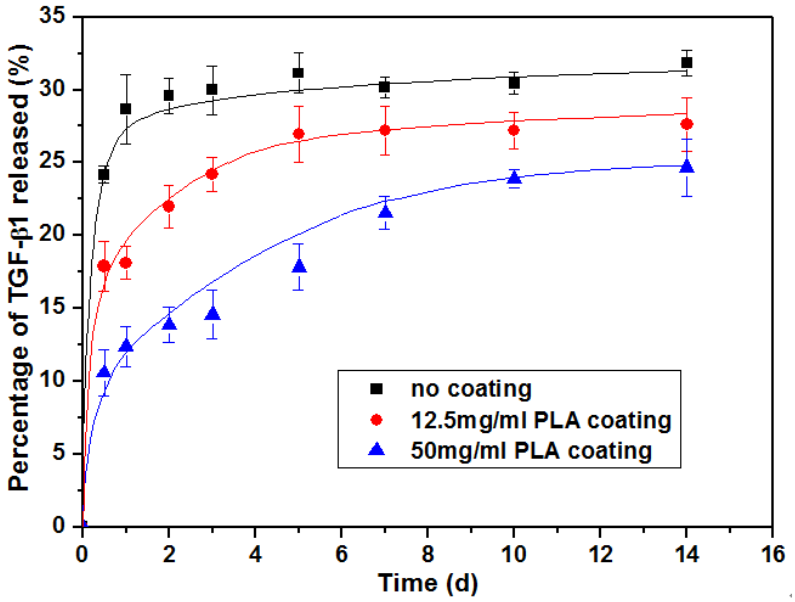

Figure 3. Cumulative release of TGF-β1 from discs composed of hollow HA microspheres into PBS as a function of time.

7.3 COMPOSITE SCAFFOLD COMPOSED OF HOLLOW HA MICROSPHERES DISPERSED IN A HYDROGEL

The combination of the hollow HA microspheres, growth factors, stem cells, and a biodegradable matrix (polymer or hydrogel) could provide a multifunctional scaffold to enhance bone regeneration in defects with a regular or irregular shape. Preliminary work has shown that the hollow HA microspheres can be dispersed in a hydrogel solution that is then gelled to form a composite scaffold. Figure 4 shows an example of a composite scaffold composed of 30 vol% hollow HA microspheres (106−150 μm) dispersed in an alginate hydrogel. An alginate solution (1% w/w) was prepared by mixing distilled water (at room temperature) with sodium alginate powder (Protanal RF 6650, FMC Biopolymer, USA). The alginate solution was then mixed with the hollow HA

microspheres and 80mM D-Gluconic acid-δ-lactone (DGL; Sigma, USA) which reacted with a small amount of the HA to release Ca^{2+} ions to crosslink the alginate polymer.

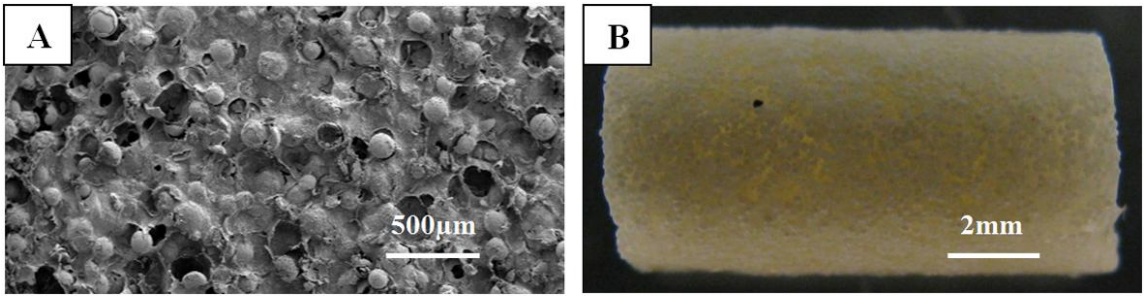

Figure 4. (A) SEM image of the cross section of a composite scaffold composed of 30 vol% hollow HA microspheres (106−150 µm) in an alginate matrix; (B) lower magnification optical image of the external surface of the composite scaffold.

7.4 SUGGESTIONS FOR FUTURE WORK

1. Determining the optimum concentration and loading method of BMP-2 in the hollow HA microspheres: As described previously, hollow HA microspheres loaded with BMP-2 showed greater capacity for bone regeneration in rat calvarial defects when compared to the microspheres without BMP-2. However, the amount of BMP-2 (1 µg/defect) loaded into the HA microspheres was based on information in the literature for other systems. Since BMP-2 is expensive, the optimum amount to be loaded into the microspheres should be investigated. The studies should consist of a combination of in vitro experiments (measuring the release kinetics of BMP-2 from the microspheres) and in vivo experiments (implantation of BMP-2 loaded microspheres in rat calvarial defects). The method used for loading the microspheres into the hollow HA microspheres should be optimized.

2. Size of hollow HA microspheres: Hollow HA microspheres with larger diameter (150−250 µm) showed greater capacity for regenerating bone when compared to

microspheres of diameter 106−150 μm. These larger microspheres should therefore be used in future work.

3. Controlling the sustained release of growth factor from the hollow HA microspheres: Measurement of the release of TGF-β1 from the hollow HA microspheres into PBS showed that the release was initially rapid and almost ceased within 2 days. Several applications would require a more sustained release. Recent work (described previously in this section; Fig. 3) showed that a more sustained release of TGF-β1 can be achieved by coating the hollow HA microspheres with a biodegradable polymer (PLA or PLGA). Experiments should be performed to determine (a) the formation of an optimal coating (biodegradable polymer composition and molecular weight; thickness and uniformity of the coating) on the HA microspheres; (b) the effect of the polymer coating on the release kinetics of a growth factor in vitro.

4. Composite (multifunctional) scaffolds: Composite scaffolds composed of hollow HA microspheres loaded with growth factors, stem cells, and a biodegradable matrix (e.g., biodegradable polymer or hydrogel) should be investigated to extend the work of this thesis to a wider range of potential applications. The composite could be used as a scaffold to fill a defect with a regular geometry or as an injectable scaffold to fill an irregular-shaped defect. Recent work described previously showed the feasibility of dispersing the hollow HA microspheres in a biodegradable alginate matrix. Future work should be performed to evaluate an appropriate matrix suitable for supporting bone regeneration (e.g., collagen, or collagen-based polymer), as well as the development and evaluation of composite scaffolds containing hollow HA microspheres.

5. Biodegradable hollow HA microspheres: Hollow HA microspheres prepared by the glass conversion process described in this thesis have a mesoporous shell wall composed of high surface area, nano size HA particles (Paper 1). The degradation of these hollow HA microspheres should be investigated. Enhancement of the degradation of the hollow HA microspheres by controlling the composition (e.g., a carbonate-substituted HA) should be studied. The ability to control the degradation rate of the hollow HA microspheres might be beneficial for improving the sustained release of growth factors as well as the total amount of growth factor released from the HA microspheres. HA has an affinity for growth factors; consequently, degradation of the HA microspheres might serve to release a greater amount of growth factor adsorbed on the HA surface. Degradation of the HA microspheres should also be beneficial for remodeling of the HA implants with new bone.

6. Microstructural modification of hollow HA microspheres: In the research described in this thesis, hollow HA microspheres were prepared by reacting borate glass microspheres in a K_2HPO_4 solution under a given set of conditions (e.g., pH = 9 or 12; temperature = 25°C, 37°C, or 60°C; solution concentration = 0.02 M, 0.10 M, or 0.25 M). The shell wall of the hollow HA microspheres typically consisted of a less porous, thin outer layer and a more porous, thicker inner layer (see Paper 1; Fig. 6). The use of borate glass particles of the same size but without the spheroidization step resulted in similar bi-layer structure of the HA shell wall; this indicated that changes in surface stress or surface composition resulting from the glass spheroidization step had little effect on the formation of the bi-layer structure. Instead, the conditions used in the glass conversion process appeared to more important. The use of varying reacting conditions (K_2HPO_4

concentration; temperature; pH) during the course of the conversion process to produce a homogeneous microstructure throughout the shell wall (instead of the bi-layer structure) should be investigated.

APPENDIX

LONG-TERM CONVERSION OF 45S5 BIOACTIVE GLASS-CERAMIC MICROSPHERES IN AQUEOUS PHOSPHATE SOLUTION

Hailuo Fu[1], Mohamed N. Rahaman[1], Delbert E. Day[1], Wenhai Huang[2]

[1]Department of Materials Science and Engineering, Center for Bone and Tissue Repair and Regeneration, Missouri University of Science and Technology, Rolla, MO 65409, USA

[2]Institute of Bioengineering & Information Technology Materials, Tongji University, Shanghai 200092, China

1 ABSTRACT

The conversion of 45S5 glass and glass–ceramics to a hydroxyapatite (HA)-like material in vitro has been studied extensively, but only for short reaction times (typically <3 months). In this paper, we report for the first time on the long-term conversion of 45S5 glass–ceramic microspheres (designated 45S5c) in an aqueous phosphate solution. Microspheres of 45S5c (75–150 μm) were immersed for 10 years at room temperature (~25°C) in K_2HPO_4 solution with a concentration of 0.01 M or 1.0 M, and with a starting pH of 7.0 or 9.5. The reacted 45S5c microspheres and solutions were analyzed using structural and analytical techniques. Only 25−45 vol% of the 45S5c microspheres were converted to an HA-like material after the 10 year reaction. In solutions with a starting pH of 9.5, an increase in the K_2HPO_4 concentration from 0.01 M to 1.0 M resulted in a doubling of the volume of the microspheres converted to an HA-like material but had little effect on the composition of the HA-like product. In comparison, reaction of the

45S5c microspheres in the solution with a starting pH of 7.0 resulted in an HA-like product in the 0.01 M K_2HPO_4 solution but a calcium pyrophosphate product, $Ca_{10}K_4(P_2O_7)_6.9H_2O$, in the 1.0 M solution. The consequences of these results for the long-term use of 45S5 glass–ceramics in biomedical applications are discussed.

2 INTRODUCTION

The silicate bioactive glass designated 45S5, often referred to by its trade name "Bioglass®", is generally considered to be the gold standard for bioactive glasses. Since its discovery by Hench et al. in 1971 [1], 45S5 glass (composition by weight: 24.5 Na_2O, 24.5 CaO, 45 SiO_2, 6 P_2O_5) has been the subject of many research and development studies [2, 3]. As a result of those studies, the bioactivity, degradation mechanisms, osteoconductivity, and bone-bonding ability of 45S5 have been well documented and explained [2, 3]. When immersed in an aqueous phosphate solution, such as the body fluid, 45S5 glass undergoes specific surface reactions, leading to the formation of a hydroxyapatite (HA)-like material on the surface of the glass [2]. It is generally acknowledged that the formation of the HA surface layer is responsible for the bioactivity and bone-bonding ability of 45S5 glass. Studies have shown that 45S5 glass converts slowly and incompletely to an HA-like material [4, 5].

Because of the narrow window between its glass transition temperature and the onset of crystallization, 45S5 glass is prone to crystallization during thermal processing, such as spheroidization of particles to form microspheres or the sintering of particles to form porous scaffolds [3, 6]. Commonly, the glass devitrifies during thermal processing to form a glass–ceramic containing the combeite crystalline phase ($Na_2O–2CaO–3SiO_2$)

predominantly. While devitrification does not inhibit the ability of 45S5 glass to form an HA-like surface layer, the glass–ceramic converts even more slowly to HA than 45S5 glass [7].

Despite the wide interest in the science and application of 45S5 glass and glass–ceramics, the conversion of these materials to HA in an aqueous phosphate solution have been studied only for short reaction times (typically less than ~3 months) [4, 5, 8]. The long-term conversion of 45S5 glass is of interest both scientifically and practically. Scientifically, it is unclear whether the glass continues to degrade slowly and eventually converts completely to a HA-like material. Practically, 45S5 glass is used in several biomedical applications [2]. While the silicon released as a result of the 45S5 degradation has been shown to be harmlessly excreted in a soluble form in the urine of rabbits [9], concerns about the long-term presence of silicon in the body, due to incomplete conversion of 45S5 glass, have been raised periodically.

The objective of this work was to evaluate the conversion of 45S5 glass–ceramic microspheres after immersion in aqueous phosphate solution at room temperature for ~10 years, far longer than any previous study. The microspheres were immersed in K_2HPO_4 solutions having two different concentrations (0.01 and 1.0 M) and two different pH values (7.0 and 9.5). Structural and analytical techniques were used to characterize the reacted microspheres and solutions.

3 EXPERIMENTAL PROCEDURE

Glass with the nominal 45S5 composition, 24.5 Na_2O, 24.5 CaO, 6.0 P_2O_5, 45.0 SiO_2 (wt%), was prepared by melting analytical grade Na_2CO_3, $CaCO_3$, NaH_2PO_4 and

SiO_2 in a platinum crucible for 1 h at 1500°C, and quenching the melt in water. The glass frit was crushed, sieved to give particles of size 75−150 μm, and spheroidized in a flame. The resulting microspheres consisted of a 45S5 glass–ceramic, denoted as 45S5c. To study the long-term conversion to a hydroxyapatite (HA)-like material, 5 g of the 45S5c microspheres were immersed in 500 ml of K_2HPO_4 (Acros Organics, Thermo Fisher Scientific, NJ) solution and kept in closed polyethylene containers at room temperature. Solutions with concentrations of 0.01 M and 1.0 M, and pH of 7.0 and 9.5 were used. After 10 years, the microspheres were removed from the solution, washed three times with distilled water, then twice with ethanol, and dried for >12 h at 90°C.

The reacted 45S5c microspheres were characterized using X-ray diffraction (XRD), and Fourier transform infrared (FTIR) spectroscopy. XRD was performed using Cu K_α radiation (λ = 0.15406 nm) at a scan rate of 1.8°/min in the 2θ range 5–70° (D/mas 2550 v; Rigaku; The Woodlands, TX, USA). FTIR (NEXUS 670 FTIR; Thermo Nicolet; Madison, WI, USA) was performed in the wavenumber range 400–2000 cm^{-1} (resolution = 8 cm^{-1}). A mass of 2 mg of the product was ground into a powder, mixed with 198 mg KBr, and pressed to form pellets for the FTIR analysis.

Cross sections of the reacted 45S5c microspheres were prepared and examined in a scanning electron microscope (SEM) to determine structural and compositional changes with distance from the surface of the microspheres. Microspheres were mounted in epoxy resin, ground with SiC paper, and polished with diamond paste down to 0.1 um, and observed in the SEM (Hitachi; S-4700) at an accelerating voltage of 10 kV and a working distance of 12 mm. The fractional volume of the 45S5c microsphere converted was determined by analyzing over five microspheres in the SEM images using Image-J

software. Energy-dispersive X-ray (EDS) analysis in the SEM (Hitachi; S-570) (accelerating voltage = 20 kV; working distance = 18 mm) was used to determine changes in the elemental composition across the sections.

To compare the long-term conversion with short-term conversion, 45S5c microspheres were immersed for 4 weeks in K_2HPO_4 solutions (0.01 M and 1.0 M) with a starting pH = 9.5 at 37°C. Sections of the reacted microspheres were prepared and examined in the SEM (Hitachi; S-4700) using the procedures described above.

The pH of the solution after the 10 year reaction was measured using a pH meter, while the concentration of Ca, Na, K and P ions in the phosphate solution was measured using inductively-coupled plasma optical emission spectrometry, ICP-OES (Optima 2000DV; Perkin Elmer, Waltham, MA).

The conversion kinetics of the 45S5c microspheres to HA in an aqueous K_2HPO_4 solution were determined from the weight loss of the microspheres as a function of time using a method described previously [4]. The microspheres were immersed for up to 4 weeks in 1M K_2HPO_4 solution (1 g microspheres per 100 ml solution) with a starting pH value of 9.5 at 37^{o}C and 60^{o}C. At selected times, the microspheres were removed from the solution, washed with deionized water and then with ethanol, and dried overnight at 90^{o}C. The fractional weight loss at time t was defined as $\Delta W = (W_o - W_t)/W_o$, where W_o is the initial weight of the glass, and W_t is the weight at time t. As described later, the activation energy for the conversion reaction was estimated from the conversion kinetics.

4 RESULTS

4.1 Composition and Phase Analysis of Reacted 45S5c Microspheres.

XRD patterns of the as-prepared 45S5 cglass–ceramic microspheres and 45S5 glass particles (no spheroidization step) are shown for reference in Fig. 1a. The glass particles showed a broad bond, centered at 30−35° 2θ, with no measurable diffraction peaks, indicating the absence of well-crystallized phases. In comparison, the 45S5c microspheres showed sharp diffraction peaks that corresponded predominantly to those of the combeite phase, $Na_2O{-}2CaO{-}3SiO_2$ (JCPDS 75-1687), as observed in other studies [10, 11].

Figure 1b shows the XRD patterns of the 45S5c microspheres after reaction for ~10 years at room temperature in K_2HPO_4 solutions with the same starting pH (7.0), but with two different concentrations (0.01 M and 1.0 M). A marked difference between the two XRD patterns is observed. For the lower concentration (0.01 M), diffraction peaks with low intensity (peak height) which can be assigned to a mixture of combeite (JCPDS 75-1687) and HA (JCPDS 72-1243) were found. In comparison, for the microspheres reacted in the 1 M K_2HPO_4 solution, sharp peaks corresponding to a calcium potassium pyrophosphate product, $Ca_{10}K_4(P_2O_7)_6(H_2O)_9$ (JCPDS 83-0912) were observed in the diffraction pattern.

XRD patterns of the 45S5c microspheres after reaction for 10 years at room temperature in 0.01 and 1.0 M K_2HPO_4 solutions with a starting pH of 9.5 are shown in Fig. 1c. For both solutions, the patterns of the reacted microspheres showed peaks corresponding to a mixture of combeite and HA, but the intensity of the HA peaks relative to the combeite peaks were higher for the microspheres reacted in the 1 M

solution. Qualitatively, the XRD patterns of the microspheres reacted in both K_2HPO_4 solutions at pH = 9.5 showed phases similar to those in the microspheres reacted in the 0.01 M K_2HPO_4 solution with a pH of 7.0.

FTIR spectra of the as-prepared 45S5c microspheres and 45S5 glass particles (no spheroidization step) are shown in Fig. 2a. Both spectra showed resonances in the region 900−1200 cm^{-1} which can be ascribed to absorption due to P–O and Si–O groups [12−14]. However, the spectra showed marked differences in the range 400−700 cm^{-1} which are presumably related to the presence of the combeite phase in the 45S5c microspheres.

Reaction of the 45S5c microspheres in the K_2HPO_4 solution for 10 years produced marked changes in the FTIR spectra. Fig. 2b shows the spectra for the microspheres reacted in the K_2HPO_4 solution with the same pH (7.0) but concentrations of 0.01 and 1.0 M. For the 0.01 M solution, the most dominant resonances corresponded to the phosphate v3 resonance, centered at ~1,040 cm^{-1}, and the phosphate v4 resonance, with peaks centered at ~560 and ~605 cm^{-1}, which are associated with the presence of HA [15, 16]. In contrast, the FTIR spectrum of the product formed in the 1.0 M solution at this pH was markedly different. The asymmetric and symmetric terminal stretching vibrations of P-O groups usually occur in the region 1,250–980 cm^{-1} [17–19]. The intense band observed at 1,175 cm^{-1} is attributed to the asymmetric P–O stretching, while the symmetric P–O stretching is located at 1,024 cm^{-1}. Resonances corresponding to P–OH vibrations are observed at 916 cm^{-1}. The resonance observed at 723 cm^{-1} is attributed to symmetric P–O–P bridge vibration, while the resonance centered at ~550 cm^{-1} can be attributed to O−P−O bending. The absorptions between 400 to 520 cm^{-1} are due to the

presences of oxygen−calcium bonds [20]. Taken together, the FTIR spectrum showed that the product formed in 1.0 M K_2HPO_4 solution at pH = 7.0 contained the $(P_2O_7)^{2-}$, $(HP_2O_7)^{3-}$ and $(PO_4)^{3-}$, indicating the presence of a pyrophosphate, as well as a phosphate material.

Fig. 2c shows the FTIR spectra for the 45S5c microspheres reacted in the K_2HPO_4 solutions with a starting pH of 9.5. The solution concentration (0.01 M and 1.0 M) had little effect on the FTIR spectra. The most dominant resonances were the phosphate v3 resonance, centered at ~1,040 cm^{-1}, and the phosphate v4 resonance, with peaks at ~605 and 560 cm^{-1}, which are associated with HA [15, 16]. In general, for K_2HPO_4 solutions with pH = 9.5, the spectra of the reacted 45S5c microspheres were similar to that for the 45S5c microspheres reacted in the 0.01 M K_2HPO_4 solution at pH = 7.0

To summarize at this stage, the results of the FTIR analysis showed good agreement with the XRD results described previously. The reaction product of the 45S5c microspheres immersed in the K_2HPO_4 solution with a starting pH of 9.5 showed little effect of the solution concentration; the results showed the presence of an HA-like product. In contrast, for a solution with a starting pH of 7.0, the results are compatible with the formation of an HA-like product for a K_2HPO_4 concentration of 0.01 M, but a pyrophosphate product with presumably a small amount of an HA-like product for a concentration of 1.0 M.

4.2 Microstructure and Microchemical Analysis of the Reacted 45S5c Microspheres.

SEM images of the surface and cross section of the as-prepared 45S5c microspheres are shown for reference in Fig. 3. The surface of the microspheres showed the presence of needle-like crystals (Fig. 3a), which presumably corresponded to the

combeite phase found previously from the XRD pattern. In comparison, the polished cross section of the as-prepared 45S5c microspheres (Fig. 3b) shows a dense homogeneous structure, with little phase contrast from the surface to the interior.

SEM images of the cross sections of 45S5c microspheres immersed for 10 years in the K_2HPO_4 solutions (concentrations = 0.01 M and 1.0 M; starting pH = 7.0 and 9.5) are shown in Fig. 4 a-d. Based on differences in contrast, the sections in Fig. 4a, c, d were divided into three regions: (1) a surface layer (A), (2) an intermediate layer (B), and (3) a core (C). EDS analysis was performed at three different positions at the midpoint of each region and the average value of the elemental concentration was taken. The section in Fig. 4b did not show large differences in contrast; only two regions, an outer region (A, B) and a core C, were vaguely discernible. Nevertheless, the letters A, B, and C show the positions at which EDS analysis was performed.

For the 45S5c microspheres reacted in the solution with pH = 7.0, the surface layer had a thickness of ~5 μm when the K_2HPO_4 concentration was 0.01 M (Fig. 4a). When the microspheres were reacted in the K_2HPO_4 solution with a starting pH = 9.5, the thickness of the surface layer A increased from ~5 μm for the 0.01 M solution (Fig. 4c) to ~10 μm for 1.0 M solution (Fig. 4d). The images indicate that for the microspheres reacted in the 0.01 M K_2HPO_4 solution, an increase in the pH from 7.0 to 9.5 apparently had little effect on the thickness (~5 μm) of the surface layer (Fig. 4a, c).

Table I summarizes the EDS data for Ca/P atomic ratio and the Na concentration (wt%) in the three regions A, B, and C shown in the cross sections of the reacted 45S5c microspheres (Fig. 4). The Ca/P ratio varied from 1.3 to 2.5 for the surface layer (A) to ~5.4 for the core (C). For comparison, the theoretical values for HA and 45S5 glass are

1.67 and 5.4, respectively. The measured Na concentration in the surface layer (A) was 0.9−1.0 wt%, except for the microspheres reacted in the 1 M K_2HPO_4 solution at pH = 7.0, in which the value was 4.8 wt%. For the core (C), the measured Na concentration was 15.7−17.7 wt% for all four reaction conditions (Table I), compared to a theoretical value of 18.2 wt% for 45S5 glass, indicating that little Na had dissolved out of the core during the 10 year reaction.

Taken with the XRD and FTIR results described previously, the results of the EDS analysis are consistent with the formation of a calcium phosphate product in the surface layer (A) and an unconverted 45S5 core (C). The region B in the cross sections is presumably an intermediate region; as described previously, for the microspheres reacted in the 1.0 M K_2HPO_4 solution at pH = 7.0, an intermediate layer was not clearly discernible.

SEM images of the cross sections of 45S5c microspheres immersed for 4 weeks in the K_2HPO_4 solutions (0.01 and 1.0 M; starting pH = 9.5) at 37°C are shown in Fig. 4e, f. Compared with the images shown in Fig. 4c, d, both the converted surface layer and the intermediate layer were thinner than those in the microspheres reacted for 10 years. For the 45S5c microspheres reacted for 4 weeks in the 0.01 M K_2HPO_4 solution, the surface layer had a thickness of 1–2 μm (Fig. 4e), while the intermediate layer had a thickness of ~1μm. After reaction of the microspheres in the 1.0 M K_2HPO_4 solution (Fig. 4f), the thickness of the surface layer was also 1–2 μm, but the thickness of the intermediate layer was much larger (~10 μm).

4.3 pH and Ionic Concentration of K_2HPO_4 Solution.

Table II shows data for the pH and ionic concentration of selected elements (Na, P, Ca, and K) in the K_2HPO_4 solutions after the 10 year reaction. For comparison, assuming that all the 45S5 glass was completely dissolved in a pure aqueous medium, the "theoretical" concentrations of the Na, Ca, and P in the aqueous medium are also shown. The ionic concentration of Na, K, Ca, and P are strongly dependent on the concentration of the starting K_2HPO_4 solution but almost independent of the starting pH. The concentration of Ca in all the solutions after the 10 year reaction was small (0.065–1.2 mmol/l), indicating that almost all the Ca ions dissolved from the glass had reacted with the phosphate ions to precipitate a calcium phosphate product, as found in previous studies [4, 5]. For the reaction in 0.01 M K_2HPO_4 solution, the Na ion concentration in the solution was 23−25 mmol/l, indicating ~30% of the Na in the starting 45S5 microspheres had dissolved into the K_2HPO_4 solution. In comparison, the Na concentration in the 1.0 M K_2HPO_4 solution was 43−47 mmol/l, indicating that 55−60% of the Na in the starting glass had dissolved into the solution.

There was an increase in the pH of the solution; for the conditions used in this work, the magnitude of the increase was dependent primarily on the K_2HPO_4 concentration and secondarily on the starting pH value. Solutions with the lower K_2HPO_4 concentration (0.01 M) showed the highest increase in pH value, from 7.0 to 11.7 and from 9.5 to 12.3 (Table II). In comparison, the pH of the 1.0 M K_2HPO_4 solution increased from 7.0 to 7.6 and from 9.5 to 10.6.

4.4 Kinetics of 45S5c Conversion to Hydroxyapatite.

Fig. 5 shows the fractional weight loss ΔW of the 45S5c microspheres as a function of immersion time *t* in 1.0 M K_2HPO_4 solution at 37°C and 60°C. The weight loss increased faster with time at the higher reaction temperature. After reaction for 4 weeks, the weight loss at 60°C was 23%, almost twice the value at 37°C (12%). Using the maximum weight loss ΔW_{max} = 42% observed for the conversion of 45S5 glass particles (150–300 μm) in 0.02 M K_2HPO_4 solution at 37°C [4], the weight loss data were normalized to show the fraction, α, of the 45S5c microspheres converted to HA as a function of time, where $\alpha = \Delta W/\Delta W_{max}$ (Fig. 6). As observed in previous studies for 45S5 glass particles [21] and 13-93 glass scaffolds [22], following an initial period (~100 h), the kinetics of 45S5c conversion to HA at both temperatures can be well fitted by a three-dimensional (3D) diffusion model (dashed lines in Fig. 5), given by the equation:

$$\left[1-(1-\alpha)^{1/3}\right]^2 = Kt \qquad (1)$$

where *K* is a temperature-dependent constant given by the Arrhenius relation:

$$K = K_o \exp(-Q/RT) \qquad (2)$$

where K_o is a constant, *Q* is the activation energy for the conversion process, *R* is the gas constant, and *T* is the absolute temperature. Least-squares fitting of the data using Eq. (1) gave $K_o = 6.8 \times 10^{-6}$ day^{-1} and Q = 66 kJ/mol.

5 DISCUSSION

The results showed that the conversion of 45S5c glass–ceramic microspheres (75–150 μm) to a calcium phosphate material was incomplete even after immersion for

10 years in an aqueous K_2HPO_4 solution (0.01 or 1.0 M) at room temperature (~25°C). Since microspheres and porous 3D scaffolds of 45S5 glass–ceramic are being used or studied for several biomedical applications [2, 3, 11, 23], these results indicate that a large fraction of unconverted 45S5 glass-ceramic material could still remain in vivo even after long implantation times.

The results of the present work also provided new information on the conversion of 45S5 glass−ceramic microspheres after long-term reaction in an aqueous phosphate solution. In a basic K_2HPO_4 solution (starting pH = 9.5), XRD and FTIR indicated that a product of the partially converted 45S5 microspheres was an HA-like material for both low concentration (0.01 M) and high concentration (1.0 M) of the K_2HPO_4 solution. This is consistent with previous observations which showed that HA was the most stable calcium phosphate phase in aqueous solution at pH values greater than 4–5 [24].

In comparison, in a K_2HPO_4 solution with a neutral starting pH (7.0), the concentration of the solution had a marked effect on the composition of the conversion product. At low concentration (0.01 M), XRD and FTIR indicated that an HA-like product was formed in the partially-converted 45S5c microspheres. However, at high concentration (1.0 M), XRD and FTIR indicated a product corresponding to a calcium pyrophosphate product. The XRD pattern showed intense peaks that corresponded to that of a reference $Ca_{10}K_4(P_2O_7)_6.9H_2O$ (JCPDS 83-0912). The formation of the pyrophosphate product can be explained in terms of the high concentration of $(HPO_4)^{2-}$ ions present at pH = 7.0, and the tendency of phosphate ions to form dimers, trimers, and polyphosphates [25]. In particular, $(HPO_4)^{2-}$ ions are known to form pyrophosphate ions in solution, according to the reaction:

$$2(HPO_4)^{2-} \leftrightarrow (P_2O_7)^{4-} + H_2O \quad (3)$$

In the presence of high concentrations of $(P_2O_7)^{4-}$ and K^+ ions, presumably the Ca^{2+} ions dissolving out of the 45S5 glass–ceramic reacted to form a pyrophosphate product, which can be described by the equation:

$$10Ca^{2+} + 4K^+ + 6(P_2O_7)^{4-} + 9H_2O \rightarrow Ca_{10}K_4(P_2O_7)_6.9H_2O \quad (4)$$

The pyrophosphate product in Eq. (4) was the dominant phase identified by XRD; however, FTIR indicated that other phosphate phases, presumably amorphous or in small concentration, might also be present.

For the pH values and concentrations of the K_2HPO_4 solutions used in this work, SEM and EDS analysis of the polished sections of the reacted 45S5c microspheres showed a core (C in Fig. 4) with a high Ca/P atomic ratio and a high concentration of Na, comparable to the values of the starting 45S5c material (Table I). These SEM and EDS observations clearly indicated an unconverted 45S5c core. ICP-OES analysis showed only limited concentrations of phosphorus (P) in the 0.01 M K_2HPO_4 solutions after the 10 year reaction (Table II), which indicated that the conversion reaction in these solutions stopped because of the lack of phosphate ions in the solution. However, the conversion reaction was also incomplete in the 1.0 M K_2HPO_4 solution with a starting pH of 9.5, despite the presence of a large concentration of P. Therefore, the incomplete conversion in this 1.0 M K_2HPO_4 solution (pH = 9.5) cannot be attributed to the lack of phosphate ions, but to other factors discussed elsewhere [4, 5].

As discussed above, when the 45S5c microspheres were reacted in the 1.0 M K_2HPO_4 solution with a starting pH of 7.0, XRD showed intense peaks of a calcium pyrophosphate phase, $Ca_{10}K_4(P_2O_7)_6.9H_2O$. EDS analysis of the near-surface region of

the reacted microspheres (A in Fig. 4b) showed a Ca/P atomic ratio of 1.33, far larger than the theoretical value (0.83) for the $Ca_{10}K_4(P_2O_7)_6.9H_2O$ phase. The reason for this larger Ca/P ratio is unclear. However, the presence an amorphous calcium phosphate material not detected by XRD but indicated from the FTIR spectrum could contribute to the higher Ca/P ratio observed.

For the other reaction conditions used in this work, XRD and FTIR showed the presence of an HA-like material in the partially converted product. SEM images showed that the reaction product of the 45S5c microspheres consisted of a surface layer (region A in Fig. 4a, c, d). Based on differences in contrast in the SEM images, this HA-like surface layer was determined to have a thickness of ~5 μm when the microspheres were reacted in a 0.01 M K_2HPO_4 (pH = 7.0 or 9.5) for 10 years. In comparison, the thickness of the HA-like layer increased to ~10 μm when the microspheres were reacted in a 1.0 M K_2HPO_4 solution (pH = 9.5) for ten years; this is compatible with an increase in the conversion rate with an increase in the reactant (K_2HPO_4) concentration.

Scanning electron microscopic images of the cross sections of the reacted microspheres (4 weeks vs. 10 years) showed that the 45S5c conversion increased slowly with reaction time. When immersed in 0.01 M K_2HPO_4 solution (pH = 9.5), the thickness of the HA-like surface layer increased from ~2 μm after 4 weeks at 37°C (Fig. 4e) to ~5 μm after 10 years at room temperature (Fig. 4c). In the 1.0 M K_2HPO_4 solution (pH = 9.5), the thickness of the HA-like surface layer increased from ~2 μm after 4 weeks at 37°C (Fig. 4f) to ~10 μm after 10 years at room temperature (Fig. 4d). The thickness of the intermediate layer also increased with reaction time (4 weeks at 37°C vs. 10 years at room temperature) in the 0.01 M and 1.0 M solutions.

EDS analysis of the surface layer of the 45S5 microspheres reacted in the 1.0 M K_2HPO_4 solution (starting pH = 9.5) showed a Ca/P atomic ratio of 1.49 (Table I) which is lower than the value (1.67) for stoichiometric HA. In previous studies, the conversion of 45S5 glass also showed a Ca/P ratio smaller than the theoretical value for HA, and was discussed in terms of a calcium-deficient HA [3]. In comparison, for the 45S5c microspheres reacted in the 0.01 M K_2HPO_4 solution, the Ca/P ratios of the surface layer are 2.13 (pH = 7.0) and 2.46 (pH = 9.5). It is not clear why these Ca/P ratios are higher than the theoretical values for HA, but two factors may be suggested. First, the surface layer may not be fully converted to an HA-like material. As described previously, the XRD patterns (Fig. 2) showed peaks corresponding to those of both HA and combeite. Because the Ca/P ratio of the 45S5 composition is 5.43, unconverted 45S5 material could lead to a marked increase in the Ca/P ratio of the surface layer. Second, even if it were fully reacted, the surface layer had a thickness of only ~5 μm (Fig. 4); partial sampling of the intermediate layer (Ca/P ratio 3.87 or 5.35) by the electron beam could result in an increase in the Ca/P ratio.

As discussed previously, based on differences in contrast in SEM images of the reacted 45S5c microspheres, a surface layer (attributed to the converted layer) of ~5 μm was determined for the microspheres reacted in the 0.01 M K_2HPO_4 solution (pH = 7.0 or 9.5) (Fig. 4a, c). Since the diameter of the microspheres was 100−120 μm, the fraction of the microspheres converted to an HA-like material was ~25 vol%. According to the ICP-OES data (Table II), the amount of Na dissolved from the glass into the solution was ~30%, which could be attributed to the Na dissolved from the converted layer (~25%), plus some Na dissolved from the intermediate layer (~5%). For the 1.0 M K_2HPO_4

solution (pH = 9.5), the thickness of the surface (converted) layer was estimated to be ~10 μm, and the fraction converted to an HA-like material is therefore ~45 vol%. In this case, the ICP data show that 55−60% of the Na from the glass was dissolved into the solution, which could be attributed to ~45% from the converted layer and 10-15% from the intermediate layer.

Over the 10 year reaction period, the pH of the K_2HPO_4 solution showed an increase which was strongly dependent on the concentration of the starting solution (Table II). A far larger increase in pH was observed for the solutions with the lower starting concentration (0.01 M). As described elsewhere [4, 5], the conversion reaction resulted in a consumption of phosphate ions from the solution and the dissolution of silicon (presumably as silicic acid) and sodium ions into the solution. Since phosphoric acid is a stronger acid than silicic acid, the consumption of a larger percentage of the phosphate ions from the 0.01 M K_2HPO_4 starting solution could result in a marked increase in the pH of the solution, as observed. In comparison, for the more concentrated 1.0 M K_2HPO_4 solution, a smaller percentage of the phosphate ions present in the starting solution is consumed in the conversion reaction, resulting in a smaller increase in the pH (Table II).

As described previously, after an initial period (~100 h), the kinetics of 45S5c conversion to an HA-like material can be well fitted by a 3D diffusion model (Eq. (1)), which is in agreement with previous studies for 45S5 glass particles [21] and silicate 13-93 glass scaffolds [22]. Using the values for K_o and Q obtained by fitting Eq. (1) to the data in Fig. 5, the rate constant K was found to be 2×10^{-5} day^{-1} at room temperature and 6×10^{-5} day^{-1} at 37°C (the body temperature). According to Eq. (1), the time required to

achieve the maximum amount of 45S5c conversion is given as $t_f = 1/K$ (when $\alpha = 1$), which is equal to ~140 years at room temperature and ~45 years at 37°C in 1.0 M K_2HPO_4 solution at pH = 9.5.

While the results of the present work indicate that the 45S5c microspheres may not fully degrade in vivo, the limitations of the present experiments in relation to the environment in vivo should be recognized. In vivo, the pH of the human body fluid is ~7.4, and the temperature is ~37.4°C. One key difference is that the $(HPO_4)^{2-}$ concentration of the body fluid (~1 mmol/l) is far lower than the K_2HPO_4 concentrations used in this work (10 and 1,000 mM). The present results showed a reduction in the thickness of the converted layer by a factor of ~2 with a reduction in the K_2HPO_4 concentration from 1 to 10 mM. A reduction in the K_2HPO_4 concentration to 1 mM is expected to result in a further reduction in the conversion rate to HA. Another difference is that the present system was generally static (little stirring of the reactants over the 10 year period) whereas environment in vivo is dynamic. As a result, ionic concentration gradients in vivo are expected to be higher than those in this work. A third difference is the absence of biomolecules and cells in the present experiments. In a previous study, the conversion of a silicate bioactive glass (designated 13-93) to HA in vivo (subcutaneous implantation in rats) was found to be faster than that in vitro (immersion in a simulated body fluid at 37°C) [26]. In that study, the converted layer in vivo was found to be ~2 times thicker than the converted layer in vitro. Presumably, a comparable increase in the conversion rate of the 45S5c microspheres could be expected in vivo. In general, despite the differences between the in vitro conditions used in this work and the in vivo

environment, it appears unlikely that full conversion could be achieved in vivo for 45S5 glass–ceramic implants with dimensions similar to or larger than those used in this work.

6 CONCLUSIONS

The results of the present work provide for the first time, information on the long-term conversion of 45S5 glass–ceramic microspheres (designated 45S5c) in an aqueous phosphate solution. Reaction of 45S5c microspheres (75−150 μm) in a K_2HPO_4 solution at room temperature for 10 years resulted in only partial conversion of the microspheres to a hydroxyapatite (HA)-like material. The fractional volume of the 45S5c microspheres converted was markedly dependent on the concentration of the K_2HPO_4 solution, increasing from ~25% (0.01 M solution) to ~45% (1.0 M solution). The starting pH of the solution (7.0 or 9.5) had little effect on the fraction of the microspheres converted in the 0.01 M K_2HPO_4 solution. For both starting pH values, the conversion product of the 45S5 microspheres immersed in the 0.01 M solution corresponded to a hydroxyapatite (HA)-like material. In contrast, the conversion product in the 1 M solution corresponded to an HA-like material for the starting pH of 9.5 and a calcium pyrophosphate material for the starting pH of 7.0. The kinetics of 45S5c conversion to HA at 37–60°C can be fitted by a 3D diffusion model, with activation energy of ~66 kJ/mol. The model predicts a time of ~45 years for conversion of the 45S5c microspheres to HA in 1.0 M K_2HPO_4 solution at 37°C, indicating that unconverted 45S5 glass ceramic material could remain in the body for an extended period.

ACKNOWLEDGMENTS: The authors would like to thank Mo-Sci Corp., Rolla, Missouri, for the 45S5 microspheres and particles used as reference materials in this work, and Eric Hallstrom for assistance with preparation of the 45S5 cross sections.

7 REFERENCES

1. Hench LL, Splinter RJ, Allen WC, Greenlee TK. Bonding mechanisms at the interface of ceramic prosthetic materials. J Biomed Mater Res. 1972;5:117–41.
2. Hench LL. Bioceramics. J Am Ceram Soc. 1998;81:1705–27.
3. Rahaman MN, Day DE, Bal BS, Fu Q, Jung SB, Bonewald LF, Tomsia AP. Bioactive glass in tissue engineering. Acta Biomater. 2011;7:2355–73.
4. Huang W, Day DE, Kittiratanapiboon K, Rahaman MN. Kinetics and mechanisms of the conversion of silicate (45S5), borate, and borosilicate glasses to hydroxyapatite in dilute phosphate solution. J Mater Sci: Mater Med. 2006;17:583–96.
5. Huang W, Rahaman MN, Day DE, Li Y. Mechanisms of converting silicate, borate, and borosilicate glasses to hydroxyapatite in dilute phosphate solution. Phys Chem Glasses-B. 2006;47:647–658.
6. Boccaccini AR, Chen Q, Lefebvre L, Gremillard L, Chevalier J. Sintering, crystallization and biodegradation behavior of bioglass-derived glass-ceramics. Faraday Discuss. 2007;136:27–44.
7. Filho OP, LaTorre GP, Hench LL. Effect of crystallization on apatite-layer formation of bioactive glass 45S5. J Biomed Mater Res. 1996;30:509–14.
8. Richard MN. Reaction of a borate glass with K_2HPO_4 solutions. M.S. Thesis; Missouri University of Science and Technology, MO, 2000.
9. Lai W, Garino J, Ducheyne P. Silicon excretion from bioactive glass implanted in rabbit bone. Biomaterials. 2002;23:213–7.
10. Clupper DC, Hench LL. Crystallization kinetics of tape cast bioactive glass 45S5. J Non-Cryst Solids. 2003;318:43–8.

11. Chen ZQ, Thompson ID, Boccaccini AR. 45S5 Bioglass®-derived glass-ceramic scaffold for bone tissue engineering. Biomaterials. 2006;27:2414–25.
12. Handke M, Sitarz M, Rokita M, Galuskin E. Vibrational spectra of phosphate-silicate biomaterials. J Mol Struct. 2003;651–653:39–54.
13. Glock K, Hirsch O, Rehak P, Thomas B, Jäger C. Novel opportunities for studying the short and medium range order of glasses by MAS NMR, ^{29}Si double quantum NMR and IR spectroscopies. J Non-Cryst Solids. 1998;232–234:113–8.
14. MacDonald SA, Schardt CR, Masiello DJ, Simmons JH. Dispersion analysis of FTIR reflection measurements in silicate glasses. J Non-Cryst Solids. 2000;275:72-82.
15. Kim CY, Clark AE, Hench LL. Early stages of calcium-phosphate layer formation in bioglasses. J Non-Cryst Solids. 1989;113:195–202.
16. Filgueiras MR, LaTorre G, Hench LL. Solution effects on the surface reaction of a bioactive glass. J Biomed Mater Res. 1993;27:445–53.
17. Harcharras M, Ennaciri A, Assaaoudi H. Vibrational spectra of double diphosphates $M_2SrP_2O_7$ (M = Li, Na, K, Rb, Cs). Can J Anal Sci Spect. 2001;46:83–8.
18. Harcharras M, Ennaciri A, Rulmont A, Gilbert B. Vibrational spectra and structures of double diphosphates $M_2CdP_2O_7$ (M = Li, Na, K, Rb, Cs). Spectrochim Acta A Mol Biomol Spectrosc. 1997;53:345–52.
19. Sarr O, Diop L. The vibrational spectra of the crystalline tripotassium hydrogen pyrophosphates $K_3HP_2O_7.3H_2O$ and $K_3HP_2O_7$. Spectrochim Acta A Mol Biomol Spectrosc. 1984;40:1011–5.
20. Parekh BB, Joshi MJ. Growth and characterization of gel grown calcium pyrophosphate tetrahydrate crystals. Cryst Res Technol. 2007;42:127–32.

21. Jung SB, Day DE. Conversion kinetics of silicate, borosilicate, and borate bioactive glasses to hydroxyapatite. Phys Chem Glasses-B. 2009;50:85–8.
22. Fu Q, Rahaman MN, Fu H, Liu X. Silicate, borosilicate, and borate bioactive glass scaffolds with controllable defradation rate for bone tissue engineering applications. I. Preparation and in vitro degradation. J Biomed Mater Res A. 2010;95:164–71.
23. Jones JR, Gentleman E, Polak J. Bioactive glass scaffolds for bone regeneration. Elements. 2007;3:393–9.
24. Nancollas GH, Zhang J. Formation and dissolution mechanisms of calcium phosphates in aqueous systems. In: Brown PW, Constantz B, editors. Hydroxyapatite and related materials. Boaca Raton: CRC Press; 1994. p.73–81.
25. House JE. Inorganic chemistry, chap. 14. New York: Elsevier/Academic Press; 2008. p.513-6..
26. Fu Q, Rahaman MN, Bal BS, Bonewald LF, Kuroki K, Brown RF. Silicate, borosilicate, and borate bioactive glass scaffolds with controllable degradation rate for bone tissue engineering applications. II. In vitro and in vivo biological evaluation. J Biomed Mater Res A. 2010;95:172–9.

Table I. EDS data for the Ca/P atomic ratio and Na concentration across the sections of 45S5c glass–ceramic microspheres (Fig. 3a-d) after reaction at room temperature for 10 years in K_2HPO_4 solutions under the conditions shown. The data are given for three positions A, B, and C in the surface layer, intermediate layer, and core, respectively, as shown in the SEM images. For comparison, the theoretical values for hydroxyapatite (HA) and 45S5 glass are also shown.

K_2HPO_4 solution: concentration; pH	Cross-sectional zone	Ca/P atomic ratio	Na concentration (wt%)
0.01M; pH = 7	Surface layer (A)	2.13	0.87
	Intermediate layer (B)	3.89	2.07
	Core (C)	5.34	17.69
1.0 M; pH = 7	Surface layer (A)	1.33	4.80
	Intermediate layer (B)	1.51	4.30
	Core (C)	5.42	15.7
0.01M; pH = 9.5	Surface layer (A)	2.46	1.0
	Intermediate layer (B)	5.35	6.83
	Core (C)	5.46	16.3
1.0 M; pH = 9.5	Surface layer (A)	1.49	0.89
	Intermediate layer (B)	1.80	0.14
	Core (C)	5.46	16.3
-	45S5 glass*	5.4	18.2
-	Hydroxyapatite*	1.67	0

*Theoretical values based on chemical composition.

Table II. Measured concentrations of Na, P, Ca and K and final pH values of K_2HPO_4 solutions (0.01 and 1.0 M), with starting pH of 7.0 and 9.5, after reacting 45S5c glass–ceramic microspheres in each solution for 10 years at room temperature. For comparison, the theoretical concentrations are shown for complete dissolution of 45S5 glass in a pure aqueous medium.

Concentration (mmol/L)	0.01M	1M	0.01M	1M	45S5 glass (Theoretical)
Na	23	47	25	43	79
P	1.5	970	1.5	1010	8.45
Ca	0.065	1.2	0.075	0.3	43.75
K	20	1980	19	2030	0
Starting pH	7.0	7.0	9.5	9.5	
Final pH	11.7	7.6	12.3	10.6	

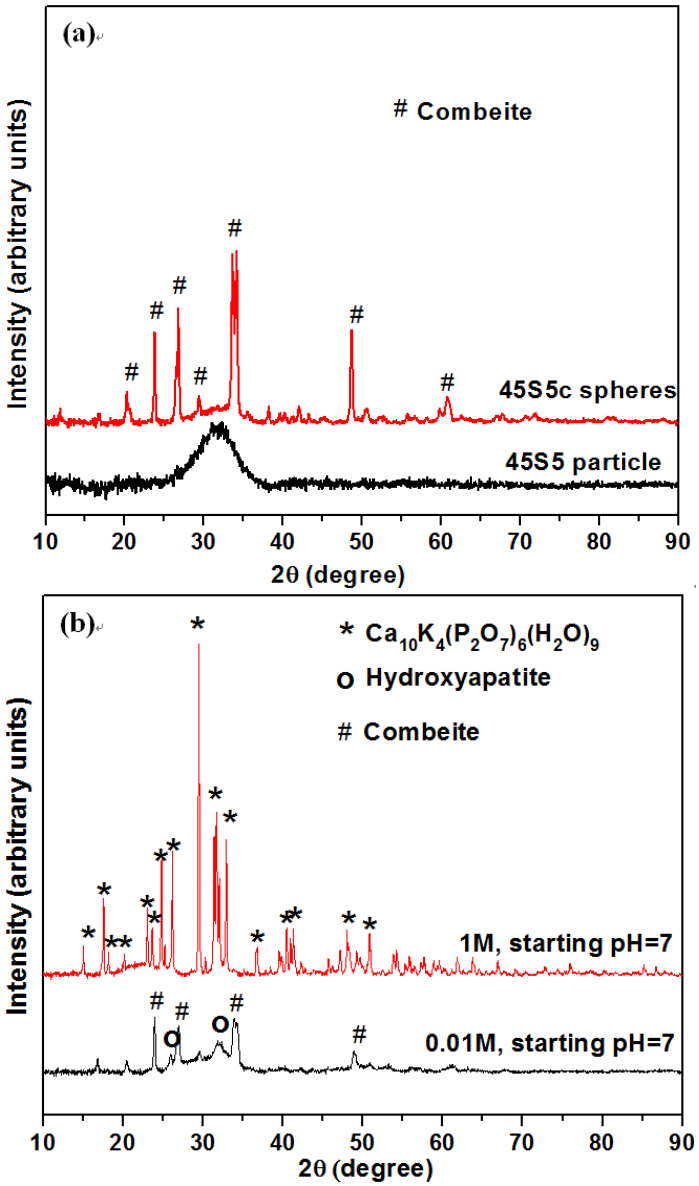

Figure 1. XRD patterns of: (a) starting 45S5c glass–ceramic microspheres; for comparison, the pattern for 45S5 glass particles without the spheroidization step is also shown. (b) 45S5c microspheres after immersion for 10 years at room temperature in K_2HPO_4 solution with a starting pH = 7.0 and concentrations of 0.01 and 1.0 M. (c) 45S5c microspheres after immersion for 10 years at room temperature in K_2HPO_4 solution with a starting pH = 9.5 and concentrations of 0.01 and 1.0 M.

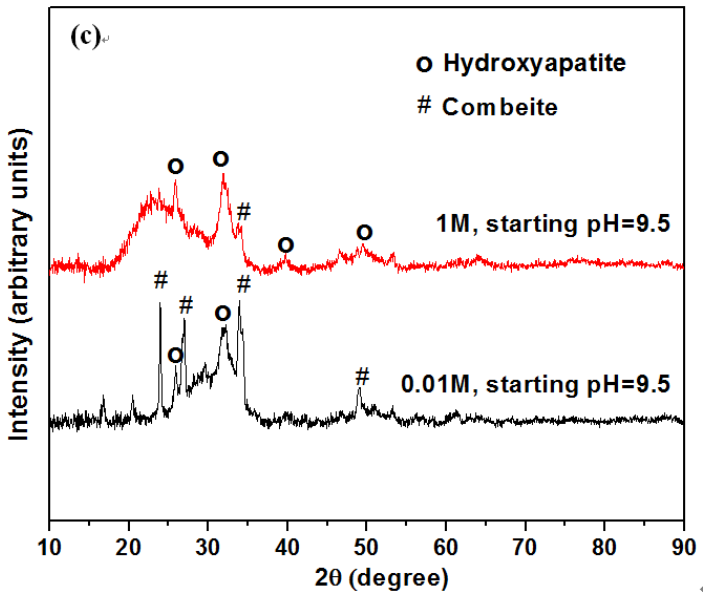

Figure 1. XRD patterns of: (a) starting 45S5c glass–ceramic microspheres; for comparison, the pattern for 45S5 glass particles without the spheroidization step is also shown. (b) 45S5c microspheres after immersion for 10 years at room temperature in K_2HPO_4 solution with a starting pH = 7.0 and concentrations of 0.01 and 1.0 M. (c) 45S5c microspheres after immersion for 10 years at room temperature in K_2HPO_4 solution with a starting pH = 9.5 and concentrations of 0.01 and 1.0 M. (Cont.)

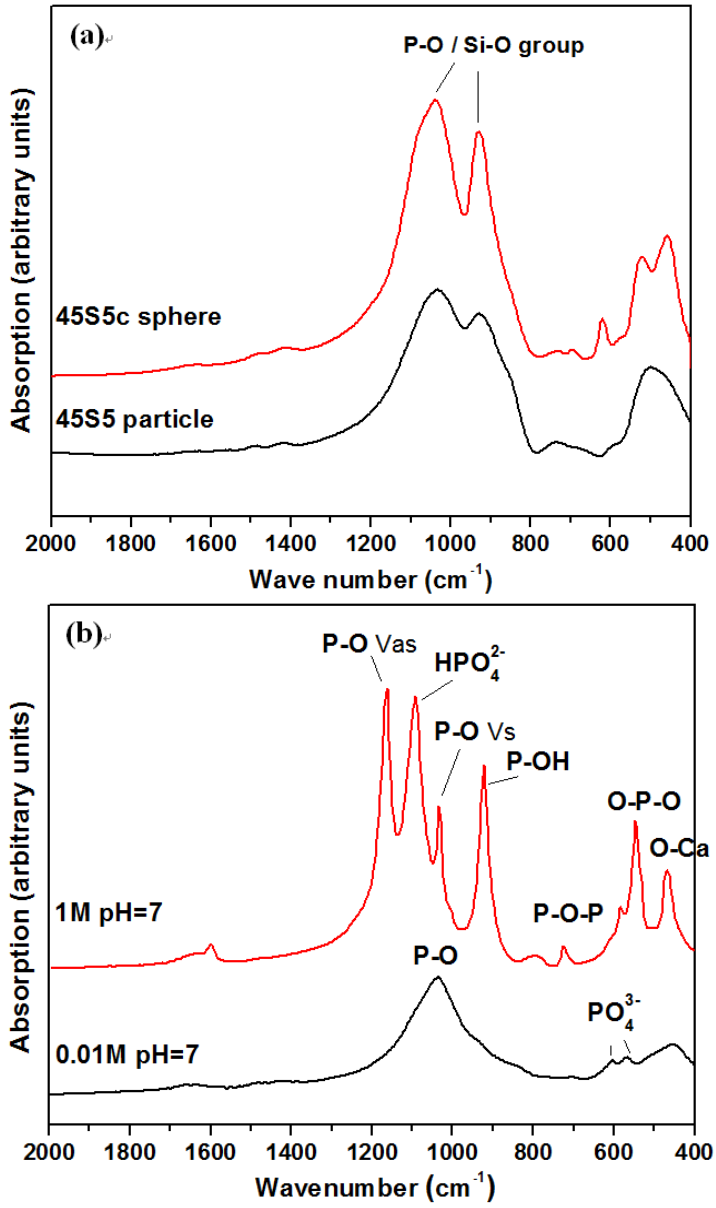

Figure 2. FTIR spectra of: (a) starting 45S5c glass–ceramic microspheres; for comparison, the spectrum of 45S5 glass particles without the spheroidization step is also shown. (b) 45S5c microspheres after immersion for 10 years at room temperature in K_2HPO_4 solution with a starting pH = 7.0 and concentrations of 0.01 and 1.0 M. (c) 45S5c microspheres after immersion for 10 years in K_2HPO_4 solution with a starting pH = 9.5 and concentrations of 0.01 and 1.0 M.

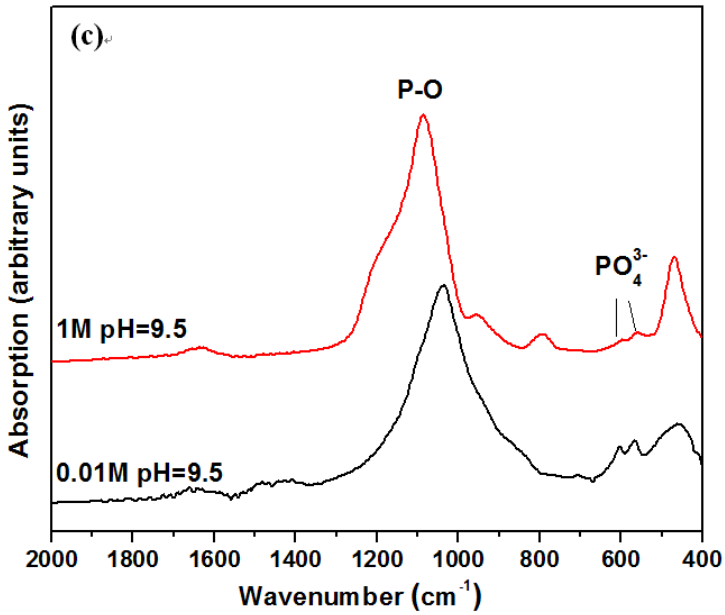

Figure 2. FTIR spectra of: (a) starting 45S5c glass–ceramic microspheres; for comparison, the spectrum of 45S5 glass particles without the spheroidization step is also shown. (b) 45S5c microspheres after immersion for 10 years at room temperature in K_2HPO_4 solution with a starting pH = 7.0 and concentrations of 0.01 and 1.0 M. (c) 45S5c microspheres after immersion for 10 years in K_2HPO_4 solution with a starting pH = 9.5 and concentrations of 0.01 and 1.0 M. (Cont.)

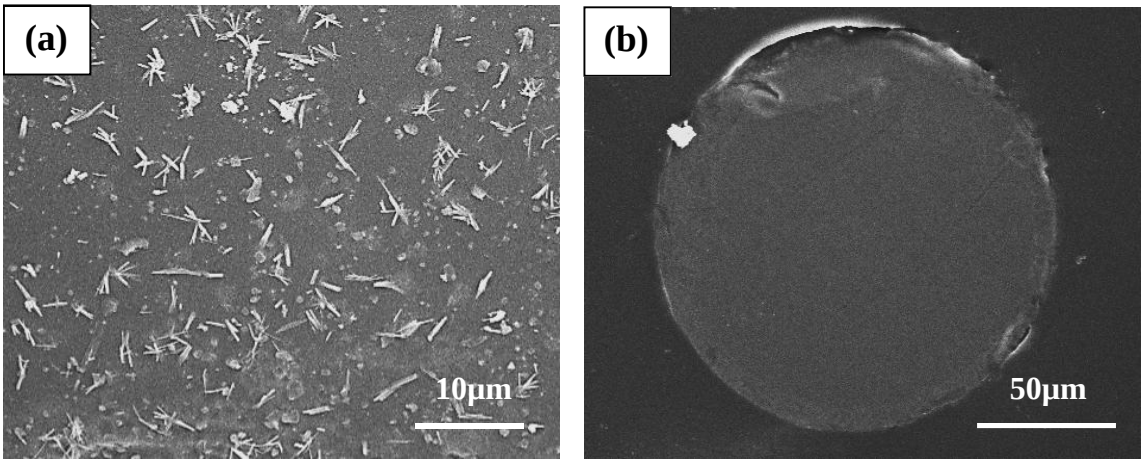

Figure 3. SEM images of: a the surface. B the polished cross section of as-prepared 45S5c microspheres.

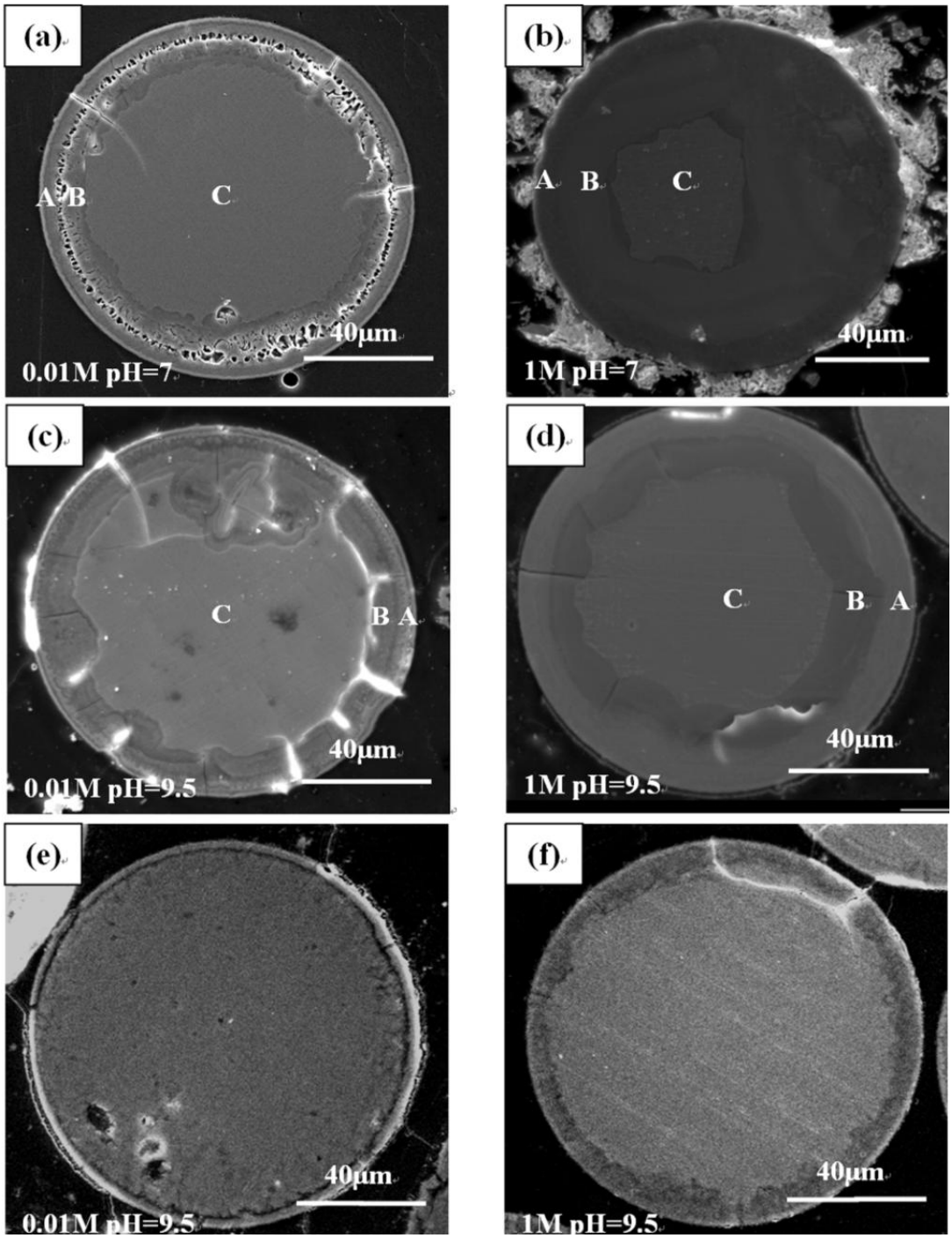

Figure 4. SEM images of the cross sections of 45S5c glass–ceramic microspheres immersed for 10 years at room temperature in K_2HPO_4 solutions with different concentrations and starting pH values: (a) 0.01 M; pH = 7.0, (b) 1 M; pH = 7.0, (c) 0.01 M; pH = 9.5, (d) 1.0 M; pH = 9.5. For comparison, SEM images of the cross sections of 45S5c microspheres immersed for 4 weeks at 37°C in K_2HPO_4 solutions (pH = 9.5) are shown for concentrations of : (e) 0.01 M, (f) 1.0 M. The letters A, B, and C show the regions where EDS analysis was performed.

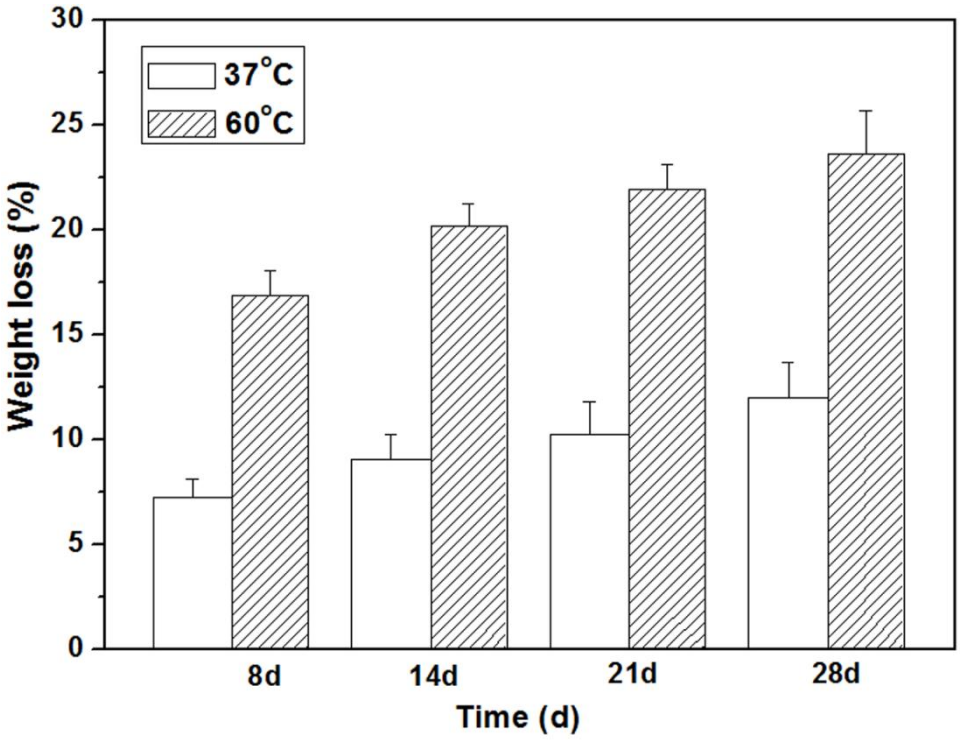

Figure 5. Fractional weight loss of 45S5c glass–ceramic microspheres as a function of immersion time in 1.0 M K_2HPO_4 solution (pH = 9.5) at the temperatures shown.

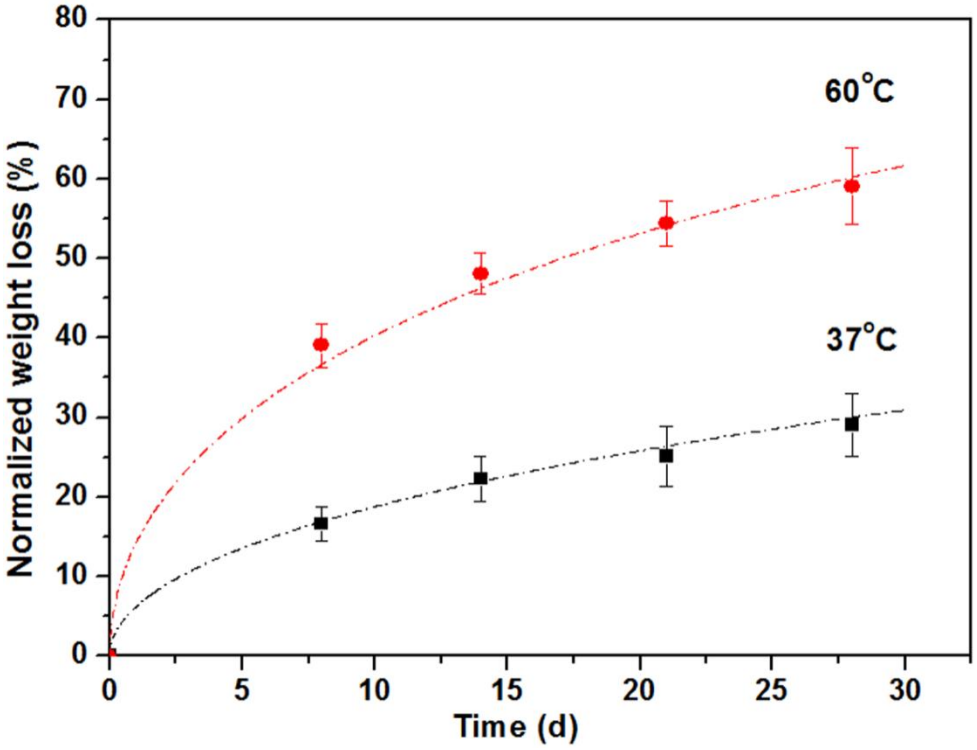

Figure 6. Fraction of 45S5c glass–ceramic microspheres converted to a hydroxyapatite (HA)-like material as a function of immersion time in 1.0 M K_2HPO_4 solution (pH = 9.5) at the temperatures shown. The dashed lines show the fit to the data using a three-dimensional diffusion model (Equation 1).

VITA

Hailuo Fu was born on March 06, 1983 in Dashiqiao, Liaoning Province, P.R. China. She lived in Dashiqiao until September 2001, when she started her undergraduate education at Tongji University, Shanghai, as a Materials Science major. During her undergraduate education, Hailuo also studied economics for 4 semesters at Fudan University, Shanghai, and German for 2 semesters. After receiving her Bachelor's degree in 2005, Hailuo remained at Tongji University for graduate studies, and she received her Master's degree in Materials Science and Engineering in 2008.

Driven by her curiosity in the area of novel materials research, in August 2008, Hailuo started her Ph.D. study under the supervision of Dr. Mohamed N. Rahaman at Missouri University of Science and Technology, Rolla, Missouri, USA. Her doctoral work resulted in 11 journal papers (8 published, one accepted for publication, and two submitted), 7 of which she is the first author; she also made 3 presentations at international meetings in the United States.